Characterization of Heterojunction Band Offsets by In Situ Photoemission Spectroscopy

（光電子分光法による半導体ヘテロ接合バンド不連続の評価）

December 21, 1992

by Yoshio HASHIMOTO

(07096)

Dissertation supervisor: Professor Toshiaki Ikoma

Contents

Chapter 1 Introduction

As an introduction to this thesis, this chapter invites all the readers to discuss about semiconductor heterostructures and energy band offsets.

1.1 Heterojunction band offset — A brief review

Semiconductor heterostructures have attracted many researchers' interests since they realize a confinement of electrons, holes, and/or photons.[1] When one look at electronic properties, this superb feature of the junction originates from abrupt changes in potentials for free electrons and holes arising very near the junction. By measuring electronic properties of a GaAs/Ge junction, Anderson found that both conduction band minimum and valence band maximum are discontinuous at the junction.[2]

Although existence of the discontinuities in the conduction band minimum (CBM) and the valence band maximum (VBM) has long been believed, their abruptness is questionable compared with their metallurgical structures. For example, molecular beam epitaxy (MBE) including growth interruptions[3] and atomic layer epitaxy utilizing self-limiting mechanisms[4] realize atomically flat interfaces. (In the following, differences in CBM and VBM at a heterojunction are called as not band discontinuities but heterojunction band offsets (HBOs) so as to express the VBM and CBM might not be discontinuous as is the atomic structure.)

Recently, needs for various optical devices have lead us to grow many junctions including a residual lattice strain by combining materials having different lattice constants from each other. At these junctions, which attract much attention because they can also modify the energy band structure in the strained material, the alignments of CBM and VBM seems to be much different from those of lattice matched systems.

Further, including GaAs/Ge and GaAs/Si, heterovalent interfaces are much more interesting since depending on an interface atomic configuration the band alignments can be greatly changed.[5,6] Moreover, several experimental works are currently devoted to apply this to a control of HBOs.[7,8]

1.2 Theoretical views of the band offsets

As shown in Ref. 1, lots of theoretical approaches have been addressed to study HBOs. Contribution of interface phenomena to the band alignments is one of the most significant issues. It is currently discussed whether the interface dipole potential varies the band offsets.[9]

By *ab initio* self-consistent calculations for (100)-, (110)-, and (111)-oriented GaAs/AlAs interfaces, Bylander and Kleinman found an interface dipole potential (~0.15 eV), which is defined by a potential energy due to a change in charge distributions compared from bulk GaAs and bulk AlAs.[10] Although the interface dipole obtained by their calculation depends on the orientation, the VBO is independent. The change in the interface charge distributions was also calculated by Baroni *et al.*,[11] Oshiyama *et al.*,[12] Massidda *et al.*,[13] and Lambrecht *et al.*[14] However, it is commonly concluded that the variation is limited only at the interface As atom to suggest an abrupt discontinuities in VBM and CBM.

It is, thus, important to study experimentally whether the change in charge distribution at an interface is really confined in the interface As atom to form a mono-atomically abrupt energy alignment.

There proposed various theories to predict VBOs by using simple models (so called model theories). Tersoff proposed that the VBO is obtained by considering a charge neutrality. In 1983, he proposed to compare so called metal induced gap state to deduce VBOs.[15] In 1984, also proposed was a simple interface charge cancellation (so called zero-dipole) model.[16] Charge neutrality levels which Flores and Tejedor used to explain an interface charge flow[17] and dielectric midgap energy proposed by Cardona and Christensen[18] give similar reference energies to determine the band alignments. Van de Walle and Martin proposed model solid theory, which consider a "model solid" to determine a potential of a material and to deduce VBOs. They claimed that the interface dipole potential depends on how one decides a reference surface.[19] Harrison's tight binding theory[20] also predicts good values of HBOs except for the GaAs/AlAs system, in which an effect of the *d*-orbital (Ga 3*d* level) seems to void the agreement of the calculation.[21,22]

Those models are in a good numerical agreement with some experiments and a use of the simple idea, to minimize interface charge flow, is convenient in predicting HBOs. However, for those theories to predict HBOs correctly, the HBO should be a value

which is determined only by bulk properties. (The existence of an interface dipole or a interface charge flow does not always violate the applicability of those theories.) We will thus clarify whether the HBOs are determined by bulk properties or not. However, we do not intend to judge whose theory is the most correct. Because the difference can be very small and a simple comparison of the determined VBOs will not make a good resolution.

1.3. Aims of this work

The following two points are addressed in this work.

(1) In order to clarify the origin of the HBOs, we study

(i) Orientation dependence of the HBOs at GaAs/AlAs

We evaluate HBOs at (100)-, (110)-, (111)*B*, and (311)*A*-oriented GaAs/AlAs.

—If the HBOs depend on the orientation, it shows that the HBOs are modified by interface phenomena (change in charge distributions near the interface).

—If not, HBOs are already determined by bulk properties.

→ Applicability of the simple model theories will be tested.

(See section 3.2)

(ii) Interface chemical shift of cation (Ga and Al) core levels

By measuring energies of Ga 3*d* and Al 2*p* levels as a function of a distance from the interface, interface chemical shifts are studied. Then, we will find how wide (in thickness) and how large (in energy) the chemical shifts are.

→ The transient in the electrostatic potential near the interface is shown.

→ Whether the mono-atomic abruptness in band alignments is or not will be resolved.

(See section 3.3)

(iii) Strain effects on InAs/GaAs HBOs

We determine the HBOs in pseudomorphic InAs/GaAs junctions

by choosing sample structure (not to generate dislocations) and

by including all the possible strain effects

both theoretically and experimentally.

By changing a substrate lattice parameter

→ Magnitude of strain effects are shown.

By changing a crystal orientation of the interface

→ Effect of non-isotropy in the strain deformation is explicitly shown.

(See chapter 4)

(2) In order to realize a control of HBOs, we study

(i) Role of Si inserted in a GaAs/Si/AlAs structure

We check the band diagram is flat in the GaAs/Si/AlAs system or not.

—If it is, the HBOs are controlled. (Then, VBO changes as reported in Ref. 7.)

—If not, Si layer is considered to introduce only a band bending. (The band bending, then, causes an apparent shift in XPS spectra.)

(ii) Analysis on the Si occupation site

Because a precise control of a Si occupation site is necessary to modify the HBOs, we study,

which site do Si atoms occupy and

whether we can control those sites.

(iii) Coupled δ-doping structure

To enable a control of the Si site, we try to insert two layers at a (311)*A* GaAs/AlAs heterojunction;

a Si δ-doping sheet and a *p*-type Si doped layer.

(See chapter 5)

Chapter 2 Evaluation of Band Offsets by Photoemission Spectroscopy

Major techniques to study HBOs by XPS and UPS are described. After a brief description about the instrumental information, an evaluation scheme of a valence band offset by using core level XPS measurements is shown. Finally, a few cautions will be given for the XPS measurements to deduce accurate values of HBOs.

2.1 What is measured by Photoemission Spectroscopy

Photoemission spectroscopy (PES) provides us a great tool to observe surface and interface chemistry and physics.[23] Utilized in this work are x-ray photoemission spectroscopy (or x-ray photo*electron* spectroscopy (XPS)) and ultraviolet photoemission spectroscopy (UPS). Briefly speaking, PES is performed as

(i) A sample is irradiated by a monochromatic photons.
(ii) Electrons are emitted from the sample through the well-known photoemission process.
(iii) An intensity of electrons is recorded as a function of an electron kinetic energy.

Then the electron kinetic energy, E_{KIN}, is given by,

$$E_{KIN} = h\nu - E_{BIN} + (\text{Correction term}), \qquad (2\text{-}1)$$

with E_{BIN}, so called an electron binding energy, which is an energy of core and valence electrons measured from the Fermi level of a sample. (Sometimes it is measured from VBM or another reference.) $h\nu$ is an incident photon energy. As shown by Eq. (2-1), an electron binding energy can be obtained. Then, we can study the density of states (DOS) for valence and core electrons. Further, by systematically measuring a shift in the peak energy, we have information of the bonding states of respective atoms. A correction term inserted in Eq. (2-1) includes an energy difference formed between the Fermi levels at a sample surface and the entrance of the electron analyzer, which shifts due to an analyzer work function, sample charging effects etc. The accuracy of the determination of E_{KIN} will be discussed in section 2.3. In the following, the obtained spectra are plotted as a function of the kinetic energy unless a particular refer-

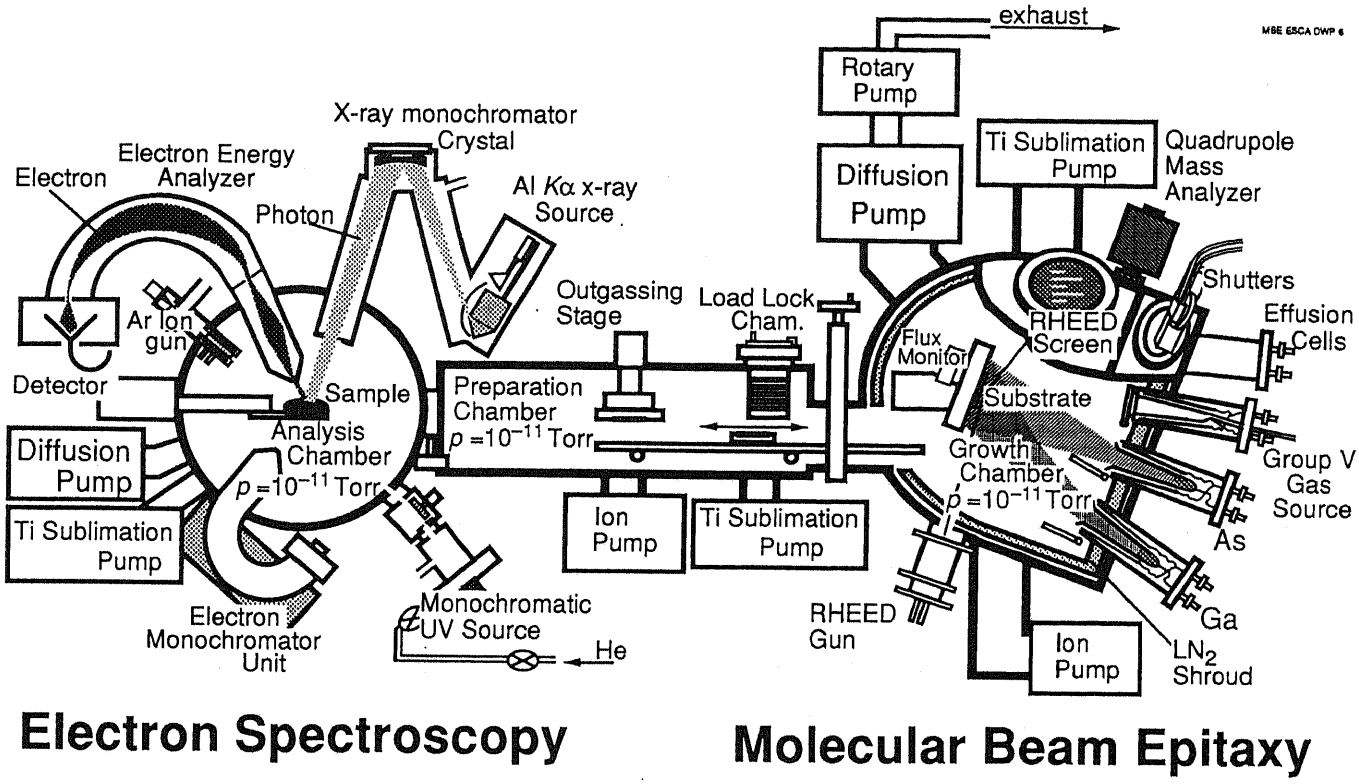

FIG. 2-1. A schematic illustration of our experimental set-up, which consists of an MBE growth chamber and an analysis chamber for XPS, UPS and LEELS combined with an UHV transfer tube.

ence level is defined, because the kinetic energy is the most direct value measured in the experiments. With use of XPS and UPS, we can study the HBOs and energy shifts in core levels as shown in the following chapters.

2.2 *In situ* measurements of MBE-grown samples

Since XPS and UPS probe only 10~100 angstroms from the very top of the sample, an oxidization and/or some contaminations of a sample surface will severely degrade obtained spectra. That is a reason why various methods to clean a surface such as a heat treatment, an ion bombardment cleaning, or a cleavage in the vacuum are required. All those techniques, however, damage a sample surface and are not suitable to study an abrupt heterointerface. With use of molecular beam epitaxy (MBE), one can grow semiconductor heterostructures under an ultra high vacuum (UHV) and its structure can be controlled in a scale of one atomic layer. By combining an MBE chamber with an UHV analysis chamber for XPS, one can measure a semiconductor heterostructure retaining a very clean surface without any damages. In Fig. 2-1, our experimental setup is schematically shown. We have grown As-based III-V semiconductors namely GaAs, AlAs, and InAs and their heterostructures in the MBE cham-

ber. Each of the grown samples was immediately transferred to the analysis chamber via a UHV transfer chamber and an XPS or UPS measurement was performed. We call these experiments as *in situ* XPS and *in situ* UPS as to express the as-grown samples are studied without exposing to the atmosphere. This is an ideal set up to study semiconductor heterostructure. Although when one study a sample during the MBE growth, the experiment is still powerful tool to reveal growth kinetics, it might severely limit the reliability of experiment by damaging an XPS optics by molecular beam or radiations etc. It is, thus, out of our scope.

The MBE chamber has 7 effusion cells allocated for Ga, Al, In, As (solid), Si, Be, and Sb elements and one for gases. (Effusion cells for Sb and gases have not yet been utilized within the experiments described in this thesis.) An excellent feasibility of the MBE system in growing high purity samples with a good temperature control and a reliable beam flux calibration has been demonstrated by persistently producing modulation doped GaAs/AlGaAs heterostructures, which show a very high electron mobility in the GaAs channel, more than $1.0\times10^6 cm^2/Vs$ (Ref. 24).

2.3 Instrumental resolution of photoemission spectroscopy

XPS has its instrumental resolution. Although the line width (0.6~1.0 eV in a FWHM of the spectrum)[25] itself is still worse than a typical magnitude of HBOs (<1 eV), we can study an energy difference in an excellent accuracy by using a monochromatized Al $K\alpha$ x-ray source and the following deconvolution procedure.

2.3.1 X-ray monochromator—Merits and Demerits

We used a Rowland-circle x-ray monochromator for an XPS photon source. Figure 2-2 shows an illustration of our monochromator. This monochromator gains an energy resolution of the Al $K\alpha$ x-ray from ~1 eV to ~0.2 eV. Simultaneously, it improves an energy dispersion of x-ray photons to be symmetric one and removes minor radiations such as $K\alpha_3$, $K\alpha_4$,.... This enables us to analyze an instrumental window function (Gaussian-Lorentzian convolution), which is necessary to deduce a VBO. However, there is a serious problem in the use of those photons. Since it depends on a photon focusing on the Rowland circle, a small spatial deviation of a sample, the crystal, or the x-ray gun (correctly, an electron beam spot on the Al coated anode) from the circle shifts the peak photon energy as well as reducing a peak photon intensity. In our system, when the sample is displaced from its optimum position by only 1 mm, photon energy is shifted by ~0.15 eV.[26] This ambiguity makes the absolute peak energy of an XPS spectrum unreliable, because the above combination of MBE and XPS chambers sacrifice a rigid adjustment of a sample position; i.e. each of the samples is mounted

on a small holder made of molybdenum which can be put on either one of the adapters for the MBE and analysis chambers. However, it gives us a good resolution when we concentrate on an energy *difference*. In other words, when we have an energy reference in the sample and determine another peak energy in an energy from that reference, the ambiguity in the absolute photon energy is mostly canceled. In the following experiment the energy difference is mainly discussed.

Moreover, an x-ray source has also a time drift in its energy. It has been found that a high-voltage source (15 kV), which is used to accelerate an electron beam to excite an x-ray anode, changes its output voltage by approximately 0.5 kV within ~ 2 hours since it has been turned on. This drift in the voltage varies the photon energy by ~0.2 eV, which might be due to a spatial shift in the electron beam spot on the anode. In order to avoid an ambiguity arising from this energy unstability, we made at least 2 hours of an idling before each experiment. In some cases, we scanned a sample more than a whole day, the peak energy does not shift during the experiment by more than 50 meV, demonstrating a stability of the system so far as an experiment during the initial 2 hours is avoided.

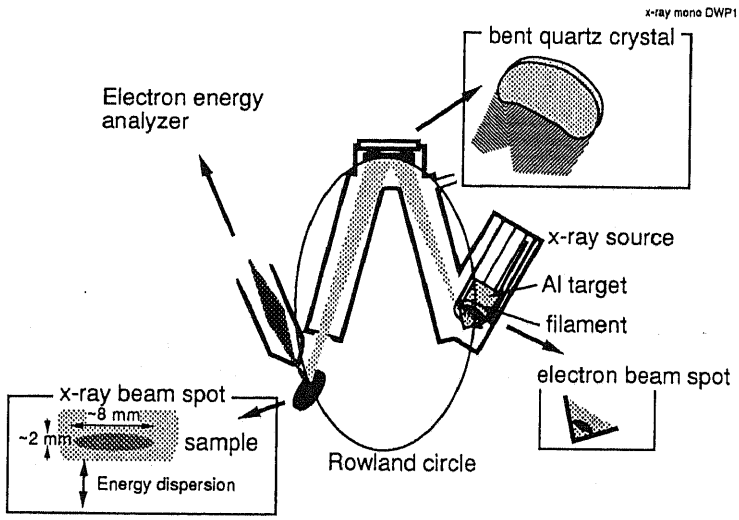

FIG. 2-2. A schematic illustration of the x-ray monochromator used for XPS measurements.

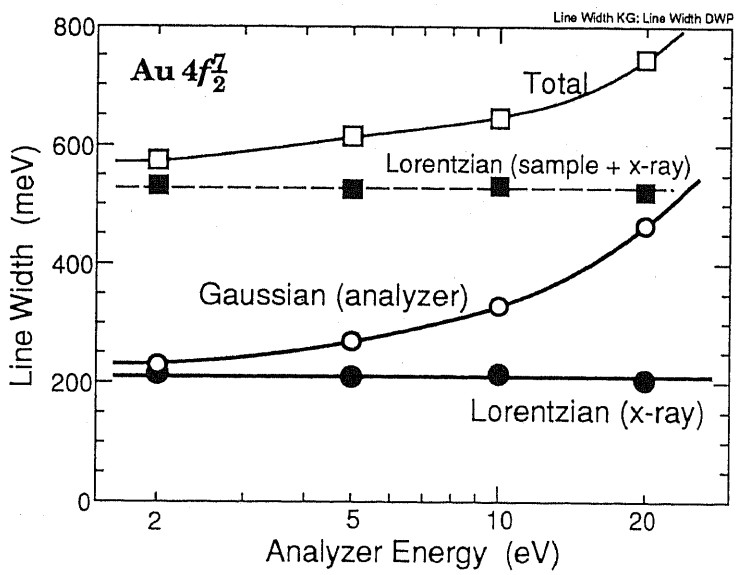

FIG. 2-3. Observed Au 4*f* line widths and deconvoluted Gaussian and Lorentzian components of the line shape shown as a function of the electron analyzer energy.

2.3.2 Analysis on a Au 4*f* spectrum

Figure 2-2 shows a variation in the line width of the Au $4f\frac{7}{2}$ XPS spectrum taken from a clean gold sample which consists on a ~0.3μm-thick poly-

crystalline gold film deposited on a molybdenum sample holder. It is known that the XPS spectra become broad due to an analyzer window function (Gaussian), a lifetime of photo-excited holes in a sample (Lorentzian broadening), and an unknown window function due to the photon source. To achieve a good determination of peak and VBM energies, we divide the three broadening components. The XPS signal has a line shape function of

$$I(E) = \int L(x)G(E-x)dx, \tag{2-2}$$

with

$$G(x) = \exp\left[-\ln 2\left(\frac{2x}{\Gamma_G}\right)\right], \tag{2-3}$$

$$L(x) = \frac{1}{1+(2x/\Gamma_L)^2}. \tag{2-4}$$

Γ_G and Γ_L denote the Gaussian and Lorentzian FWHMs. In Fig 2-2, also plotted are the Gaussian and Lorentzian line widths, which were obtained by a fit to the XPS spectra with use of Eq. (2-2~4). An intrinsic Au $4f\frac{7}{2}$ line has a Lorentzian line shape with a FWHM of 335 meV.[27] By subtracting 335 meV from the Lorentzian FWHM, we have 205 meV of the Lorentzian component of the instrumental broadening. An independence of the Lorentzian components on the analyzer energy indicates that this 205 meV-broadening is due to the x-ray optics, which agrees with a value reported by Gelius *et al.* (0.21V).[28]

2.3.3 Tips

Although the monochromatized Al $K\alpha$ line is relatively low in its intensity, in our experiment we have gathered enough signals by using three channeltrons and a 300W (20 mA×15 kV) x-ray source for typically 20 hours (in some cases, several days). This experiment cannot be performed without the following techniques and conditions.

(1) The analysis chamber is kept in very low pressure as ~5×10^{-11} Torr during an XPS measurement, which is achieved by using a diffusion pump with a liquid nitrogen cooled trap, Ti sublimation pumps, which evaporates only when the sample is in the MBE chamber, a small ion pump to evacuate the x-ray source, and a thin Al window to isolate the sample chamber from a room for the x-ray source. AlAs is especially sensitive to the surface contamination. Surface vibration measurements suggest that some hydrocarbon (not oxygen) molecules may contaminate the AlAs surface.

(2) Each of the samples was transferred from the MBE chamber to the analysis chamber immediately after the growth. Besides keeping an UHV of the transfer

chamber we took a care of the MBE chamber. (i.e. Liquid nitrogen has been supplied until the sample is taken to the analysis chamber.)

(3) During an XPS measurement, all the energy regions of the interest are repeatedly and circularatingly scanned for more than a hundred times: e.g. region 1, region 2, region 3, region 1, region 2, region 3, region 1,... This procedure has two merits:

(i) When an unknown trouble terminates the experiment, it damages very slightly the circularatingly scanned data (i.e. When the data acquisitions are stopped at the midpoint a region in the 100th scan, the ambiguity is reduced to be 1%, which is, in most cases, much less than the white noise appearing in the spectrum. However, those troubled data are not included for the most serious experiments as will be described in Figs. 3-6~7.

(ii) Although the time-drift of x-ray is avoided by procedure shown in section 2.3.1, a long duration of XPS measurement might be suffered from some time-dependent fluctuations. For example;

(a) A sample might be displaced from its initial position.

(b) A spectral peak intensity can change. (In most cases the intensity slightly decreases by a few percent during a scan of ~20 hours.)

(c) A shift in the brightness of the sample chamber can affect a surface pinning to shift the spectra. (In our experiments the sample chamber has been lighted with a halogen lump constantly during a measurement to ease us by sighting a sample during an experiment.)

(d) A slight contamination causes (depending on the surface material) a time-dependent shift in the spectra.

(d) The data recording computer rarely stops counting one of the 3 channeltron files to degrade an integrated spectrum, which seems to be a trouble particular to our apparatus.

Thus, it is best to scan circularatingly the important levels and check those drifts by a peak line width.

(4) When one huge noise is detected by the computer system, data for all the cannels except the one for the noise are recorded to be zero (in our system). To minimize this damage, no less than 2 regions must be allocated for each one of the important energy regions. When a noise eliminates the whole data of a region, another region of the spectra gives us an important information only by lowering the signal to noise (S/N) ratio to be $1/\sqrt{2}$ of the successful experiment.

(5) For most of the samples analyzed in this work, the thicknesses of the epitaxially grown layers must be finely evaluated and (depending on experiments) it must be exactly controlled (e.g. one monolayer-thick GaAs layers were inserted for the sample used in the experiment depicted by Fig. 3-6,7.). The growth rates

of GaAs, AlAs, AlGaAs, InAs and InGaAs were calibrated by measuring RHEED intensity oscillations.

2.4 Derivation of the band offset

2.4.1 The basic idea

Margaritondo *et al.* reported a determination scheme of a valence band offset by measuring valence energy distribution curve (EDC).[29] For example, they grew Si on a CdS substrate and measured its XPS spectra by increasing a thickness of the Si overgrown layer. In the CdS/Si system there is ~1.5 eV of VBO, which made them possible to distinguish a Si EDC from that of CdS. Thus, by comparing those EDCs the offset in the VBM was deduced. However this idea is not advantageous when one would evaluate a relatively small magnitude of VBOs, which includes GaAs/AlAs and InAs/GaAs systems, although they are a great interest of today.

As reported by Kraut *et al.*,[30] we can perform a precise measurement of a VBO by using core levels in the following way. The essence of this idea is to utilize a shallow core level as a *marker* of the energy in the respective material. Figure 2-4 shows energy band diagrams at a heterojunction between materials a and b, (a) for a thick heterojunction and (b) for a particular structure used for an XPS measurement. Shown in Fig. 2-4(b) are the VBMs of a and b, E_v^a and E_v^b, shallow core level of the material a, E_{CL}^a, and that of the material b, E_{CL}^b, energy difference from the VBM to the core level (binding energy) for a and b, E_{v-CL}^a and E_{v-CL}^b, the VBO, ΔE_v, and the core level energy difference, ΔE_{CL}. In Fig. 2-4(a), conduction band minima, E_c's, conduction band offset ΔE_c , and the Fermi level, E_f are also included. ΔE_v, ΔE_c, and ΔE_{CL} are shown with Δ as to express that they are differences between the respective energy in a and that in b. When the doping density is enough low in a sample for XPS, we can assume that the band diagram is flat as shown in Fig 2-4(b). Then the VBO is given by the following formula,

$$\Delta E_v = \Delta E_{CL} + E_{v-CL}^a - E_{v-CL}^b . \qquad (2\text{-}5)$$

Another important point in measuring ΔE_v is that E_{v-CL}^a and E_{v-CL}^b are bulk properties. This means

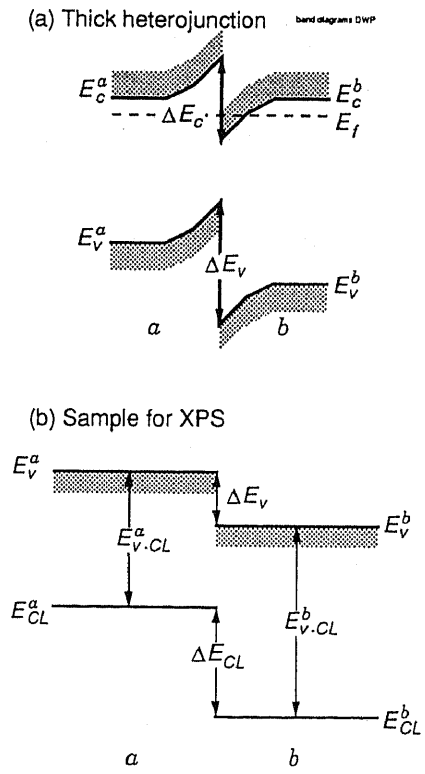

FIG. 2-4. Energy band diagrams of an a/b heterojunction.

that E^a_{v-CL} is determined only by the property of material a and can be determined by measuring sample a. Then we can evaluate the VBO by substituting E^a_{v-CL} and E^b_{v-CL} measured on bulk samples, which are grown by MBE, and ΔE_{CL} determined on a heterojunction.

A line shape of an XPS spectrum of one core level does not change as far as a flat band condition as shown in Fig 2-4(b) is fulfilled. Then, by appropriately defining a peak position, a core level energy is accurately determined. In this work, as well as Kraut *et al.*, it is defined to be a midpoint of two energies at which the XPS intensity is a half of the maximum. However, it is more difficult to determine the energies of the VBM, because the valence XPS spectrum has a shape which is given by a convolution of valence density of states and the window function of the equipment. We determined the VBM energy by a least squares fit to a valence XPS spectrum by a theoretical curve, which was calculated by a convolution of theoretical DOS broadened by taking into account the window function, Gaussian and Lorentzian convolution, determined in section 2.3. In order to keep an accuracy of the determination, we used the DOS calculated by the same theory for both sides of a heterojunction. In Table II-I, determined $E_{v\text{-}CL}$'s are summarized for GaAs/AlAs and InAs/GaAs systems. Because we do not know a theorist who has calculated all of GaAs, AlAs, and InAs in the same manner, we used different values for the GaAs depending on the system is GaAs/AlAs or InAs/GaAs. This makes two values for the Ga 3*d* binding energy. However, by using the DOS by Ihm and Joannopoulos, we include a difference in the valence DOS between GaAs and AlAs, which has been neglected by Kraut *et al.* The determination accuracy of ± 0.05 eV for the VBM is achieved.[31] It is much worse than the determination of a core level energy (± 0.01 eV) because the VBM has a weaker feature than the core levels and the theoretical DOS themselves have also another ambiguity.[32] In chapter 3 and 4 the VBO will be determined by using Eq. (2-5).

2.4.2 Important cautions

Finally, described here are a few important cautions, which should be informed of before measuring HBOs as shown in 2.4.1.

(i) Although some of the authors claim that the HBOs are correctly evaluated

TABLE II-I. Determined core level binding energies.

system	energy	value	theory
GaAs/AlAs	$E_{v\text{-Ga }3d}$	18.83±0.05	Ihm and Joannopoulos
	$E_{v\text{-Al }2p}$	72.80±0.05	(Ref. 33)
InAs/GaAs	$E_{v\text{-Ga }3d}$	18.75±0.05	Chelicowsky and Cohen
	$E_{v\text{-In }4d}$	17.36±0.05	(Ref. 34)

when the overgrown layer thickness is only 5~10Å, this is too much approximated. It is known that there is a surface chemical shift, which amount to ~0.2 eV on (110) surfaces, will severely affect the spectra. Moreover, the interface chemical shift can also affect the spectra. As will be clarified in chapter 3, the interface atoms do show a chemical shift of several tens meV. To minimize those ambiguities, it is recommended to use relatively large electron escape depth, λ_e, (A high $h\nu$ and a small electron take off angle are to be used) and to grow a sample with a thick overgrown layer. Practically, the overgrown layer thickness cannot be raised more than ~λ_e while keeping a good S/N ratio. In our experiment, we use $h\nu$ = 1486.6 eV (Al $K\alpha$) and a photoelectron take-off angle of ~30° from the normal to the sample surface. Under that configuration, the photoelectron escape depth is determined to be ~25Å for GaAs and AlAs with an electron kinetic energy E_{KIN} ~ 1.4 keV, which includes Ga 3*d* and 3*p*, Al 2*p*, As 3*d*, In 4*d*, and VBMs. This value was acquired by a fit to the XPS peak intensity ratio of Ga 3*d*/Al 2*p* measured on AlAs/GaAs heterostructures, including AlAs/GaAs single and double heterostructures, for those structures the intensity ratio, $I_{\mathrm{Ga}\,3d}/I_{\mathrm{Al}\,2p}$ is given by;

$$\frac{I_{\mathrm{Ga}\,3d}}{I_{\mathrm{Al}\,2p}} = \frac{C_{\mathrm{Ga}\,3d}}{C_{\mathrm{Al}\,2p}} \frac{\int_{\mathrm{GaAs\ layers}} \exp(-x/\lambda_e)\mathrm{d}x}{\int_{\mathrm{AlAs\ layers}} \exp(-x/\lambda_e)\mathrm{d}x}, \qquad (2\text{-}6)$$

Here, $C_{\mathrm{Ga}\,3d}/C_{\mathrm{Al}\,2p}$ shows a ratio of Ga 3*d* and Al 2*p* photoemission cross section (constant). x is a depth from the sample surface. By comparing those values measured on heterostructures, λ_e ~ 25Å is obtained.

(ii) The determination of a VBO with use of Eq. (2-5) depends on the binding energies $E_{v\text{-}CL}$'s to be *bulk* values. Thus, the following cases should be avoided.

1) Measuring $E_{v\text{-}CL}$'s by crystalline bulk samples and the ΔE_{CL} by a polycrystalline or amorphous sample might deduce wrong value. (All of our samples were epitaxially grown single crystals.)

2) When the extremely flat band diagram in an XPS scale as shown in Fig. 2-4(b) is not fulfilled the determined offsets are affected by a band bending, which will be discussed in sections 3.2 and 5.2.

3) When the experiment is performed with a very intense photon source such as a beam line from a storage ring, the thermal equilibrium might be broken to shift the spectra. (In those cases one cannot consider the Fermi level is leveled over the sample.) An absence of those effects will be demonstrated in section 3.2.

4) Sample structures shown in Fig. 2-5 are not suitable to deduce a VBO by Eq. (2-5). Because the surface Fermi level tends to be pinned and its energy depends

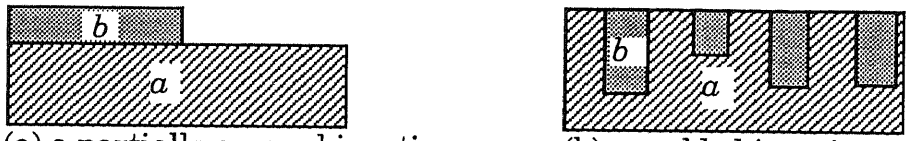

(a) a partially covered junction (b) a molded junction

FIG. 2-5. Sample structures which are affected by a difference in surface Fermi level (or a difference in a surface dipole potential).

on the material (near the mid gap). When a sample shown in Fig 2-5(a) is measured, the evaluated ΔE_{CL} is expressed as

$$\Delta E_{CL} = (E_F^a - E_{CL}^a) - (E_F^b - E_{CL}^b), \tag{2-7}$$

with E_F's the Fermi level for material a and b, and E_{CL}'s core level energies for material a and b, respectively. This shows that the energy has different physical meaning. Of course, by measuring the energy positions of the surface Fermi level pinning, $E_{f\text{-}v}$'s, one can obtain a VBO as reported by Gualtieri *et al.* [35] The structure shown in Fig. 2-5(b) should be carefully analyzed taking into account a surface pinning and also a band bending.

2.5 Summary

We use an experimental apparatus, which consists of an MBE growth chamber and an analysis chamber for the photoemission spectroscopy combined with an UHV transfer chamber. This enables us to perform an *in situ* XPS and UPS measurements on semiconductor heterostructures without exposing a sample to the atmosphere. By improving an accuracy of the peak detection and utilizing core levels to evaluate a VBO, we can conduct precise measurements of core level energies and VBOs as will be described in the following chapters. However, it requires us to take a great care to prevent any artifacts from affecting the measured energies as shown in section 2.4.2.

Chapter 3 Effects of Interface Charge Distributions on Band Alignments

Heterojunction band offsets at GaAs/AlAs heterostructures are investigated. This chapter describes not only an evaluation of the HBOs in this system but a pursuit to identify the origin of the band offsets. First, shown is an orientation independence of the valence band offset, which supports an idea that the HBOs are dominated by bulk properties within lattice matched systems. Second, by performing two series of XPS measurements on GaAs/AlAs heterostructures, spatial variations were scanned in energies of Ga 3*d* and Al 2*p* levels. Determined interface chemical shifts of these levels indicate that interface-specific charge distributions exist over at least 4 monolayers at the interface. The magnitudes of these energy shifts agree with chemical shifts found in an AlGaAs alloy.

3.1 Introduction

It has long been believed since an early stage of a research on semiconductor heterostructures, that abrupt discontinuities in VBM and CBM are created at a heterojunction.[2] If the heterojunction band offsets (HBOs) are determined by only the bulk properties, proposed model theories[15-20] can correctly predict the HBOs. Further, MBE provides us atomically abrupt heterointerfaces.[3,4] From a viewpoint of a metallurgical structure the abruptness of an MBE-grown interface can be almost perfect.[36] It has been demonstrated by finely contrasted TEM images from $(GaAs)_4/(AlAs)_4$ superlattices (SLs)[37] and sharp photoluminescence peaks observed from AlGaAs/GaAs/AlGaAs quantum wells.[38] Accordingly, we normally assume abrupt discontinuities of the band edges at the interfaces and design heterostructure devices using this "assumption." When two semiconductors are joined to form a heterojunction, however, the local electronic structure is perturbed near the interface.[9] The energetical transition should be completed in a finite thickness at the interface.

We can, then, raise two important questions concerning the origin of the HBOs;

(i) Whether the HBOs are determined by bulk properties or the HBOs are determined by the interface charge distributions. If the HBOs are determined by the interface properties, it requires us to perform a complicated calculation including

detailed charge distributions near the interface before we get correct values of HBOs.
(ii) How thick are the interface-specific charge distributions. Regardless of the answer to the question (i), a change in the interface charge distributions can exist to form a transient electronic structure. Then, we have to clarify the spatial extension of the transient, because the HBOs are considered to be formed after the energetical transient. Only a few studies have been made for that local energetical structure,[10-14] although it is necessary to study short period SLs and very small quantum structures (in the order of monolayers).

We study the GaAs/AlAs system to determine the HBOs in this system and to answer the above questions. We performed the following experiments;

(i) Orientation dependence of the VBOs is evaluated. This experiment will answer whether the HBOs are determined by the bulk properties or not.
(ii) Spatial variations in energies at Ga and Al atoms at the interface (interface chemical shifts) are measured. The existence of the chemical shifts will demonstrate a transient in the electronic structure.
(iii) By measuring the chemical shift in AlGaAs alloy, the validity of the chemical shifts found on the heterojunction are confirmed.

3.2 Orientation independence of HBO at GaAs/AlAs heterointerfaces

A valence band offset, ΔE_v, is studied at GaAs/AlAs interfaces. In order to clarify whether the interface charge distributions vary the VBO, we discuss a dependence of the VBO on a crystal orientation. Studied in this work were GaAs/AlAs heterojunctions grown on GaAs substrates with different orientations, namely, (100), (110), (111)*B*, and (311)*A*. Because an atomic bond configuration at a heterointerface depends on the crystal orientation, the orientation dependence of HBOs informs us a lot about the origin of HBO.

3.2.1 A determination of VBO

As shown in the previous chapter, the VBO is determined by using a core level energy difference ($\Delta E_{\mathrm{Ga}\ 3d\text{-}\mathrm{Al}\ 2p}$ in this system), which is accurately measured by XPS. Since $E_{v\text{-}\mathrm{Ga}\ 3d}$ and $E_{v\text{-}\mathrm{Al}\ 2p}$ are quantities specific to the constituent bulk materials, all the information on the band lineups is condensed in $\Delta E_{\mathrm{Ga}\ 3d\text{-}\mathrm{Al}\ 2p}$. Then, Eq. (2-5) is rewritten as

$$\begin{aligned} \Delta E_v &= \Delta E_{\mathrm{Ga}\ 3d\text{-}\mathrm{Al}\ 2p} + E_{v\text{-}\mathrm{Ga}\ 3d} - E_{v\text{-}\mathrm{Al}\ 2p} \\ &= \Delta E_{\mathrm{Ga}\ 3d\text{-}\mathrm{Al}\ 2p} + 53.97\ \mathrm{eV}. \end{aligned} \tag{3-1}$$

Therefore, by measuring only $\Delta E_{\text{Ga } 3d\text{-Al } 2p}$ for different interfaces, we can discuss an orientation dependence of the VBO. Although $E_{v\text{-Ga } 3d}$ and $E_{v\text{-Al } 2p}$ are measured less accurate than $\Delta E_{\text{Ga } 3d\text{-Al } 2p}$, this method cancels its ambiguity as far as its orientation dependence is concerned.

3.2.2 Samples

GaAs/AlAs heterojunctions were grown on (100), (110), (111)*B*, and (311)*A* GaAs substrates by MBE. Each of the samples was grown in the following way.

(1) For a (100) interface, an AlAs on GaAs interface was prepared by growing successively a 0.3~1μm-thick Si-doped *n*-type GaAs buffer layer and a 30 Å-thick undoped AlAs layer on an *n*-type GaAs substrate. A GaAs on AlAs structure consists of a 0.3~1μm-thick *n*-type GaAs buffer layer, a 100 Å-thick undoped AlAs layer, and a 30 Å-thick undoped GaAs layer. The Si doping density was ~ 1×10^{16} cm^{-3}.

(2) A (110) GaAs surface is known to be a difficult for an MBE growth. For a (110) interface, we made two types of samples in order to prevent Ga droplet formations and obtain a mirror surface. (i) A relatively thick InAs buffer was grown immediately after the oxide desorption from a GaAs substrate. Although a large lattice mismatch generates a lot of dislocations, when a GaAs layer is grown on that InAs layer, a clean mirror surface can be obtained.[39] (ii) Alternatively, by applying a large As_4 to Ga ratio, a sample with a mirror surface is grown without an InAs layer.[40]

(3) For a (111)*B* interface, by using a slightly misoriented substrate a mirror surface is obtained.[41] Then, the buffer layer and the heterostructures were grown in the same way as has been done for the (100) samples.

(4) For a (311)*A* interface, an undoped 1 μm-thick GaAs buffer layer and a 30 Å-thick AlAs top layer were grown to form an AlAs on GaAs interface. A 1 μm-

TABLE III-I. Growth conditions of buffer layers. AlAs/GaAs and GaAs/AlAs heterostructures were grown on the buffer layer shown bellow at the same T_s and As flux as were used for the buffer.

Orientation	T_s	Buffer layers
(100)	550-600°C	A 0.3-1μm n^--GaAs buffer layer A doping density is ~$1\text{x}10^{16}cm^{-3}$
(110)	400-450°C	600Å InAs and 0.3μm n^--GaAs
	400-450°C	A ~1μm n^--GaAs (As_4/Ga ratio > 10)
(111)*B*	550-600°C	A 0.3μm-thick GaAs buffer grown on (111)*B* substrates 2° misoriented toward (100)
(311)*A*	550-600°C	A 1 μm-thick undoped GaAs buffer

thick buffer layer, a 100 Å-thick AlAs layer, and a 30 Å-thick GaAs top layer were successively grown as to form a GaAs on AlAs interface. Since a Si doped (311)*A* GaAs shows *p*-type conductivity, the buffer layer was not doped with Si in order to prevent from forming a *p-n* junction.

Table III-I summarizes structures of the buffer layers. Each of the samples has 30Å-thick top AlAs (GaAs) layer grown on GaAs (AlAs) layer. This value (30Å) has been chosen to most accurately evaluate a VBO. Because in our experimental configuration, the photoelectron escape depth is ~25Å, the heterointerface should be formed nearly in this dimension from the surface. By forming an AlAs 30Å grown on GaAs structure give almost the same peak intensity for Ga 3*d* and Al 2*p*. The accuracy of a measurement is gained by increasing a peak signal intensity.[42] The MBE-grown samples were immediately transferred to the XPS chamber. XPS measurements were performed to scan energy regions which cover Ga 3*d* and Al 2*p* core levels for about 20 hours.

3.2.3 Determined ΔE_v and discussions

Figure 3-1 shows a typical XPS spectrum taken from an AlAs/GaAs (110) heterostructure. An energy difference, $\Delta E_{\text{Ga } 3d\text{-Al } 2p}$, was determined from the spectrum. Table III-II summarizes the obtained values of $\Delta E_{\text{Ga } 3d\text{-Al } 2p}$ for different orientations and growth sequences. $\Delta E_{\text{Ga } 3d\text{-Al } 2p}$ (= 54.41 ± 0.03 eV) is constant within an experimental uncertainty,[43] clearly indicating an orientation independence of ΔE_v. By substituting the obtained values of $\Delta E_{\text{Ga } 3d\text{-Al } 2p}$ into Eq. (3-1), ΔE_v is determined to be 0.44 ± 0.05 eV. This result is in agreement with the recent theoretical results by *ab-*

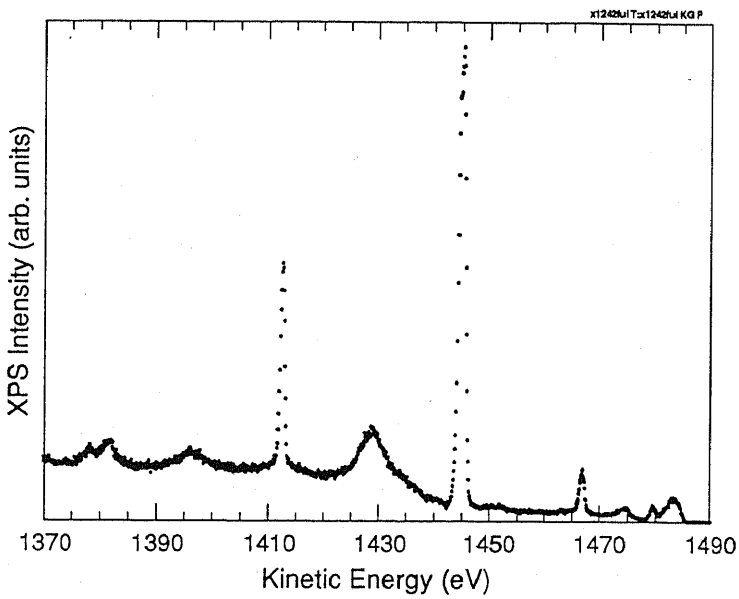

FIG. 3-1. A typical XPS spectrum taken from an AlAs/GaAs (110) heterostructure.

TABLE III-II. Measured $\Delta E_{\text{Ga } 3d\text{-Al } 2p}$'s.

Orientation	Growth Sequence	$\Delta E_{\text{Ga } 3d\text{-Al } 2p}$ (eV)
(100)	GaAs on AlAs	54.41, 54.42
	AlAs on GaAs	54.42, 54.42
(110)	GaAs on AlAs	54.41, 54.42
		54.40[a]
	AlAs on GaAs	54.42, 54.42
(111)*B*	GaAs on AlAs	54.40, 54.40
	AlAs on GaAs	54.42, 54.39
(311)*A*	AlAs on GaAs	54.36

[a]InAs layer was not used for this sample.

initio band calculations.[10,11,13,19]

Waldrop *et al.*[44] reported ~0.2 eV-dependence of $\Delta E_{\text{Ga } 3d\text{-Al } 2p}$ on the crystallographic orientation and/or the growth-sequence, although the origin of this discrepancy is not clear at present, the following possibilities are to be considered.

(i) As Ohno *et al.* reported, when GaAs and/or AlAs layers are heavily doped (intentionally or unintentionally), a surface band bending induces an apparent change in the determined VBO.[45] This ambiguity amounts to ~0.2 eV when the doping density is in the order of 10^{18} cm^{-3}.
(ii) A photovoltage effect has been reported to affect the spectra.[46] Although the experimental condition of Waldrop *et al.* is not known, our result of a growth sequence independence also demonstrates that our experiments use enough weak x-ray not to shift the spectra by introducing a voltage drop due to the photoexcitation. This is one of the important bases for our measurement to study energy shifts in Ga 3*d* and Al 2*p* levels as will be shown in the following sections.
(iii) As will be discussed in chapter 5, when a thin Si or Ge layer is inserted at the interface, the apparent VBO decreases for an AlAs/GaAs structure and increases for a GaAs/AlAs structure. Since it had been commonly used to deposit Ge on GaAs etc., a slight contamination from residual atoms such as Ge might cause an orientation dependence. As will be discussed later, we also tried to grow a heterointerface with 1~5 minutes of a growth interruption. The core energy difference measured on a single heterojunction does not vary by using a growth interruption, demonstrating that in our sample a contamination due to a degassing from the MBE chamber does not affect the spectra.
(iv) Although in early papers, Waldrop *et al.* commented the origin of growth sequence dependence might be due to a variation of interface dipole potential at the interface,[47] it is not likely because the orientation independence shown by our experiments more clearly indicates that the magnitude of the interface dipole contribution (if any) to the VBO is constant.

Our experimental observation of the orientation independence of ΔE_v strongly suggests that the band lineups at lattice-matched isovalent heterojunctions are determined by the bulk properties of the two constituent materials which form a heterojunction, rather than by the detail of the heterointerface such as bond configurations. This result, however, does not deny the presence of the interface dipoles; it indicates that the interface dipole potential, if it exists, is also orientation independent. This fact supports the idea that the interface dipole potential is determined by the bulk properties of the host semiconductors, such as the dielectric susceptibilities and the charge neutrality levels.[15-20]

3.3 Transient of local electronic structure at a heterointerface

Another important point to be clarified is

(i) Is there an interface dipole, the magnitude of which is independent of the crystal orientation?
(ii) If it is, how wide (in thickness) and how high (in energy) the potential varies to form the interface dipole (and the band lineups)?

In order to answer the above two questions, spatial variations of core level energies at a heterointerface are studied.

3.3.1 Core level energy and potential lineups

By XPS measurements on GaAs/AlAs structures, cation core level energies, $E_{\mathrm{Ga}\ 3d}$ and $E_{\mathrm{Al}\ 2p}$, are traced as a function of a distance from a heterointerface.[48] Each of these energies shifts when one changes the species of neighboring atoms; i.e., for a Ga atom bonded to interface As atoms, Al atoms replace 4 of the second-nearest Ga atoms. This change in bond configuration is considered to cause a chemical shift in core level energies. A chemical shift of an atom i, δE_i, is given by,[49]

$$\delta E_i = \delta E(q_i) + e^2 \sum_{j \neq i} \frac{q_j}{r_{ij}}. \qquad (3\text{-}2)$$

Here, q_i denotes a free ion charge of atom i and r_{ij} denotes a distance between atoms i and j. $-e$ is a charge of an electron. $\delta E(q_i)$ shows a shift in E_i due to a change in q_i. It is clearly shown that not only the potential due to the other atoms (latter component) but a contribution of a change in an atomic charge (former component) affects a chemical shift. In the present case, all of the Ga and Al atoms are bonded only to As atoms and the valence charge distributions can be changed at the junction. We can, then, discuss shifts in *the electrostatic potential* on the cation sites by measuring $E_{\mathrm{Ga}\ 3d}$ and $E_{\mathrm{Al}\ 2p}$. (In the following, these shifts of core level energies are called as *interface chemical shifts*.) If the valence electron density changes from that in bulk GaAs to that in bulk AlAs abruptly within one atomic layer at the heterointerface,[50] then $E_{\mathrm{Ga}\ 3d}$ and $E_{\mathrm{Al}\ 2p}$ should be *position independent*. However, if the spatial extension of the electronic perturbation due to cation substitution is larger than the size of the Wigner-Seitz cell of the zincblende structure and the valence electron density changes gradually over a finite distance, then $E_{\mathrm{Ga}\ 3d}$ and $E_{\mathrm{Al}\ 2p}$ near the interface are expected to be *shifted* from their respective bulk values. Therefore, by checking the position dependence (interface chemical shifts) of $E_{\mathrm{Ga}\ 3d}$ and $E_{\mathrm{Al}\ 2p}$, we can study microscopic valence charge distributions in the interface region. In the following, depicted are two series

of XPS measurements on GaAs/AlAs heterostructures, which indicates ~0.06 eV of a chemical shift in the both of cation core levels.

3.3.2 Formulation

In order to discuss the interface chemical shifts quantitatively, let us consider the following simple model. Figure 3-2 shows a metallurgical cross section and an energy band diagram of a GaAs/AlAs heterojunction. For simplicity, As atoms are omitted in the figure. a_i is defined as a chemical shift of Ga 3*d* level (nearly a change in the electrostatic potential on the Ga site) which is induced by the *i-th* Al plane from the Ga plane of the interest (See Fig. 3-2(a).). Then, the chemical shifts of the Ga 3*d* (Al 2*p*) level for the *n-th* Ga (Al) plane from the interface, $\delta E_{\mathrm{Ga}\ 3d}(n)$ and $\delta E_{\mathrm{Al}\ 2p}(n)$, are expressed as;

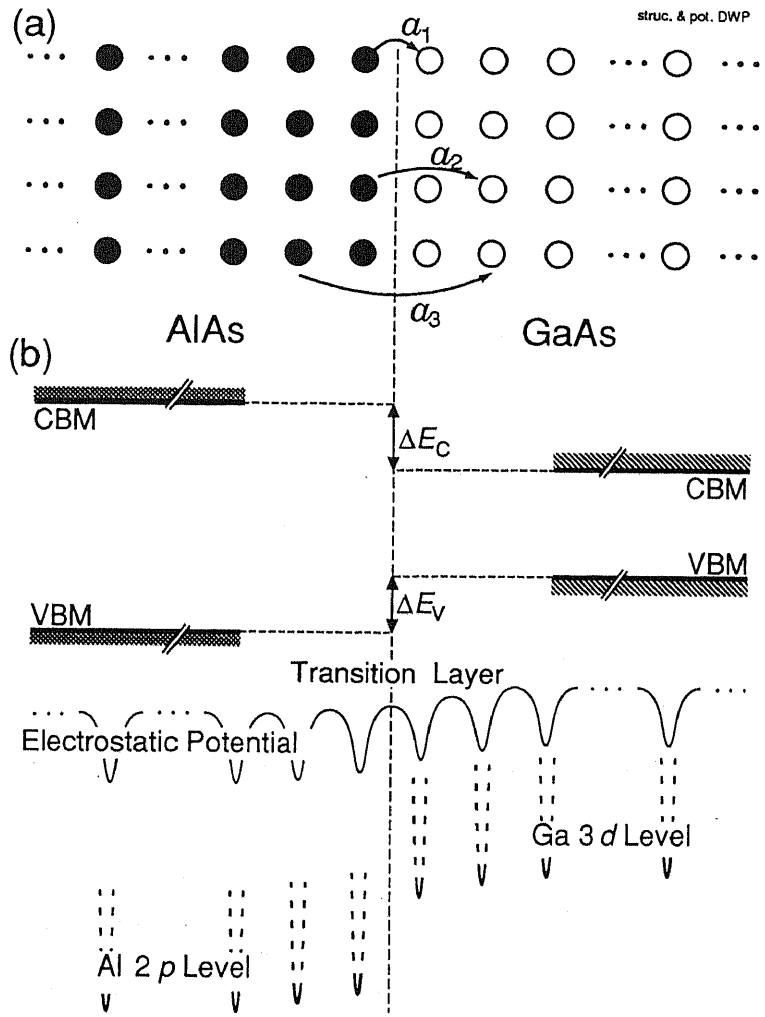

FIG. 3-2. (a) A cross section of the AlAs/*d* ML-thick GaAs/AlAs double heterostructure. Only group-III atoms are shown for simplicity. Shown with arrows are the chemical shift of the Ga 3*d* level induced by the neighboring Al planes. (b) energy diagram for CBM, VBM core levels, and electrostatic potential.

$$\delta E_{\mathrm{Ga}\ 3d}(n) \equiv \left[E_{\mathrm{Ga}\ 3d}(n) - E^{bulk}_{\mathrm{Ga}\ 3d}\right] = \sum_{i=n}^{\infty} a_i, \tag{3-3}$$

and

$$\delta E_{\mathrm{Al}\ 2p}(n) \equiv \left[E_{\mathrm{Al}\ 2p}(n) - E^{bulk}_{\mathrm{Al}\ 2p}\right] = \sum_{i=n}^{\infty} a'_i, \tag{3-4}$$

where $E^{bulk}_{\mathrm{Ga}\ 3d}$ and $E^{bulk}_{\mathrm{Al}\ 2p}$ denote Ga 3*d* and Al 2*p* core level energies in the respective bulk. The use of a simplified linear superposition for the interface chemical shift is considered to be valid, since the induced chemical shifts are less than 1% of the unperturbed core level binding energy. These coefficients, a_i's, quantify the magnitude and

the spatial extension of the perturbation to the local electronic structure by the heterointerface formation.

3.3.3 Ideas for Experiments

The following two types of samples, which are shown in Table III-III, were studied. One is a double heterostructure (DH), which consists of a GaAs (AlAs) layer embedded by AlAs (GaAs) layers. Core level energy difference is expected to vary with increasing d as shown in Table III-III reflecting an interface chemical shift. By varying a thickness of an inserted GaAs layer while keeping thick enough both of the AlAs layers, one can study a chemical shift in the GaAs layer. The essence of this experiment is that when d is 2 MLs or thinner than that, all of the Ga atoms are *interface Ga atoms*, for which 4 or more of the second nearest group-III atoms are replaced by Al, in contrast to the sample with $d \gg 2$ MLs (e.g. d = 20 MLs) where the Ga 3d signal is dominated by emissions from *bulk Ga atoms*, which locates at a certain distance from the interface. Then, an energy of the Ga 3d level measured from the Al 2p level reflects a chemical shift in the Ga 3d level. The reversed structure, where an AlAs layer

TABLE III-III. Sample structures and theoretical variation of energy differences.

Type	Structure	Energy
I	 (i) An AlAs/GaAs/AlAs double heterostructure (DH)	For a GaAs inserted DH, an energy difference is given by $\Delta E_{\text{Ga }3d\text{-Al }2p} \approx \frac{\sum_{n=1}^{d} E_{\text{Ga }3d}(n)\exp\left(-\frac{nd_0}{\lambda_e}\right)}{\sum_{n=1}^{d}\exp\left(-\frac{nd_0}{\lambda_e}\right)} - E^{bulk}_{\text{Al }2p}$, (3-5) with $E_{\text{Ga }3d}(n) = E^{bulk}_{\text{Ga }3d} + \sum_{i=n}^{\infty} a_i + \sum_{i=d-n}^{\infty} a_i$. (3-6)
	 (ii) A GaAs/AlAs/GaAs DH	For an AlAs inserted DH, an energy difference is given by $\Delta E_{\text{Ga }3d\text{-Al }2p} \approx E^{bulk}_{\text{Ga }3d} - \frac{\sum_{n=1}^{d} E_{\text{Al }2p}(n)\exp\left(-\frac{nd_0}{\lambda_e}\right)}{\sum_{n=1}^{d}\exp\left(-\frac{nd_0}{\lambda_e}\right)}$, (3-7) with $E_{\text{Al }2p}(n) = E^{bulk}_{\text{Al }2p} + \sum_{i=n}^{\infty} a'_i + \sum_{i=d-n}^{\infty} a'_i$. (3-8)
II	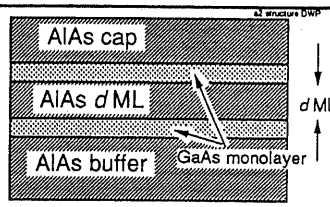 Two GaAs monolayers were inserted and spaced from each other by d ML.	An energy difference is given by $\Delta E_{\text{Ga }3d\text{-Al }2p} = 2\sum_{i=1}^{\infty} a_i - a_{d+1}$, (3-9) By comparing the values, a_i's are deduced as $a_i = \Delta E_{\text{Ga }3d\text{-Al }2p}(d \to \infty) - \Delta E_{\text{Ga }3d\text{-Al }2p}(d \to i-1)$. (3-10)

is inserted in GaAs layers, is also measured to study a shift in the Al 2*p* level. The theoretical variation of $\Delta E_{\text{Ga } 3d\text{-Al } 2p}$ in those samples is also shown in Table III-III.

Another type of sample consists of two GaAs monolayer sheets inserted among AlAs layers. A spacing between the GaAs monolayers, *d*, is varied. The theoretical variations in $E_{\text{Ga } 3d\text{-Al } 2p}$ for these structures are also shown in Table III-III. As can be seen from Eq. (3-10), the chemical shift a_i is explicitly given by comparing two values, $E_{\text{Ga } 3d\text{-Al } 2p}$'s for $d = i-1$ (i = 1,2,... MLs) and d=∞. The sample for $d = \infty$ consists of only one GaAs monolayer inserted in AlAs layers.

3.3.4 Samples and growth procedures

(i) Type I samples

Two series of DH samples were grown by MBE. Each of the AlAs/GaAs/AlAs (GaAs inserted) DHs was prepared by successively growing a 1 μm-thick Si-doped *n*-type GaAs buffer layer, a 100 Å-thick undoped AlAs, a *d* ML-thick GaAs inserted layer, and a 30 Å-thick undoped AlAs capping layer. The reversed AlAs inserted DH consists of a 1 μm-thick *n*-type GaAs layer, a *d* ML-thick AlAs inserted layer and a 30 Å-thick GaAs capping layer. The Si doping density for the GaAs buffer layer was ~1×10^{16} cm^{-3}. The substrate temperature during the growth was ~550°C. Growth was interrupted at each heterointerface for 1 minute to reduce the interface roughness. The thickness *d* of the inserted layer was varied from 0.5 to 20 MLs. Therefore, the uncertainty in the inserted layer thickness is at most ± 1 ML due to interface roughness.

(ii) Type II samples

Each of the type II samples consists of a 1 μm-thick Si-doped GaAs buffer layer, a 100 Å-thick AlAs, a 1 ML-thick GaAs bottom probing layer, a *d* ML-thick AlAs inserted layer, a 1 ML-thick GaAs top probing layer, and a 30 Å-thick AlAs layer, successively grown on an *n*-type (100) GaAs substrate by MBE. The Si doping density for the GaAs buffer is 1×10^{16} cm^{-3}. The growth has been conducted more carefully than has been done for the growth of type I samples as to reduce a step density in four heterointerfaces above and below the GaAs probing layers. Because when there are too much density of steps at each of the heterointerfaces, Eqs. (4-9,10) can not be applied to this system.[51] To enhance surface migrations of Ga and Al atoms, the substrate temperature during the growth was kept around 600°C, which is higher than that used to grow the type I samples. Growth was interrupted at each interface for 1~5 minutes to smooth out the interface roughness. Because it is more difficult to smooth out a GaAs on AlAs heterointerface, the growth was interrupted for 5 minutes at 600°C with reduced As pressure (~2×10^{-7} Torr) after the growth of each AlAs layer.[52] The RHEED

intensity was monitored during the growth to control the deposition thickness. It was also used to check the flatness of the heterointerfaces above and below the GaAs monolayers. The samples were immediately transferred to the analysis chamber to be studied by XPS. For the growth of each GaAs probing monolayer, especially, it is confirmed that the RHEED intensity variation shows one decline and one restoration in accordance with a growth of one monolayer.[53]

5.3.5 XPS spectra and changes in $\Delta E_{\text{Ga } 3d\text{-Al } 2p}$

(i) A survey spectrum and a determination of $\Delta E_{\text{Ga } 3d\text{-Al } 2p}$

Figure 3-3 shows a typical XPS spectrum measured on the heterostructure described above, one of the type II samples for d = 1 ML. As seen from the inset of Fig. 3-3, there is an AlAs related background around the Ga 3d level, which is a plasmon satellite of the valence DOS for AlAs. Before a determination of the peak position for the Ga 3d level from each of the spectra, the background intensity was subtracted. An XPS spectrum from an AlAs sample was fit by the peak energy and the intensity of the Al 2p level. The experimental uncertainty in determining the peak position is

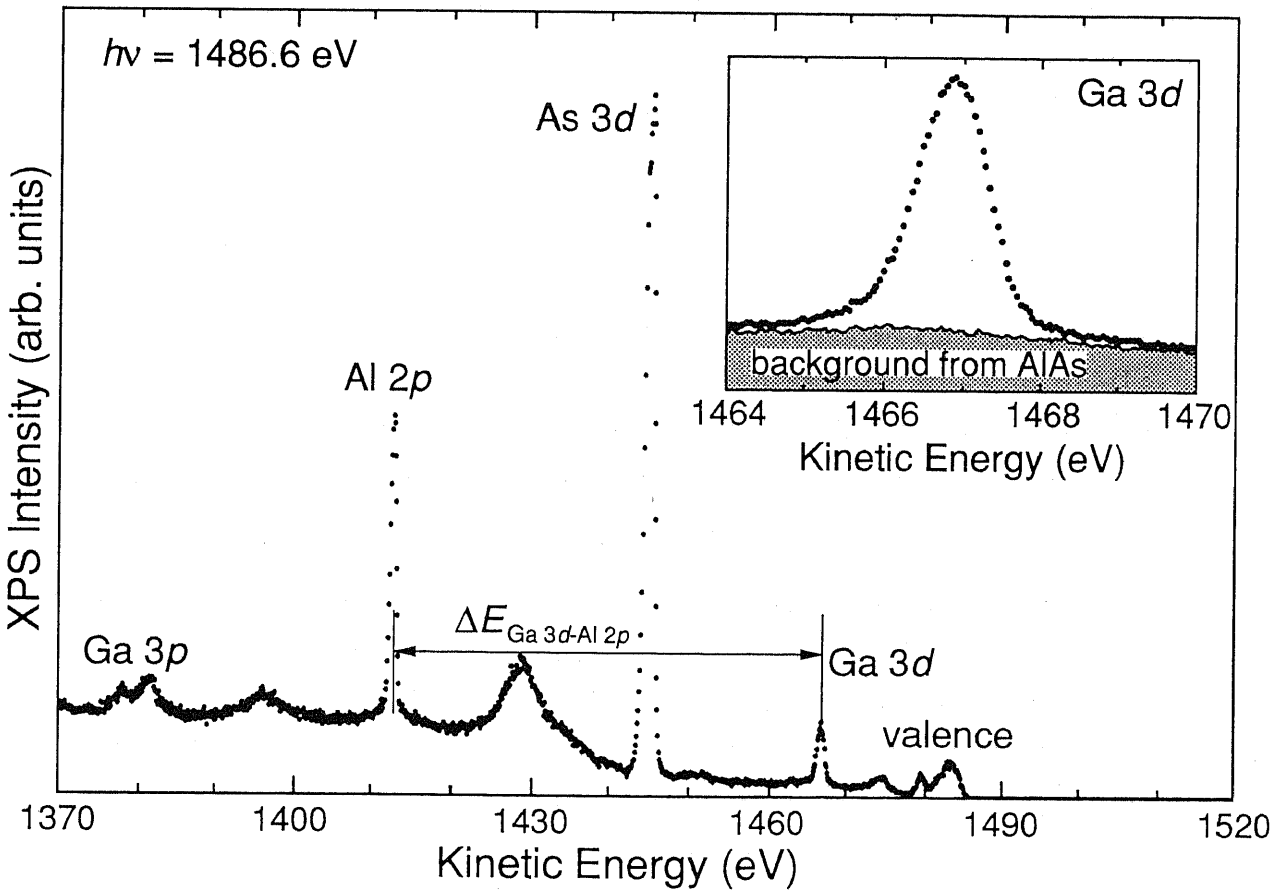

FIG. 3-3. A typical XPS spectrum taken on the GaAs/AlAs heterostructure described in the text. The inset shows the blowup of the XPS spectrum, which was used to determine the peak energy of the Ga 3d core level.

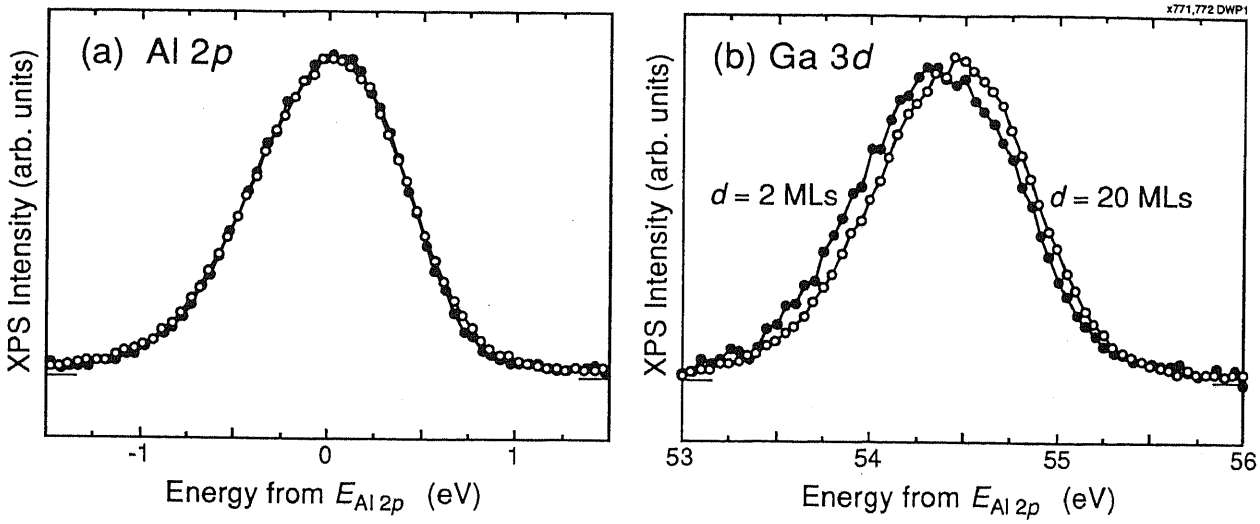

FIG. 3-4. XPS spectra around (a) the Al 2*p* level and (b) the Ga 3*d* level taken on the AlAs/*d* ML-thick GaAs/AlAs (100) double heterostructures. The origin of the energy scale is set at the peak energy of the Al 2*p* level. The full circles are data from the sample with d = 2 MLs and the open circles are from that with d = 20 MLs. The background intensity emitted from the top AlAs layer is subtracted from each Ga 3*d* spectrum.

thus minimized. For type II samples it is less than ± 10 meV except for the sample for $d = \infty$, which has an accuracy of ± 20 meV. We systematically measured the energy difference between Ga 3*d* and Al 2*p*, $\Delta E_{\text{Ga }3d\text{-Al }2p}$, as a function of the inserted layer thickness d.

(ii) Results on the type I samples

Figure 3-4 shows XPS spectra around (a) Al 2*p* and (b) Ga 3*d* core-levels measured on the AlAs/GaAs/AlAs DHs with inserted layer thickness d = 2 MLs and 20 MLs. Although the peak line width is approximately 1 eV as shown in Fig. 3-4, we can discuss a shift in the core level energy difference, $\Delta E_{\text{Ga }3d\text{-Al }2p}$, with an accuracy of ± 0.02 eV (and ± 0.01 eV for type II samples) by the following reasons;

(1) The quantity relevant to the following discussion is not the absolute energy position, which can be easily shifted by the surface pinning and/or the charging effect, but the energy difference between the core levels of the same sample. Although the surface band bending due to the background carrier density and/or the photo carriers by the x-ray can give a systematic shift in $\Delta E_{\text{Ga }3d\text{-Al }2p}$, as shown in section 3.2.3, the growth-sequence independence of $\Delta E_{\text{Ga }3d\text{-Al }2p}$ demonstrates that this effect is negligible in our experiments, which measure samples with low doping density ($1\times10^{16}\text{cm}^{-3}$) by an enough weak photoexcitation.

(2) Because the peak line shapes are insensitive to d, we can discuss the energy shift by comparing the two peaks as shown in Fig. 3-4. We found ~ 0.1 eV of the energy shift in $\Delta E_{\text{Ga } 3d\text{-Al } 2p}$, as clearly seen from Fig 3-4 (b). By defining a peak position as described in section 2.4 and by checking the peak line widths (0.95 eV for Al $2p$ and 1.03 eV for Ga $3d$ level) are maintained, we can evaluate a change in that energy difference in an excellent accuracy (± 0.01 eV).

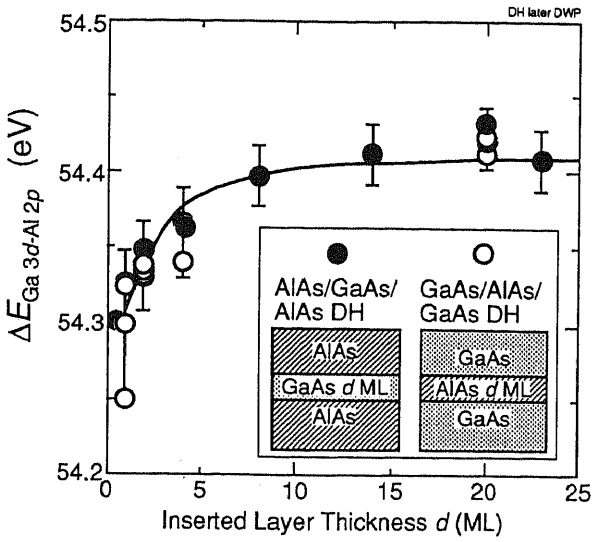

FIG. 3-5. The core level energy differences, $\Delta E_{\text{Ga } 3d\text{-Al } 2p}$'s, obtained from the AlAs/d ML-thick GaAs/AlAs double heterostructures (DHs) (full circles) and the GaAs/d ML-thick AlAs/GaAs DHs (open circles) are plotted as a function of the inserted layer thickness d. The solid curve shows the theoretical curve obtained by using a_i's shown by Eqs. (3-11~13).

Figure 3-5 plots $\Delta E_{\text{Ga } 3d\text{-Al } 2p}$ measured on the type I samples as a function of d. $\Delta E_{\text{Ga } 3d\text{-Al } 2p}$'s measured on both of DHs fall on a single curve and increases gradually from 54.30 ± 0.05 eV to 54.42 ± 0.02 eV with increasing d from 1 to 20 MLs. This increase in $\Delta E_{\text{Ga } 3d\text{-Al } 2p}$ indicates that the Ga $3d$ core level becomes ~ 0.1 eV-deeper by going closer to the interface, while the Al $2p$ level becomes shallower by the same amount. These energy shifts clearly indicate that the charge distributions on the cation site near the interface is perturbed by the presence of the different cation species on the next cation plane and that the electrostatic potential in the crystal gradually changes from the value in bulk GaAs to that in bulk AlAs over a finite distance.

(iii) Results on type II samples

The result on type I samples, however, does not directly show the values of chemical shifts in Ga $3d$ and Al $2p$ levels. As listed in Table III-III, if $\Delta E_{\text{Ga } 3d\text{-Al } 2p}$ measured on type II samples changes as a function of the thickness d of the inserted AlAs layer, chemical shifts a_1, a_2,... will be shown. Figure 3-6 shows Ga $3d$ and Al $2p$ XPS spectra measured on type II samples for d = 0 ML and for $d = \infty$ ML. Although the peak shift is smaller than that has been seen from Fig. 3-4, a peak shift of ~ 30 meV is found from the spectra. This is achieved by integrating higher peak intensity than type I samples to obtain a better accuracy of 0.01 eV. Figure 3-7 shows measured $\Delta E_{\text{Ga } 3d\text{-Al } 2p}$'s as a function of the thickness d of an AlAs inserted layer. Each of data

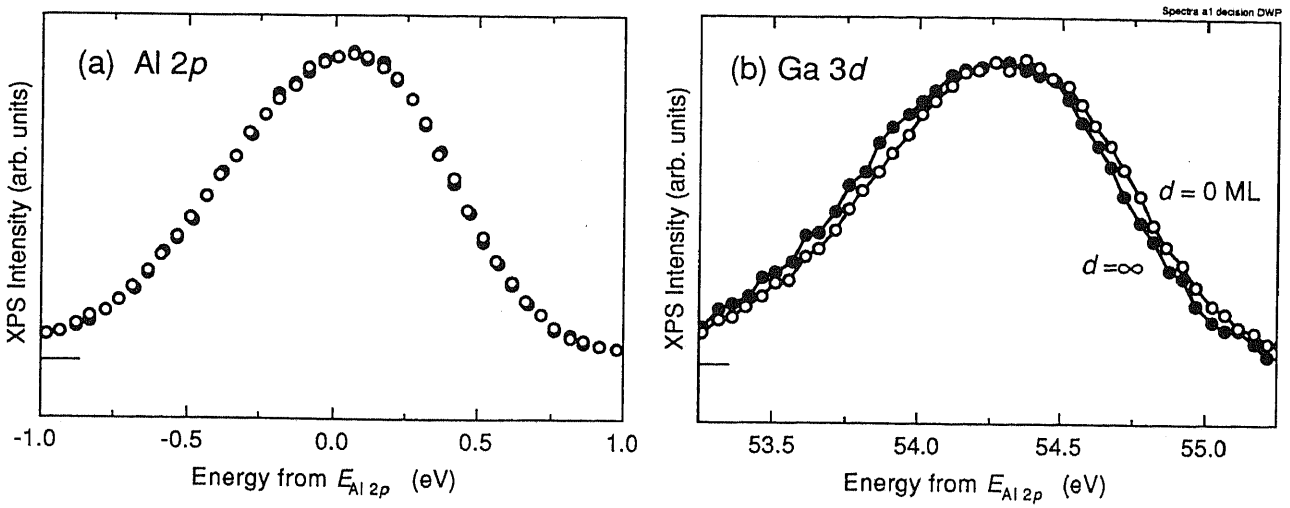

FIG. 3-6. XPS spectra around (a) the Al 2*p* level and (b) the Ga 3*d* level taken from the type II heterostructures. The energy scale is identical to that in Fig 3-4. The full circles are from a sample with $d = \infty$ and the open circles are from that with d = 1 ML. Both of Ga 3*d* and Al 2*p* spectra are normalized as to agree the peak intensities of the Al 2*p* levels to each other.

points stands for an independent experimental run.[54] $\Delta E_{\mathrm{Ga}\ 3d\text{-}\mathrm{Al}\ 2p}$ decreases from 54.28 eV to 54.25 eV when d increases from 0 ML to ∞ (*i. e.*, only one GaAs layer is inserted). By substituting the measured $\Delta E_{\mathrm{Ga}\ 3d\text{-}\mathrm{Al}\ 2p}$'s into Eq. (3-10),

$$a_1 = -31 \pm 20 \text{ meV}, \tag{3-11}$$

$$a_2 = -18 \pm 20 \text{ meV}, \tag{3-12}$$

and

$$a_3 = -7 \pm 20 \text{ meV} \tag{3-13}$$

were obtained. Although the magnitude of a_3 is marginal as compared with the experimental uncertainty, this result clearly indicates that a_1 and a_2 are non-zero.

3.3.6 Discussions

These values of a_i's are compared with the result obtained from type I samples. The solid line in Fig. 3-5 shows the theoretical variation in $\Delta E_{\mathrm{Ga}\ 3d\text{-}\mathrm{Al}\ 2p}$ obtained by substituting the determined values of a_i's into Eq. (3-5,7) and by using the following expression for the observed

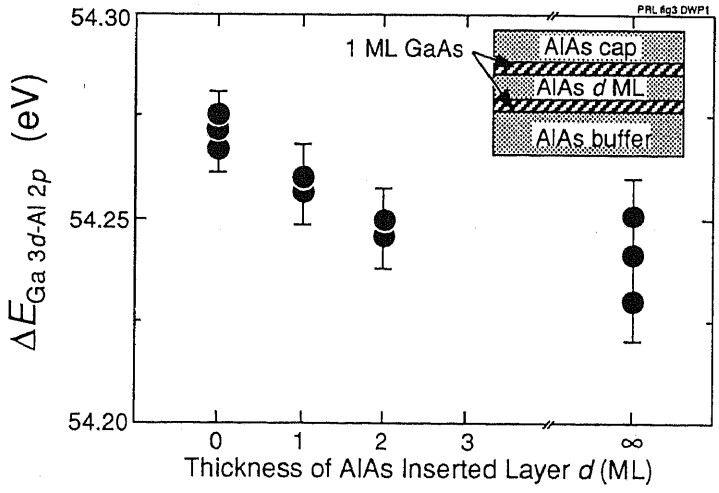

FIG. 3-7. $\Delta E_{\mathrm{Ga}\ 3d\text{-}\mathrm{Al}\ 2p}$ measured from type II samples plotted as a function of the thickness d of the inserted AlAs layer.

$\Delta E_{\text{Ga } 3d\text{-Al } 2p}$ for the AlAs/GaAs/AlAs DHs;[55]

$$\Delta E_{\text{Ga } 3d\text{-Al } 2p} \approx \frac{\sum_{n=1}^{d} E_{\text{Ga } 3d}(n)\exp\left(-\frac{nd_0}{\lambda_e}\right)}{\sum_{n=1}^{d}\exp\left(-\frac{nd_0}{\lambda_e}\right)} - E_{\text{Al } 2p}^{bulk}, \qquad (3\text{-}14)$$

where $E_{\text{Al } 2p}^{bulk}$ denotes the bulk Al $2p$ energy and $E_{\text{Ga } 3d}(n)$ the Ga $3d$ core level energy of the Ga atoms on the n-th cation plane from the top AlAs/GaAs interface. d_0 is the inter-cation plane distance (d_0 = 2.83 Å for GaAs and AlAs (100) planes). The exponential weighting function takes into account the finite electron escape depth λ_e. The excellent agreement between the experimental results and the calculated curve further supports the reliability of a_i's determined in the present work.

In should be noted that the theoretical curve for Fig. 3-5 is obtained by considering a value for $d = \infty$ as a fitting parameter and the absolute value of $\Delta E_{\text{Ga } 3d\text{-Al } 2p}$ does not agree with that of Fig. 3-7 due to the following two reasons;

(i) We performed the measurements on type II samples more than one year later than the measurements on type I samples, single heterostructures as shown in section 3.2, and AlGaAs alloy samples which will be shown in section 3.4. Because of an unstability of our apparatus, the value has been slightly changed during that one year; i.e. the energy difference $\Delta E_{\text{Ga } 3d\text{-Al } 2p}$ for an AlAs (30 Å)/ GaAs single heterojunction decreased from 54.41 eV to 54.38 eV.
(ii) We took a special care in growing type II samples, because it requires us to form very flat interfaces. However, the type I samples are considered to have ± 1 ML roughness at the interfaces, which change $\Delta E_{\text{Ga } 3d\text{-Al } 2p}$ for small d's. Then, the data points for d=1 and 2 MLs became ~0.04 eV larger than found on type II samples.

Although it is practically impossible to conduct a measurement on the reversed structure of type II, the coincidence of the data points on type I samples shows that the magnitude of chemical shift in the Al $2p$ level is identical to that found on the Ga $3d$ level. Thus, there is a relation as,

$$a_i' = -a_i. \qquad (3\text{-}15)$$

It agrees with an idea that because the chemical shifts originate from the difference in the valence charge distribution between GaAs and AlAs, the Al $2p$ core level shift is considered to have the same magnitude but the opposite sign of that of the Ga $3d$ level. Then, by substituting Eq. (3-11~13,15) into Eq. (3-3) the chemical shifts at a single heterojunction are given as

$$\delta E_{\mathrm{Ga}\,3d}(1) = -\,\delta E_{\mathrm{Al}\,2p}(1) = -\,57 \pm 20\ \mathrm{meV}\,, \tag{3-16}$$

$$\delta E_{\mathrm{Ga}\,3d}(2) = -\,\delta E_{\mathrm{Al}\,2p}(2) = -\,25 \pm 20\ \mathrm{meV}\,, \tag{3-17}$$

and

$$\delta E_{\mathrm{Ga}\,3d}(3) = -\,\delta E_{\mathrm{Al}\,2p}(3) = -\,7 \pm 20\ \mathrm{meV}\,. \tag{3-18}$$

The negative (positive) sign of the values means that the Ga 3*d* level (Al 2*p* level) becomes deeper (shallower) in the vicinity of the interface (See Fig. 3-2(b).). The error limit put on the values for Eqs. (3-15~17) is given by considering the result for both types of experiments: i.e. by using only type I experiment and a least squares fit by considering $\delta E_{\mathrm{Ga}\,3d}(1)$ and $\delta E_{\mathrm{Ga}\,3d}(2)$ to be fitting parameters the values are obtained as[56]

$$\delta E_{\mathrm{Ga}\,3d}(1) = -\,\delta E_{\mathrm{Al}\,2p}(1) = -\,60 \pm 10\ \mathrm{meV}\,, \tag{3-19}$$

and

$$\delta E_{\mathrm{Ga}\,3d}(2) = -\,\delta E_{\mathrm{Al}\,2p}(2) = -\,25 \pm 10\ \mathrm{meV}\,. \tag{3-20}$$

These values, in agreement with Eqs. (3-16,17) demonstrate the accuracy of Eqs. (3-16~18). In should be noted that the interface roughness, especially for type II sample with $d = \infty$ and type I sample with $d < 2$ ML, must exist to affect the obtained values. For type I samples, it mainly affects the samples with small d's and decreases the obtained value of the interface chemical shifts. For type II samples, it is rather complicated than for type I samples and it introduces the following ambiguities;

(i) Even if one considers only a_1 (a chemical shift of the first layer), by including ± 1 ML roughness at the four interfaces (above and below the GaAs monolayers), the observed trend in Fig. 3-7 ($\Delta E_{\mathrm{Ga}\,3d\text{-}\mathrm{Al}\,2p}$ decreases with increasing d) can be mostly explained. However, the agreement of the determined data (including non-zero a_2 and a_3) with type I experiments indicates a reliability of the experiments.

(ii) The accuracy of the experiments is limited by the data point for $d = \infty$, which is measured in an accuracy of ± 0.02 eV

The microscopic electronic structure at the GaAs/AlAs interface has been discussed theoretically. The general consensus among the detailed *ab-initio* band structure calculations[10-14] is that the charge density deformations are localized near the interface As atoms of the (100) interface and the first As-plane away from the interface already retains its charge distribution in the bulk; *i. e.* the transient layer is thinner than 2 MLs. This is a theoretical base of the use of $(GaAs)_3/(AlAs)_3$ supercells for the heterojunction band offset (HBO) calculations. However, our result strongly suggests that the size of the $(GaAs)_3/(AlAs)_3$ supercell is not sufficient to deduce HBOs in an accuracy of a few ten meV and that at least $(GaAs)_5/(AlAs)_5$ is recommended. Our result also implies that it is very important to take into account such a transient in the elec-

trostatic potential near the interface in predicting the electronic properties of short period superlattices such as $(GaAs)_1/(AlAs)_1$ and $(GaAs)_2/(AlAs)_2$.

3.4 Core level chemical shift and energy lineups in AlGaAs alloy

In this section shown are our *in situ* XPS measurements of the valence band maximum and the core levels in $Al_xGa_{1-x}As$. The chemical shifts of cation core levels are shown to be compared with the interface chemical shift discussed in section 3.3. A lineup of VBM is displayed in consistent with a VBO determined on the heterojunction to deduce a modified version of so called natural energy lineups.

3.4.1 Introduction

An orientation independence of HBOs at GaAs/AlAs heterointerfaces (See section 3.2) and a transitivity of the HBOs in the HgTe-CdTe-ZnTe system[57] strongly support the idea that the HBOs are predominantly determined by the difference of bulk properties. It is, then, considered to be able to establish so called a natural energy lineup of the VBM. When one knows a universal reference level and VBM energies of constituent materials measured from that level, the VBO is trivially given from a difference. Although a lot of theoretical and also experimental works have been addressed,[15-20] it is not clear so far which level can be the reference. It is, thus, necessary to determine the natural lineups of the VBMs and other levels without assuming an energy level to be a common reference level a priori.

Further, in the previous section, it has been shown that the energies of Ga 3*d* and Al 2*p* levels shifts in the vicinity of the interface. In AlGaAs alloy each of the Ga atoms for example has some second nearest Al atoms. Then, it is considered that a similar chemical shift should appear and that we can compare those result to check the reliability of the interface chemical shift shown in the last section.

In this section we study the VBM and the atomic core levels in $Al_xGa_{1-x}As$. By photoemission measurements, one can study the energy of those levels; Ludeke *et al.*,[58] Ireland *et al.*,[59] and Okumura *et al.*[60] studied the $Al_xGa_{1-x}As$ alloy by XPS. However, as has been stated in section 2.3, the difficulty to evaluate the absolute energy has made it necessary to estimate an energy by using a reference level; *i.e.* the contamination C 1*s* peak was used by Ireland *et al.* The cation core level binding energies were also a candidate to be a reference level, which Shih and Spicer applied to the CdTe/HgTe system.[61] We study the $Al_xGa_{1-x}As$ by *in situ* XPS and propose a new scheme to obtain lineups of the VBM and core levels.

We used the measured energy difference, $\Delta E_{\text{Ga } 3d\text{-Al } 2p}$,. It should be noted that the value of the Ga $3d$ or Al $2p$ core level measured without assuming a reference level (absolute zero) is ambiguous, but their difference is a universal value. By comparing the value of $\Delta E_{\text{Ga } 3d\text{-Al } 2p}$ for a GaAs/AlAs heterojunction (HJ) and that for $Al_xGa_{1-x}As$ alloy, the chemical shift of the Ga $3d$ and Al $2p$ core levels will be determined. Further, the energy positions of the VBM and an anion core level were obtained by adding determined chemical shift to the measured energy difference from those cation core levels. The determined energy shifts of the VBM and core levels are compared with recent theoretical predictions.[13,22]

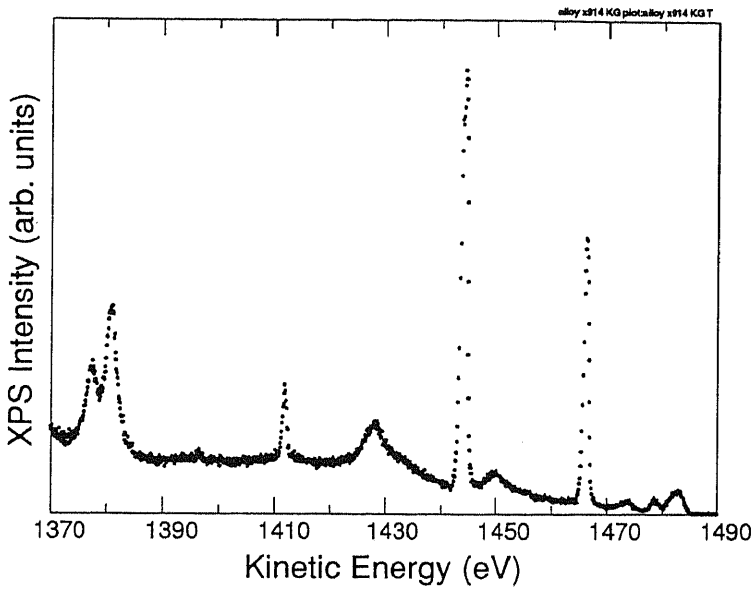

FIG. 3-8. A typical XPS spectrum taken on an MBE-grown $Al_xGa_{1-x}As$.

3.4.2 Experiment

Each of the samples measured in this work consists of a 1 μm-thick lightly Si-doped n-type GaAs layer (doping density is $1\times10^{16}cm^{-3}$) and a 1000 Å-thick $Al_xGa_{1-x}As$ alloy (x = 0 ~ 1) layer successively grown on Si-doped a n^+-GaAs (100) substrate by MBE. The AlAs content x was calibrated by comparing RHEED oscillations for GaAs and AlGaAs layers. Kinetic energy regions including the VBM and the Ga $3d$, As $3d$, Al $2p$, and Ga $3p$ core levels were repeatedly scanned for 20~40 h. The VBM was determined by comparing the XPS spectrum with the theoretical density of states (DOS) for $Al_xGa_{1-x}As$ broadened by the instrumental resolution.[62]

Figure 3-8 shows a typical XPS spectrum taken on an $Al_xGa_{1-x}As$ sample. First, an energy difference, $E^{\text{alloy}}_{\text{Ga } 3d\text{-Al } 2p}$, is evaluated in the same manner as used for the heterojunctions (HJs). Thus, the value can be compared with the result for HJs.[63] In Fig. 3-9, $E^{\text{alloy}}_{\text{Ga } 3d\text{-Al } 2p}$ is plotted as a function of the AlAs content x. $E^{\text{HJ}}_{\text{Ga } 3d\text{-Al } 2p}$ denotes the $\Delta E_{\text{Ga } 3d\text{-Al } 2p}$ measured on a GaAs/AlAs heterojunction, which is shown as a difference in binding energies of GaAs and AlAs, respectively, as;

$$E^{HJ}_{Ga\ 3d\text{-}Al\ 2p} = E^{GaAs}_{Ga\ 3d} - E^{AlAs}_{Al\ 2p}. \quad (3\text{-}21)$$

It is clearly seen that $E^{alloy}_{Ga\ 3d\text{-}Al\ 2p}$ (= 54.27 ± 0.04 eV) is almost independent of x and smaller than that in the heterojunctions, $E^{HJ}_{Ga\ 3d\text{-}Al\ 2p}$, by 0.14 eV. The Al 2$p$ level energy in $Al_xGa_{1-x}As$ ($x \to 0$) is deeper than the Ga 3d level in GaAs by $E^{alloy}_{Ga\ 3d\text{-}Al\ 2p}$ in contrast to the same level in AlAs, which is deeper than the Ga 3d level in GaAs by $E^{HJ}_{Ga\ 3d\text{-}Al\ 2p}$ as shown by Eq. (3-21). Thus, the 140 meV-difference in $E_{Ga\ 3d\text{-}Al\ 2p}$'s shows that the Al 2p level energy in the alloy shifts by −140 meV when x increases from 0 to 1. In the same way, the Ga 3d level also shifts −140 meV when x increases from 0 to 1.

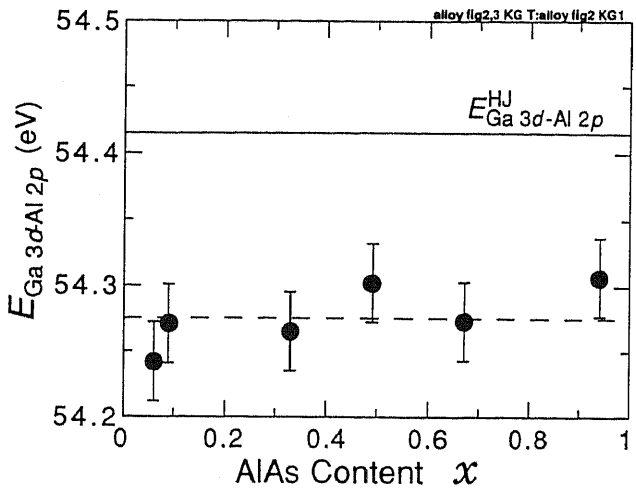

FIG. 3-9. Energy difference between the Ga 3d and Al 2p core levels in $Al_xGa_{1-x}As$ is plotted as a function of the AlAs content x. The solid line shows the value obtained on the GaAs/AlAs heterostructure.

3.4.3 *p-d* repulsion effect

The Ga 3d and Al 2p chemical shifts are due to the 12 x atoms of the second nearest Al atoms which replace Ga atoms. It has been theoretically predicted that shallow d levels such as the Ga 3d level in GaAs interact with the valence p orbital and push the VBM up (p-d repulsion effect).[21,22] We study the energy separation between the Ga 3d level and the Ga 3p level (approximately 100 eV-deeper than VBM) to check the Ga 3d level can be a good marker to study the electronic structure of GaAs by its energy shift from the Ga 3p level, which does not interfere with the valence bands. The energy of Ga 3p level is acquired by a fit using two Gaussian-Lorentzian convolution functions (for $3p\frac{3}{2}$ and $3p\frac{1}{2}$ levels) and evaluated by a weighted average of the spin-orbital split levels. Because of a broadness and a low intensity of the Ga 3p level, the energy difference $E_{Ga\ 3d\text{-}Ga\ 3p}$ has an uncertainty of ~0.03 eV. Figure 3-10 shows $E_{Ga\ 3d\text{-}Ga\ 3p}$ as a function of the AlAs content x. It is clearly shown in Fig.

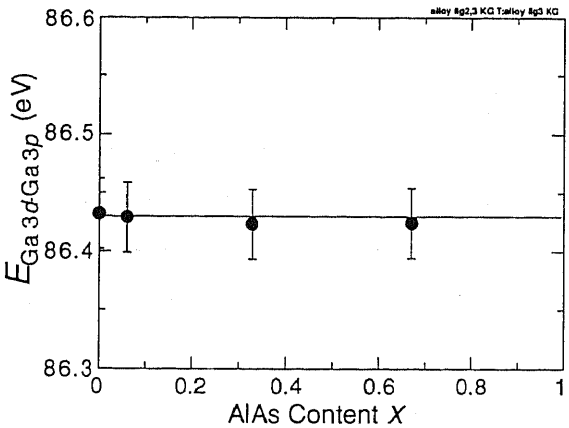

FIG. 3-10. Energy difference between the Ga 3d and Ga 3p core levels in $Al_xGa_{1-x}As$ is plotted as a function of the AlAs content x.

3-10 that $E_{\text{Ga }3d\text{-Ga }3p}$ is independent of x. It is, therefore, justified to consider that the energy shift of the Ga $3d$ level as well as a deeper core level of Ga $3p$ level represents the electrostatic potential shift on the cation site.

3.4.4 Natural energy lineups

The contribution of each second nearest atom to the core level chemical shift is very small and can be considered by the following simple linear model; the shifts of electrostatic potentials at the Ga and Al cores are proportional to the number of the second nearest Al atoms (AlAs content on the average). Then, the Ga $3d$ energy in $Al_xGa_{1-x}As$ $E_{\text{Ga }3d}(x)$, is estimated by;

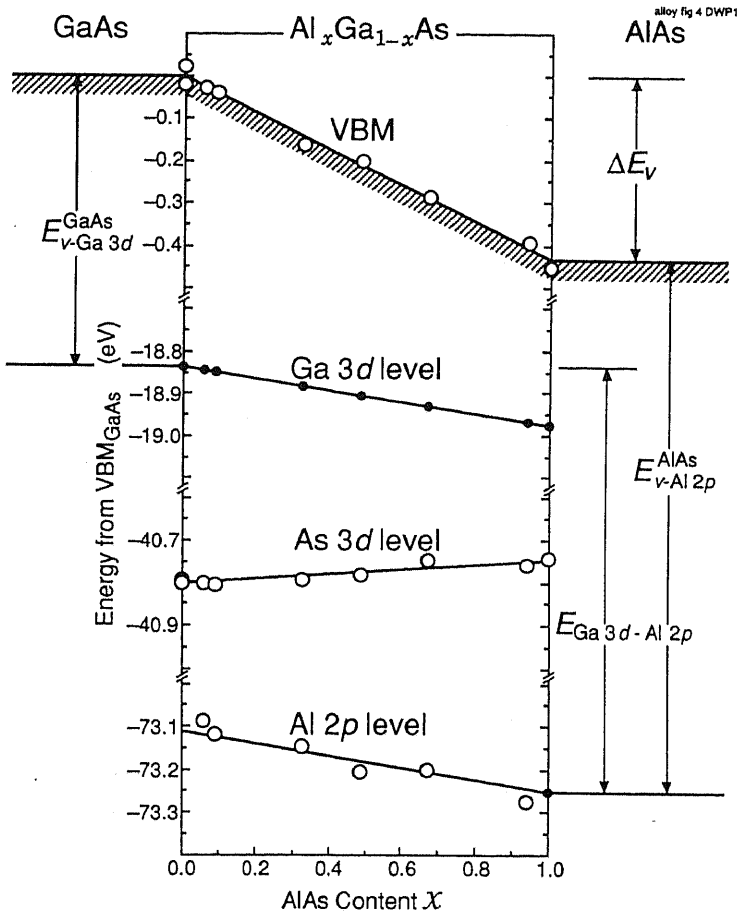

FIG. 3-11. Determined energy lineups of the VBM and core levels (Ga $3d$, As $3d$, and Al $2p$ levels).

$$E_{\text{Ga }3d}(x) = E^{\text{GaAs}}_{\text{Ga }3d} + x\delta E_{\text{Ga }3d}, \qquad (3\text{-}22)$$

Here, $E^{\text{GaAs}}_{\text{Ga }3d}$ denotes the energy of the Ga $3d$ level in GaAs and $\delta E_{\text{Ga }3d}$ (= −140 meV) represents the chemical shift of Ga $3d$ level in $Al_xGa_{1-x}As$ ($x \to 1$). The zero energy is set at the VBM of GaAs.

Since the Ga $3d$ core level is most clearly resolved and is located very near the VBM, we can minimize the experimental uncertainty by using the energy separations from the Ga $3d$ level to the VBM or the core levels of the interest. By using the measured energy differences and Eq. (3-22) for the energy of the Ga $3d$ level, the energy of the VBM and the As $3d$ and Al $2p$ core levels in $Al_xGa_{1-x}As$, $E_{\text{VBM}}(x)$, $E_{\text{As }3d}(x)$, and $E_{\text{Al }2p}(x)$, are, respectively, given by;

$$E_{\text{VBM}}(x) = E_{\text{Ga }3d}(x) + E_{v\text{-Ga }3d}(x), \qquad (3\text{-}23)$$
$$E_{\text{As }3d}(x) = E_{\text{Ga }3d}(x) - E_{\text{Ga }3d\text{-As }3d}(x), \qquad (3\text{-}24)$$
$$E_{\text{Al }2p}(x) = E_{\text{Ga }3d}(x) - E_{\text{Ga }3d\text{-Al }2p}(x). \qquad (3\text{-}25)$$

Here, $E_{\text{v-Ga }3d}(x)$, $E_{\text{Ga }3d\text{-As }3d}(x)$, and $E_{\text{Ga }3d\text{-Al }2p}(x)$ denote the experimental energy difference from the VBM to the Ga $3d$ level and those from the Ga $3d$ level to the As $3d$ and Al $2p$ core levels, respectively. Equations (3-22~25) lead us to show the energy lineups of the VBM and the core levels as plotted in Fig. 3-11. In Fig. 3-11, the energy zero is set at the VBM of GaAs, and the shown energies correspond to the level of interest in an $Al_xGa_{1-x}As$ at a GaAs/$Al_xGa_{1-x}As$ heterojunction measured from the VBM of GaAs. The energy of the VBM linearly shifts by -0.43 ± 0.05 eV when x increases from 0 to 1, indicating that the natural valence band offset (NVBO) at GaAs/AlAs is 0.43 ± 0.05 eV in agreement with the value obtained by measuring the HJs (ΔE_v = 0.44 ± 0.05 eV). It is because we defined the energy line up in this system as to coincide the NVBO with VBO determination by the HJ samples. Eq (2-5) and Eq (3-1) are rewritten as;

$$\Delta E_v = E^{\text{HJ}}_{\text{Ga 3d-Al 2p}} + E^{\text{GaAs}}_{v\text{-Ga }3d} - E^{\text{AlAs}}_{v\text{-Al }2p}. \qquad (3\text{-}26)$$

Here, $E^{\text{GaAs}}_{v\text{-Ga }3d}$ and $E^{\text{AlAs}}_{v\text{-Al }2p}$ denote the energy differences between the VBM and the core levels (Ga $3d$ and Al $2p$) in GaAs and AlAs, respectively. As shown in Fig. 3-11, the definition of the natural energy lineup agrees with Eq. (3-26).

The energy of the As $3d$ level depends on x by only +0.06 eV in contrast to the Ga $3d$ and Al $2p$ core levels which shift by –0.14 eV depending on the AlAs content x, although nearest-neighboring cation atoms are altered for the As atoms.

3.4.5 Discussions

By Al $L_{2,3}$ soft x-ray emission measurement on $Al_xGa_{1-x}As$, Nithianandam and Schnatterly estimated the shift in the energy of VBM, $E_{\text{v-Al }2p}(x)$, measured from the Al $2p$ core level.[64] $E_{\text{v-Al }2p}(x)$ changes gradually by –0.31 eV when x increases from 0 to 1. This value of 0.31 eV is smaller than the GaAs/AlAs VBO (0.44 eV), suggesting that the natural band lineup assuming the constancy of the cation (Al $2p$) core level does not provide a proper value of the HBO in this system. Further, by adding our value of the Al $2p$ core level chemical shifts (–0.14 eV), their value of the shift in $E_{\text{v-Al }2p}(x)$ corresponds to the VBO of 0.45 eV, which agrees quite well with our value of 0.43 eV.

Shih and Spicer proposed a natural energy lineup of the $Hg_xCd_{1-x}Te$, which is obtained by using the cation core level as a reference and predicted a proper value of NVBO in that system.[65] However, our data of chemical shifts in cation core levels show that the constancy of the cation core level is invalid for the $Al_xGa_{1-x}As$ system.

Wei and Zunger estimated the cation chemical shifts at a GaAs/AlAs (100) heterojunction to be 0.04 eV, which corresponds to the 0.12 eV shift in the alloy from GaAs to AlAs, although the sign of the shift (Ga core becomes shallower in the alloy) is opposite to ours.[22] Their value of the As chemical shift (0.42 eV) is much larger than our value of 0.06 eV. A still larger magnitude of the anion chemical shift (0.8 eV) is calculated by Massidda et al.,[13] although their values of the cation chemical shift agree with ours. The reason of the discrepancy for the anion chemical shift is not clear at present.

Akimoto *et al.* estimated that an Al atom loses 0.03 electron in the $Al_xGa_{1-x}As$ by ^{27}Al nuclear magnetic resonance measurements.[66] A simple estimation from the XPS chemical shift shows that the Ga atoms lose and the Al atoms gain the valence electrons, which contradict to the result by Akimoto *et al.* However, the Ga 3*d* level chemical shift $\delta E_{Ga\ 3d}$ is the electrostatic potential energy difference between the Ga atom in GaAs and that in the $Al_xGa_{1-x}As$ ($x \sim 1$). Since the Ga 3*d* chemical shift is the energy difference between a Ga atom in GaAs and another Ga atom in $Al_xGa_{1-x}As$ in a GaAs/$Al_xGa_{1-x}As$ ($x \rightarrow 1$) heterojunction, we must consider the charge distribution at the heterointerface as well as that at the Ga atom. It is, thus, very difficult to show the charge distribution in the $Al_xGa_{1-x}As$ alloy from only the XPS chemical shifts, but it will be clarified by the further theoretical approaches to explain the cation chemical shifts of –0.14 eV and the smaller shift in the As 3*d* level.

3.4.6 Comparison of chemical shifts — alloy and heterointerface —

In order to verify the magnitude of chemical shifts a_1, a_2, and a_3, which were deduced in section 3.3, a comparison is made with chemical shift 0.14 eV found on the alloy.

A chemical shift in alloy, CS_{alloy} (a Ga atom in the $Al_xGa_{1-x}As$ $x \rightarrow 1$ is considered.) is expressed by a_i's as,

$$CS_{alloy} = \sum_{i=-\infty}^{\infty} a_i . \qquad (3\text{-}27)$$

ai's for negative i denote chemical shifts due to the layer below the Ga atom and a_0 denotes the chemical shift due to the other group III atoms located in the same layer. Because there are same number of second nearest group III atoms (4 atoms) and second nearest to one of the second nearest group III atoms (8 atoms) and farther atoms for a_1 and a_0 we can approximate a_0 as,

$$a_0 \sim a_1 . \qquad (3\text{-}28)$$

Since a_{-i} is identical to a_i, CS_{alloy}, is given by

$$CS_{alloy} = \sum_{i=-\infty}^{\infty} a_i = a_0 + 2\sum_{i=1}^{\infty} a_i \sim 3a_1 + 2a_2 + 2a_3 + \ldots. \quad (3\text{-}29)$$

By adding a_i's, *CSalloy* is ,then, calculated from the values of Eqs. (3-11~13) as

$$CS_{alloy} = 135 \pm 30 \text{ meV}. \quad (3\text{-}30)$$

This value agrees with the observed chemical shift in AlGaAs (140 meV). This fact confirms the validity of the interface chemical shifts.

3.5 Conclusions

(1) The valence band offset at GaAs/AlAs interface is determined as:

$$\Delta E_v = 0.44 \pm 0.05 \text{ eV},$$

which depends on neither the interface orientation nor the growth sequence.
This result supports the so called model theories[15-20] to predict HBOs.

(2) By measuring Ga 3*d* and Al 2*p* level energy at the GaAs/AlAs heterointerface, the following features of heterointerface have been found:

(i) Interface chemical shift of Ga 3*d* and Al 2*p* levels are found as
$\delta E_{\text{Ga } 3d}(1) = -\delta E_{\text{Al } 2p}(1) = -57 \pm 20$ meV ,
$\delta E_{\text{Ga } 3d}(2) = -\delta E_{\text{Al } 2p}(2) = -25 \pm 20$ meV ,
and
$\delta E_{\text{Ga } 3d}(3) = -\delta E_{\text{Al } 2p}(3) = -7 \pm 20$ meV .
These values mean that Ga 3*d* (Al 2*p*) level becomes deeper (shallower) in the vicinity of the heterointerface.
(ii) There is a transient in the electronic structure at the interface (no thinner than ~11Å). This result presents us a caution that the atomically abrupt HBOs are not a real picture.

(3) $\Delta E_{\text{Ga } 3d\text{-Al } 2p}$ is 140 meV-smaller for AlGaAs alloy indicating a 140 meV of chemical shift in the alloy.
This value agrees with our experiments on heterostructures and confirms a validity of the measured interface chemical shifts.
Further, by including the above chemical shift, an energy diagram (so called natural energy lineups) for AlGaAs is given as Figure 3-11.

Chapter 4 Strain Effects on InAs/GaAs Heterojunction Band Offsets

Strain effects on the HBOs are studied with XPS measurements on pseudomorphic InAs/GaAs structures and a theoretical consideration for the core level binding-energies to obtain a valence band offset (VBO). For (100) interfaces, two extreme cases are examined; one is an InAs layer pseudomorphically grown on a GaAs (100) substrate (type I) and the other a GaAs layer grown on an InAs (100) substrate (type II). Energy difference between In 4*d* and Ga 3*d* core levels is almost independent of the substrate lattice parameter. However, the VBO deduced by including a splitting of the VBM is very different; 0.53 eV for type I and –0.16 eV for type II. This clearly indicates an effect of strain on the VBO (~0.7 eV) in this system. Further, band lineups are studied for pseudomorphic InAs/GaAs heterostructures grown on (110) and (111)*B* GaAs substrates. Because of non-isotropic stain components, the VBO varies by ~0.15 eV with the crystal orientation.

4.1 Introduction

A strained semiconductor heterostructure such as InGaAs/GaAs is one of the today's highlights because it does not only extend a variety of the materials used for device fabrications but also presents a lot of interesting phenomena in the band structure. It is well known that hole bands (heavy hole, light hole and spin-orbit bands) are mixed and the valence band maximum is split. Strain effects on the band alignments as well as a stability of the structure is the most important issue to have been studied before the strained heterostructure devices gain a lot of uses. Because of this technological interest in conjunction with a physical interest of the band offset formation in the strained system, we have studied the HBOs at strained InAs/GaAs heterostructures. In addition, an InAs/GaAs short period superlattice is also attracting much attention for its possibility to replace a disordered $In_xGa_{1-x}As$ alloy to reduce an alloy scattering effects on electron devices.[67] In spite of its importance,[68] only a few experiments have been done to determine the InAs/GaAs HBOs. A very thin critical thickness for a generation of misfit dislocations (as thin as 2 monolayers (MLs) for this system)[69] is one of the reasons that make it very difficult to determine HBOs accurately.

Kowalczyk *et al.* reported the valence band offset, ΔE_v, at InAs/GaAs to be 0.17 eV from their XPS measurements.[70] However, their measurement was carried out on an InAs/GaAs single heterojunction with a 20 Å-thick InAs layer, which is much thicker than the critical thickness. Hence, the lattice strain is considered to be relaxed in their samples. Therefore, to study the HBOs at InAs/GaAs heterointerfaces including the strain effects, the structural parameters of the specimen must be carefully chosen.

In this work, we studied the HBOs at pseudomorphic InAs/GaAs interfaces by *in situ* XPS measurements with an emphasis on the strain effects. As described in chapter 2, XPS evaluates energy difference between core levels in the heterostructures as well as core level binding-energies of bulk materials. To deduce ΔE_v in this strained system we have taken the following cares.[71]

1) A very thin InAs (GaAs) was deposited on GaAs (InAs) substrates to preserve strain effects on energy alignments of core levels.
2) Core level binding energies for strained InAs and GaAs are determined by XPS measurements and a theoretical consideration.

Further, in order to quantitatively discuss the strain effects, ΔE_v 's were measured by changing the strain configuration as

1) InAs/GaAs heterostructures were grown on GaAs and InAs (100) substrates. By changing the substrate lattice parameter the strain effect on GaAs and InAs layer are separately discussed.
2) The heterostructures are grown on GaAs substrates with different surface orientations.

4.2 Theoretical background

Figure 4-1 shows a schematic energy band diagram at the InAs/GaAs heterointerface. The valence band offset defined by $\Delta E_v \equiv E_v(\text{InAs}) - E_v(\text{GaAs})$ is given by;

$$\Delta E_v = -E^v_{\text{Ga }3d} + E^v_{\text{In }4d} + \Delta E_{\text{In }4d\text{-Ga }3d}. \quad (4\text{-}1)$$

$E^v_{\text{Ga }3d}$, $E^v_{\text{In }4d}$, and also $\Delta E_{\text{In }4d\text{-Ga }3d}$ can be affected by a lattice strain.[72] Let us consider two extreme cases as strained InAs/GaAs heterostructures; one is the case where an

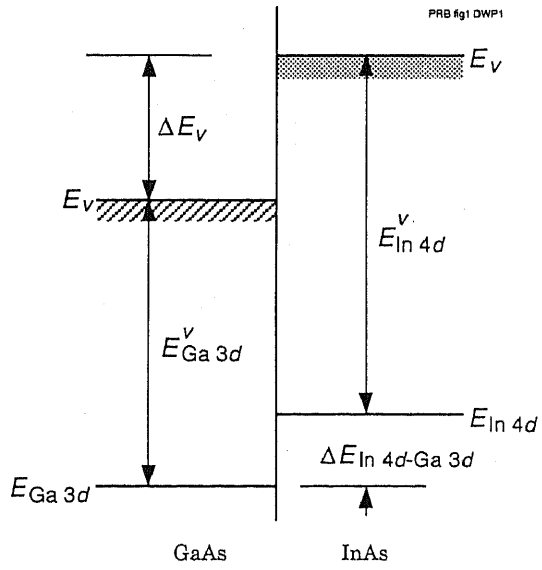

FIG. 4-1. A schematic energy band diagram at an InAs/GaAs hetero-junction.

InAs layer is pseudomorphically grown on a GaAs substrate (InAs strained case; type I), and the other is the case where a GaAs layer is grown on an InAs substrate (GaAs strained case; type II). Then, Eq. (4-1) can be shown as the followings in order to express the strain effects explicitly;

$$\Delta E_v = -E^{vo}_{\mathrm{Ga}\ 3d} + E^{vs}_{\mathrm{In}\ 4d} + \Delta E^{\mathrm{I}}_{\mathrm{In}\ 4d\text{-}\mathrm{Ga}\ 3d} \qquad \text{(type I)}, \qquad (4\text{-}2)$$

$$\Delta E_v = -E^{vs}_{\mathrm{Ga}\ 3d} + E^{vo}_{\mathrm{In}\ 4d} + \Delta E^{\mathrm{II}}_{\mathrm{In}\ 4d\text{-}\mathrm{Ga}\ 3d} \qquad \text{(type II)}. \qquad (4\text{-}3)$$

Here, the superscript s denotes the values for strained layers and o the unstrained bulk values. $\Delta E^{\mathrm{I}}_{\mathrm{In}\ 4d\text{-}\mathrm{Ga}\ 3d}$ and $\Delta E^{\mathrm{II}}_{\mathrm{In}\ 4d\text{-}\mathrm{Ga}\ 3d}$ are determined by XPS measurements on strained heterojunctions. $E^{vo}_{\mathrm{Ga}\ 3d}$ and $E^{vo}_{\mathrm{In}\ 4d}$ can be obtained from XPS spectra on unstrained bulk GaAs and InAs, respectively. However, it is very difficult to determine $E^{vs}_{\mathrm{Ga}\ 3d}$ and $E^{vs}_{\mathrm{In}\ 4d}$ experimentally. Kowalczyk *et al.* replaced $E^{vs}_{\mathrm{Ga}\ 3d}$ and $E^{vs}_{\mathrm{In}\ 4d}$ with the unstrained values. However, this approximation is not always correct. Therefore, in order to determine the HBOs in strained InAs/GaAs systems, we estimated $E^{vs}_{\mathrm{Ga}\ 3d}$ and $E^{vs}_{\mathrm{In}\ 4d}$ by the following theoretical consideration and also by XPS measurements on strained GaAs layers.

The biaxial strain associated with pseudomorphic epitaxy can be decomposed into the hydrostatic part and the uniaxial part. Van de Walle and Martin have theoretically

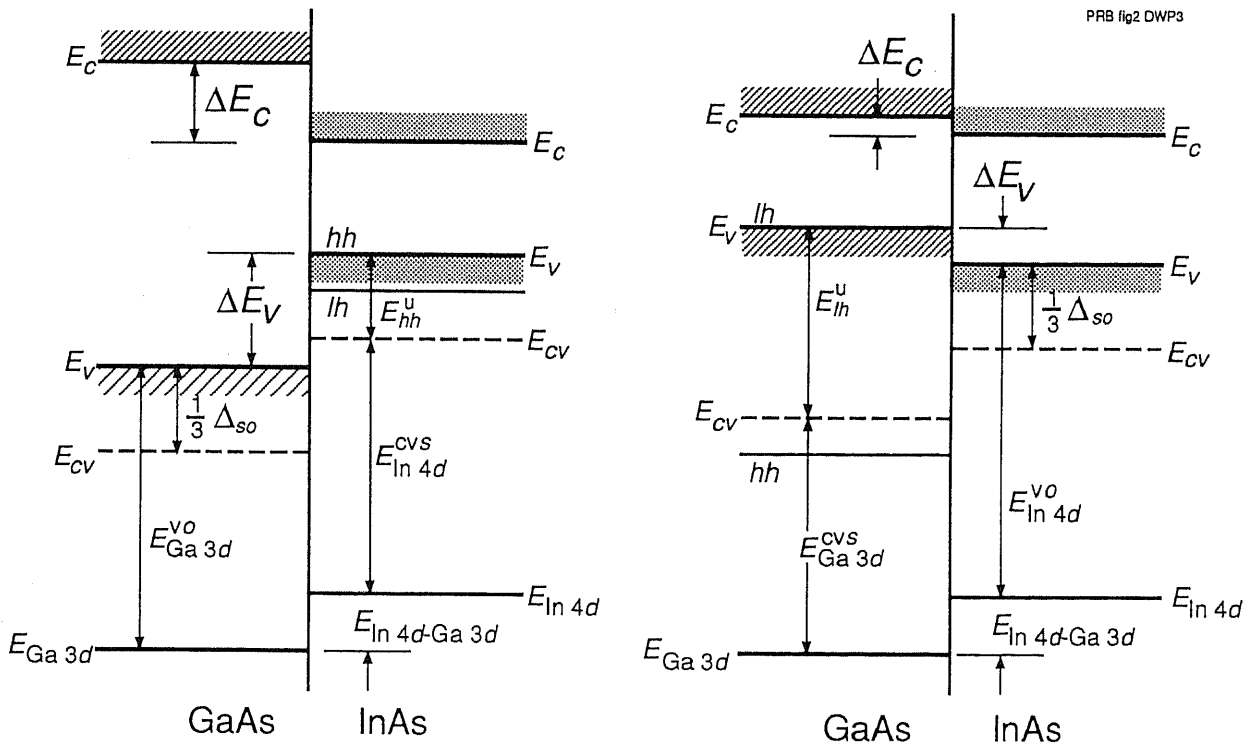

(a) InAs strained (type I)

(b) GaAs strained (type II)

FIG. 4-2. Band lineups at strained type I and type II heterointerfaces.

shown that the energy difference between the centroid of the valence band maximum (CVBM) and the core level is influenced only by the hydrostatic part and that the uniaxial part splits the valence bands around the centroid.[73] By taking into account these strain effects, the energy band diagrams are shown in Fig. 4-2 for type I and II systems.

TABLE IV-I. Material parameters.

Constant	Unit	GaAs	InAs
a_0	Å	5.642	6.058
a	eV	−9.2	−6.0
b	eV	−2.0	−1.8
d	eV	−6.0	
S_{11}	10^{-12} cm^2/dyne	1.172	
S_{12}	10^{-12} cm^2/dyne	−0.365	
S_{44}	10^{-12} cm^2/dyne	1.683	
C_{11}	10^{11} dyne/cm^2	8.329	11.88
C_{12}	10^{11} dyne/cm^2	4.526	5.38
C_{44}	10^{11} dyne/cm^2	3.959	5.98
E_g^o	eV	1.43	0.36
Δ_{so}	eV	0.34	0.38

For a (100) interface, the strain components arising from the pseudomorphic epitaxy are given by;

$$e_{xx} = e_{yy} = \left(\frac{a_{//}}{a_0} - 1\right), \tag{4-4}$$

$$e_{zz} = \left(\frac{a_{\perp}}{a_0} - 1\right), \tag{4-5}$$

where a_0 denotes the bulk lattice parameter, $a_{//}$ and $a_{\perp}$ the strained lattice parameter parallel and normal to the interface, respectively. By using the elastic constants S_{11} and S_{12}, e_{zz} is expressed as;

$$e_{zz} = \frac{2S_{12}}{S_{11}+S_{12}}\left(\frac{a_{//}}{a_0} - 1\right). \tag{4-6}$$

This biaxial strain can be decomposed into the hydrostatic component e_h and uniaxial component e_u as;

$$\begin{pmatrix} e_{xx} & e_{xy} & e_{xz} \\ e_{yx} & e_{yy} & e_{yz} \\ e_{zx} & e_{zy} & e_{zz} \end{pmatrix} = \begin{pmatrix} e_h & 0 & 0 \\ 0 & e_h & 0 \\ 0 & 0 & e_h \end{pmatrix} + \begin{pmatrix} -e_u & 0 & 0 \\ 0 & -e_u & 0 \\ 0 & 0 & 2e_u \end{pmatrix}, \tag{4-7}$$

with

$$e_h = \tfrac{1}{3}(e_{xx} + e_{yy} + e_{zz}) = \frac{2}{3}\frac{S_{11}+2S_{12}}{S_{11}+S_{12}}\left(\frac{a_{//}}{a_0} - 1\right), \tag{4-8}$$

and

$$e_u = \tfrac{1}{2}(e_{zz} - e_h) = e_h - e_{xx} = e_h - e_{yy}. \tag{4-9}$$

The hydrostatic part of strain shifts CVBM relative to the core levels. $E^{cvs}_{\mathrm{In}\,4d}$ and $E^{cvs}_{\mathrm{Ga}\,3d}$ denote the shifted CVBM measured from the In 4*d* core level in strained InAs and that measured from the Ga 3*d* core level in strained GaAs, respectively, which are different from the unstrained bulk values of $E^{cvo}_{\mathrm{In}\,4d}$ for InAs and $E^{cvo}_{\mathrm{Ga}\,3d}$ for GaAs. Furthermore, the uniaxial part of the strain splits the three-fold degenerate VBM into heavy hole (*hh*), light hole (*lh*), and spin-orbit split-off (*so*) bands around the CVBM. The splittings of *hh* and *lh* bands relative to CVBM, E^{u}_{hh} and E^{u}_{lh}, can be estimated by using appropriate deformation potential constants. $E^{vs}_{\mathrm{In}\,4d}$ and $E^{vs}_{\mathrm{Ga}\,3d}$ are, then, obtained by $E^{cvs}_{\mathrm{In}\,4d} + E^{u}_{hh,\,lh}$ and $E^{cvs}_{\mathrm{Ga}\,3d} + E^{u}_{hh,\,lh}$ for *hh* and *lh* bands, respectively.

First, let us evaluate the effects of the hydrostatic part of strain. Because of the core-hole relaxation effect during XPS measurements, the measured binding energy of the core electrons relative to the CVBM, E^{cv}_{CL}, is different from the unperturbed binding energy. This shift (so called "a final state effect") can be treated by using a Born-Haber cycle. Using the tight-binding (TB) theory with universal parameters and also using the Z+1 approximation, the unstrained E^{cvo}_{CL} is given by;[74]

$$E^{cvo}_{CL} = \Delta E_{bond} + E_{cv} + \Delta E_{met} + I_{core}. \tag{4-10}$$

Here, ΔE_{bond} and ΔE_{met} denote the differences in the bond formation energy and the metallization correction between in the initial and final states, respectively. E_{cv} denotes the theoretical CVBM, and I_{core} the core level ionization energy in a free atom.[75] Under the hydrostatic strain with an isotropic strain component of e_h, we can calculate the binding energy of a core electron in the same manner and obtain E^{cvs}_{CL}. Because of the Z+1 approximation and the TB approach, the absolute values of the calculated E^{cvs}_{CL} and E^{cvo}_{CL} have uncertainties, but the calculated strain-induced shifts, $[E^{cvs}_{CL} - E^{cvo}_{CL}]$, are reliable. Therefore, we will use the following approximation;

$$E^{cvs}_{CL} \equiv E^{cvo}_{CL}(expt) + \left[E^{cvs}_{CL}(theor) - E^{cvo}_{CL}(theor)\right], \tag{4-11}$$

with

$$E^{cvo}_{CL}(expt) = E^{vo}_{CL}(expt) - \tfrac{1}{3}\Delta_{so}, \tag{4-12}$$

TABLE IV-II. Energies for strained GaAs and InAs (in eV) calculated by using Eqs. (4-4~16) and material parameters listed in Table IV-I. The subscript *CL* represents the Ga 3*d* or In 4*d* core levels in GaAs or InAs, respectively. To obtain E^{cvs}_{CL} by Eq. (4-5), we used the values of E^{vo}_{CL} measured by XPS, which are shown in TABLE IV-III.

	$E^{cvs}_{CL}(theor) - E^{cvo}_{CL}(theor)$	E^{cvs}_{CL}	E^{u}_{hh}	E^{u}_{lh}	E^{cs}_{cv}
InAs (type I)	0.02	17.25	0.39	0.18	0.90
GaAs (type II)	− 0.11	18.53	− 0.17	0.59	0.86

where (*expt*) and (*theor*) denote the quantities obtained experimentally and theoretically, respectively. Δ_{so} is the spin-orbit splitting energy. By using parameters summarized in Table IV-I, the strain-induced shifts are calculated as listed in Table IV-II.

With the deformation potential constant b,[76] the splittings of the heavy and light hole bands relative to the CVBM, E^u_{hh} and E^u_{lh}, are respectively given by;[77]

$$E^u_{hh} = \tfrac{1}{3}\Delta_{so} - \tfrac{1}{2}\delta E_{001}, \tag{4-13}$$

$$E^u_{lh} = -\tfrac{1}{6}\Delta_{so} + \tfrac{1}{4}\delta E_{001} + \tfrac{1}{2}\left(\Delta^2_{so} + \Delta_{so}\delta E_{001} + \tfrac{9}{4}\delta E^2_{001}\right)^{\frac{1}{2}}, \tag{4-14}$$

with

$$\delta E_{001} = 2b\left(\frac{a_\perp}{a_0} - \frac{a_{//}}{a_0}\right). \tag{4-15}$$

Here, a_0 denotes the bulk lattice parameter, $a_\perp$ and $a_{//}$ the strained lattice parameter parallel and normal to the growth direction, respectively. In uniaxially expanded (biaxially compressed) InAs the VBM is the heavy hole band, while in uniaxially compressed (biaxially expanded) GaAs it is the light hole band.

The conduction band relative to the CVBM, E^{cs}_{cv}, can be calculated by using the hydrostatic deformation potential constant a, as the following;

$$E^{cs}_{cv} = E^o_g + \tfrac{1}{3}\Delta_{so} + a\left(\frac{a^2_{//}a_\perp}{3} - 1\right). \tag{4-16}$$

Here, E^o_g denotes the direct band gap for unstrained bulk material. These values are also tabulated in Table IV-II.

4.3 Samples and XPS measurements

4.3.1 Core level energy distance

All the samples were grown by MBE and XPS measurements were performed on them immediately after the growth. In order to investigate the strain effects on HBOs, two types of heterostructures (HS's) were prepared; i. e., an InAs layer grown on a GaAs (100) substrate (type I HS) and a GaAs layer grown on an InAs (100) substrate (type II HS). To avoid the generation of misfit dislocations, the thickness of the heterojunction overlayers was only 2 MLs. However, the XPS signals from such thin overlayers are strongly affected by the surface and interface chemical shifts. To minimize this ambiguity, thin overlayers were grown to cap the strained thin layers; i. e., 5 ML-thick GaAs layers for type I structures and 5 ML-thick InAs layers for type II structures.

Thus, the samples measured in these experiments are double heterostructures; i. e., GaAs/InAs/GaAs structures (type I HS) and reversed InAs/GaAs/InAs structures (type II HS).

Although the electronic structure of 2 ML-thick InAs is much different from bulk InAs, in these experiments we concentrate on an energy alignment of In 4*d* and Ga 3*d* core levels without introducing a lattice relaxation. For type I HS, a 1μm-thick Si-doped GaAs buffer layer, a 2 ML-thick undoped InAs strained interlayer, and a 5 ML-thick GaAs capping layer were successively grown on a Si-doped GaAs (100) substrate. For type II HS, a 1μm-thick undoped InAs buffer, a 2 ML-thick undoped GaAs interlayer, and a 5 ML-thick undoped InAs capping layer were grown on an undoped n-type InAs (100) substrate.

Clean mirror surfaces were obtained at substrate temperatures around 450°C under As-rich condition. For the growth of InAs, especially, a high As overpressure is necessary. In this case the flux ratio was As_4/In ~10. The RHEED patterns were photographically recorded to ensure

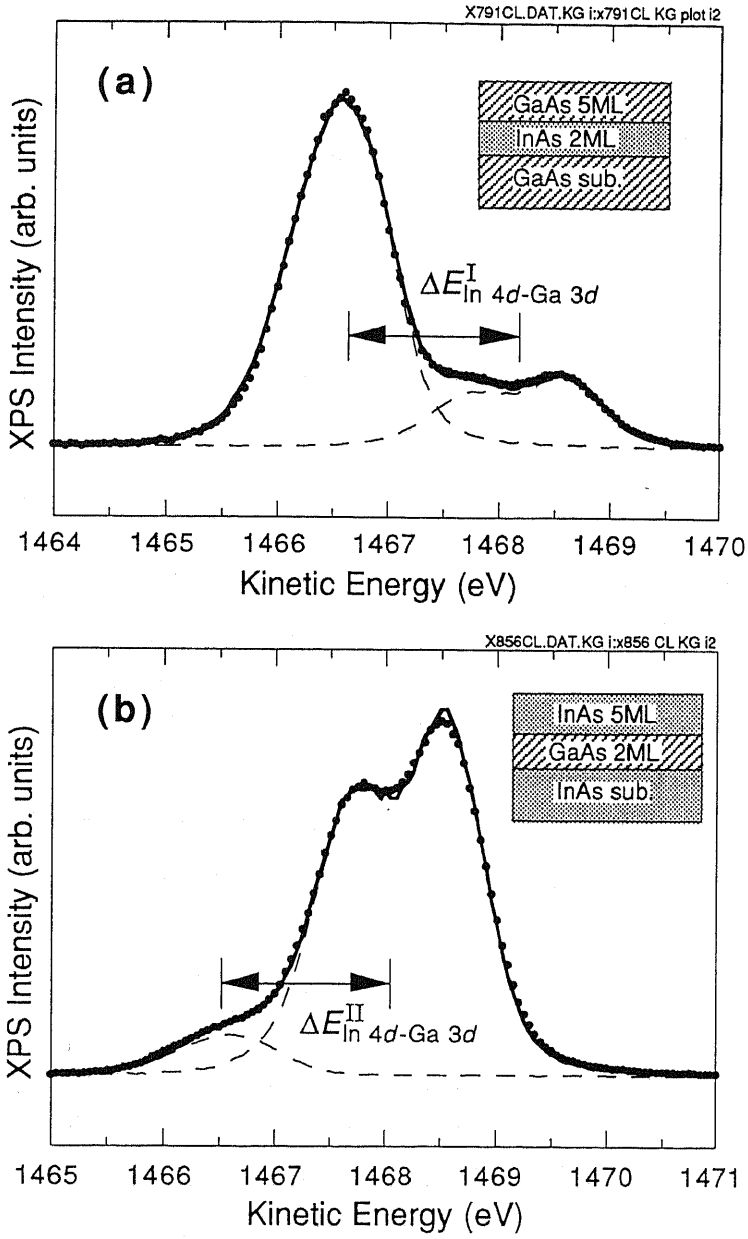

FIG. 4-3. Typical XPS spectra taken from (a) type I and (b) type II samples. The backgrounds are subtracted as described in the text. The dots are the XPS data and the solid lines are fitting curves by using the Ga 3*d* and In 4*d* core level spectra (broken lines) which are obtained from XPS measurements on respective bulk materials. The insets show the sample structures.

that the lattice relaxation did not occur in these samples.

TABLE IV-III. Measured energy differences.

Sample	energy	value (eV)
InAs/GaAs (type I)	$\Delta E^{I}_{In\ 4d\text{-}Ga\ 3d}$	1.647
		1.626
		1.647
	av.	**1.64 ± 0.02**
GaAs/InAs (type II)	$\Delta E^{II}_{In\ 4d\text{-}Ga\ 3d}$	1.585
		1.616
		1.608
	av.	**1.60 ± 0.02**
bulk GaAs	$E^{vo}_{Ga\ 3d}$	**18.75 ± 0.05**
bulk InAs	$E^{vo}_{In\ 4d}$	**17.36 ± 0.05**

First, $E^{vo}_{Ga\ 3d}$ and $E^{vo}_{In\ 4d}$ were measured on MBE-grown unstrained bulk GaAs and InAs samples, respectively. In the XPS spectra the background intensity which is proportional to the integrated peak intensity was subtracted from each core level spectrum. Here, we simply define the peak position of each core level as the midpoint of the two energies at which the intensity is half of the maximum intensity. As shown in section 2.4.1, to determine the energy position of VBM, E_v, the theoretical densities of states[78] for GaAs and InAs broadened by the instrumental lineshape were fit to the XPS spectra around VBM. The obtained values of $E^{vo}_{Ga\ 3d}$ and $E^{vo}_{In\ 4d}$ are tabulated in Table IV-III.

The XPS spectra were, then, taken on type I and II HS's to determine $\Delta E^{I}_{In\ 4d\text{-}Ga\ 3d}$ and $\Delta E^{II}_{In\ 4d\text{-}Ga\ 3d}$. Typical XPS spectra are shown in Fig. 4-3. We made three independent experiments for each type of structures to assure the accuracy. The least squares fitting by the Ga 3*d* and In 4*d* core level spectra taken on bulk GaAs and InAs samples, respectively, was used to separate the two closely spaced core levels.[79] The $\Delta E_{In\ 4d\text{-}Ga\ 3d}$'s thus determined were 1.64 ± 0.02 eV and 1.60 ± 0.02 eV for type I and II samples, respectively. This result shows that $\Delta E_{In\ 4d\text{-}Ga\ 3d}$ only slightly depends on the in-plane lattice constant.

4.3.2 Strain induced shift in the core level binding energy

In order to check the accuracy of the theoretical prediction of the core level binding energy measured from the VBM, $E^{cvs}_{CL} - E^{cvo}_{CL}$, the strain induced shift in the Ga 3*d* level binding energy in GaAs was systematically measured as a function of the in-plane lattice constants $a_{//}$.[80] A 1 μm thick $In_xGa_{1-x}As$ buffer layer (x = 0 ~ 0.37) and a 50 Å thick GaAs probing layer were successively grown on an n^+-GaAs substrate by MBE and *in situ* XPS measurements were performed. The lattice constant in the $In_xGa_{1-x}As$, which is considered to be the same as the in-plane lattice constant in the strained GaAs overlayer unless the lattice relaxation occurs in the overlayer, is determined by using the x-ray diffraction spectrum. The 50 Å-thick GaAs overlayer is enough thicker than the photoelectron escape depth (~ 25 Å) and dominates the XPS

signal from these samples. The energy positions of Ga 3*d* level and VBM are determined by comparing the strained XPS spectrum with that of unstrained GaAs.

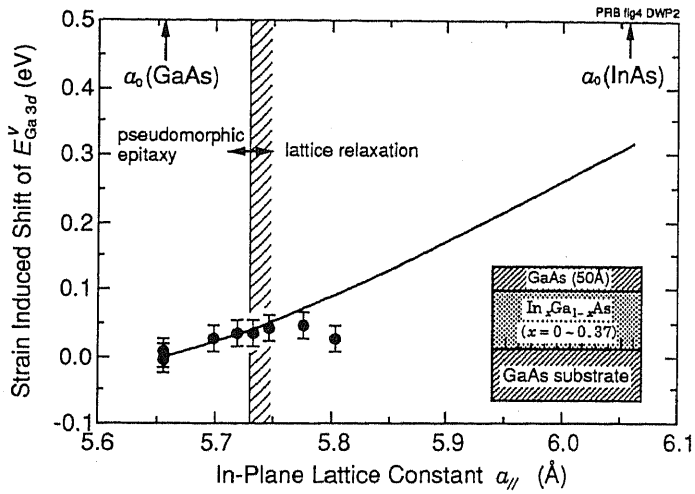

FIG. 4-4. Shift in the Ga 3*d* core level binding energy measured from the VBM plotted as a function of the in-plane lattice constant, $a_{//}$. The inset shows a sample structure.

In Fig. 4-4, the shift in the Ga 3*d* core level binding energy is plotted as a function of the in-plane lattice constant $a_{//}$. The binding energy increases gradually by approximately 50 meV when $a_{//}$ increases from 5.65 Å (GaAs) to ~5.75 Å, clearly indicating the strain induced shift in that energy. The solid curve in Fig. 4-4 shows the theoretical estimation obtained by substituting the respective $a_{//}$ into Eqs. (4-11~15). This agrees well with experiment while $a_{//} < 5.73$ Å. Although with larger $a_{//}$ the experimental strain shift is lower than the theoretical prediction, the critical thickness for the generation of misfit dislocations is lower than the overlayer thickness and the most lattice strain in the overlayer is considered to be relaxed. This experiment strongly supports the validity of the theoretical prediction by Eqs. (4-11~15) in order to predict the strain effect at InAs/GaAs heterojunctions.

4.4 Derivation of band offsets and discussions

$E^{cvs}_{In\ 4d}$ and $E^{cvs}_{Ga\ 3d}$ are obtained by substituting into Eqs. (4-11,12) the calculated energy shifts $[E^{cvs}_{CL}(theor) - E^{cvo}_{CL}(theor)]$ and the measured values of $E^{vo}_{In\ 4d}$ and $E^{vo}_{Ga\ 3d}$. Then, by combining these values with $\Delta E^{I}_{In\ 4d\text{-}Ga\ 3d}$ and $\Delta E^{II}_{In\ 4d\text{-}Ga\ 3d}$, the offsets of the CVBM, ΔE_{cv} [$\equiv E_{cv}$(InAs) – E_{cv}(GaAs)], are obtained as;

$$\Delta E_{cv} = -E^{cvo}_{Ga\ 3d} + E^{cvs}_{In\ 4d} + \Delta E^{I}_{In\ 4d\text{-}Ga\ 3d} \quad \text{(type I)}, \tag{4-17}$$

$$\Delta E_{cv} = -E^{cvs}_{Ga\ 3d} + E^{cvo}_{In\ 4d} + \Delta E^{II}_{In\ 4d\text{-}Ga\ 3d} \quad \text{(type II)}. \tag{4-18}$$

The determined ΔE_{cv}'s are 0.25 eV and 0.30 eV for type I and II HS's, respectively. Furthermore, by taking into account the effect of the uniaxial strain as described in section 4.2, the energy band diagrams are determined as shown in Fig. 4-5. A ΔE_v of 0.53 eV and a conduction band offset, ΔE_c [$\equiv E_c$(InAs) – E_c(GaAs)], of –0.38 eV are obtained for the type I structure. In this case, both *hh* and *lh* bands in InAs are above the VBM in GaAs. The VBM in the strained InAs is *hh* band. In contrast, a charac-

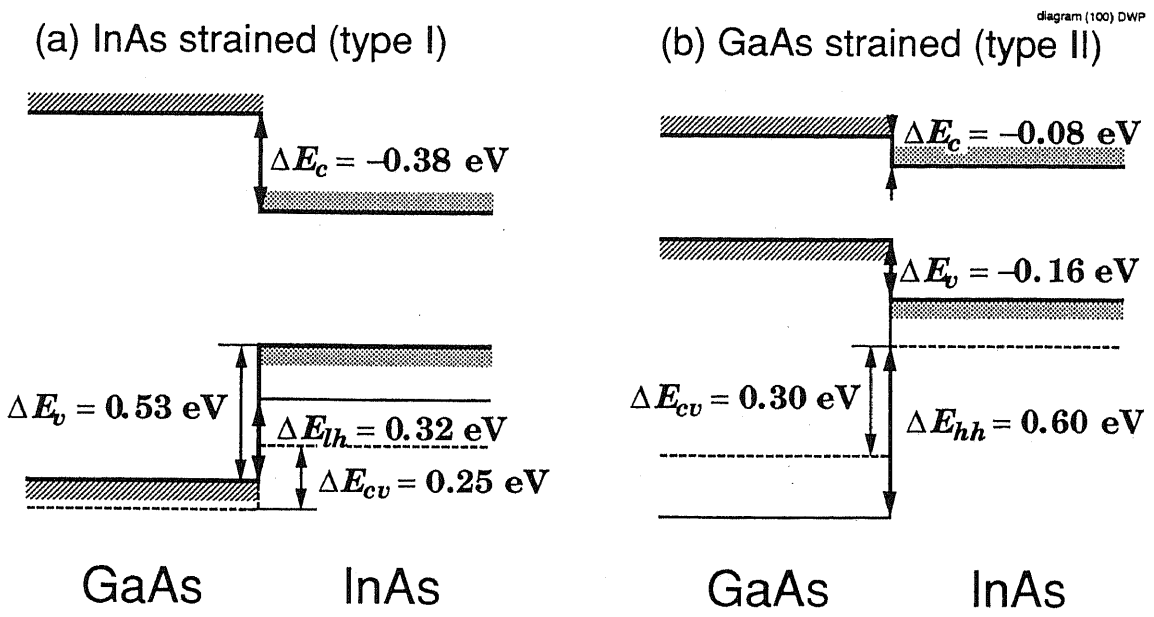

FIG. 4-5. Determined energy band diagrams for type I and type II InAs/GaAs heterostructures.

teristic band alignment is expected for the type II structure, where *lh* (*hh*) band in the strained GaAs layer is higher (lower) than VBM in the InAs by 0.16 eV (0.60 eV) and the conduction band offset is 0.08 eV.

Table IV-IV shows our results with recent reported experimental and theoretical values. First, let us compare our result with experimental values reported for type I structures. Kowalczyk *et al.* reported ΔE_v of 0.17 eV determined by XPS measurements on an InAs/GaAs single heterojunction. The discrepancy between their result and ours is considered to be due to the lattice relaxation in their sample, since the

TABLE IV-IV. A comparison of determined valence band offsets at InAs/GaAs heterointerfaces (in eV).

	ΔE_{cv}		ΔE_v	
	type I	type II	type I	type II
This work (XPS)	**0.25**	**0.30**	**0.53**	**−0.16**
Core level XPS[a]			0.17	
Light-scattering[b]	0.49 ± 0.1			
DME theory[c]	0.18		0.52	
Tight binding[d]	0.09	0.19	0.47	−0.34
Pseudopotential[e]	0.02	0.01	0.31	−0.49

[a] S. P. Kowalczyk et al., J. Vac. Sci. Technol. **20**, 705 (1982).
[b] J. Menéndez et al., Phys. Rev. B **36**, 8165 (1987).
[c] M. Cardona and N. E. Christensen, Phys. Rev. B **35**, 6182 (1987).
[d] C. Priester et al., Phys. Rev. B **38**, 9870 (1988).
[e] A. Taguchi and T. Ohno, Phys. Rev. B **39**, 7803 (1989).

InAs layer in their sample is much thicker than the critical thickness for dislocation generation. On the other hand, Menéndez *et al.* predicted much larger band offset (ΔE_{cv} = 0.49 ± 0.1 eV) by extrapolating the value obtained by light-scattering experiments on $In_{0.05}Ga_{0.95}As$/GaAs quantum wells.[81] This is still larger than our results. Although the origin of this discrepancy is not clear at present, such a simple extrapolation procedure might exaggerate the strain effects.

Second, our results are compared with theoretical values. Cardona and Christensen predicted ΔE_{cv} = 0.18 eV and ΔE_v = 0.52 eV for type I from their dielectric midgap energy (DME) theory,[82] which is in good agreement with ours (ΔE_{cv} = 0.25 eV and ΔE_v =0.53 eV). On the other hand, Priester *et al.* theoretically predicted ΔE_{cv} to be 0.09 eV for type I and 0.19 eV for type II by self-consistent tight binding calculations,[83] and Taguchi and Ohno obtained ΔE_{cv} = 0.02 eV for type I and 0.01 eV for type II by ab-initio self-consistent pseudopotential method.[84] Our values of ΔE_{cv}'s (0.25 eV for type I and 0.30 eV for type II) as well as ΔE_v's are much larger than these theoretical predictions, calling for further refinement in the theories.

4.5 Orientation dependence of InAs/GaAs HBOs

The uniaxial part of the stain introduces the most significant change in the valence band offset. The VBO can be, then, changed by a crystal orientation of the substrate. This section shows an analysis on strain effects on HBOs at InAs/GaAs structures grown on (110)- and (111)-oriented GaAs substrates in order to check the orientation dependence.

4.5.1 A (110) interface

First, by decomposing the strain arising from the lattice mismatch to calculate the isotropic and non-isotropic strain effects, which is not *uni*axial in this case. On a (110) plane, two stresses, $\mathbf{X}_{110}$ along [110] axis and $\mathbf{X}_{001}$ along [001] axis as shown in Fig. 4-6, should be considered, because [110] and [001] axes, which are in the $(\bar{1}10)$ plane, are not equal. Then, the strain components are shown by

$$e_{xx} = e_{yy} = S_{12}X_{001} + \tfrac{1}{2}(S_{11} + S_{12})X_{110}, \quad (4\text{-}19)$$

$$e_{zz} = S_{11}X_{001} + S_{12}X_{110}, \quad (4\text{-}20)$$

and

$$e_{xy} = \tfrac{1}{4}S_{44}X_{110}. \quad (4\text{-}21)$$

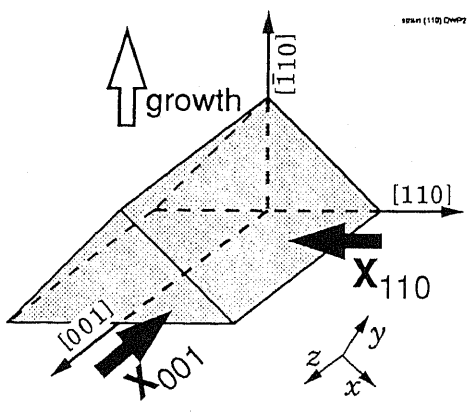

FIG. 4-6. Stress components of heterostructure grown on a (110) surface.

A changes in an in-plane lattice constant $a_{//}$ and that in a vertical lattice constants $a_{\perp}$ are shown by those strain components as

$$\frac{a_{//}}{a_0} - 1 = e_{xx} + e_{yx} = e_{zz}, \tag{4-22}$$

and

$$\frac{a_{\perp}}{a_0} - 1 = e_{yy} - e_{yx}. \tag{4-23}$$

By solving Eqs. (4-19~23), X_{110} and X_{001} are shown by using $a_{//}$ and $a_{\perp}$ as

$$X_{110} = \frac{2(S_{11} - S_{12})}{S_{11}^2 + S_{11}S_{12} - 2S_{12}^2 + \frac{1}{2}S_{11}S_{44}} \left(\frac{a_{//}}{a_0} - 1 \right), \tag{4-24}$$

and

$$X_{001} = \frac{1}{S_{12}} \left[\left(\frac{a_{//}}{a_0} - 1 \right) - S_{12}X_{110} \right]. \tag{4-25}$$

Then, a change in volume from its unstrained value, $\Delta V/V$, is given by

$$\Delta V/V \sim 2\left(\frac{a_{//}}{a_0} - 1 \right) + \left(\frac{a_{\perp}}{a_0} - 1 \right) = (2 - D_{110}) \left(\frac{a_{//}}{a_0} - 1 \right), \tag{4-26}$$

with

$$D_{110} = -1 + \frac{S_{44}(S_{11} - S_{12})}{S_{11}^2 + S_{11}S_{12} - 2S_{12}^2 + \frac{1}{2}S_{11}S_{44}}. \tag{4-27}$$

A change in the bond length d is approximately given by using $\Delta V/V$ as

$$d \propto V^{1/3}. \tag{4-28}$$

By substituting d into Eq. (4-10), an isotropic strain effect $E^{cvs}_{\text{In }4d} - E^{cvo}_{\text{In }4d}$ is obtained in the same manner as Eq. (4-11). This value, only 0.03 eV to raise the VBM, is included in Table IV-V.

The effect of the non-hydrostatic part of the strain is calcu-

TABLE IV-V. Orientation dependence of measured and calculated values at InAs/GaAs structures grown on various GaAs substrates.

Orientation	(100)	(110)	(111)*B*
$\Delta E_{\text{In }4d\text{-Ga }3d}$ (eV)	1.647	1.575	1.660
	1.626	1.609	1.665
	1.647	—	—
av.	**1.64±0.02**	**1.59±0.03**	**1.66±0.02**
$E^{cvo}_{\text{Ga }3d}$ (eV)		18.64 ± 0.05	
$E^{cvo}_{\text{In }4d}$ (eV)		17.23 ± 0.05	
a_0 (InAs) (Å)		6.058	
$a_{//}$ (InAs) (Å)		5.643	
$a_{\perp}$ (InAs) (Å)	6.510	6.338	6.323
$\Delta V/V$	−0.063	−0.091	−0.094
$E^{cvs}_{\text{In }4d} - E^{cvo}_{\text{In }4d}$ (eV)	+0.02	+0.03	+0.03
δE^{u}_{hh} (eV)	0.39	0.36	0.23
δE^{u}_{lh} (eV)	0.18	0.16	0.09
ΔE_{cv} (eV)	0.25	0.21	0.28
δE^{cs}_{cv} (eV)	0.90	1.05	1.05
ΔE_c (eV)	**−0.38**	**−0.27**	**−0.20**
ΔE_{hh} (eV)	0.53	0.46	0.40
ΔE_{lh} (eV)	0.32	0.26	0.26
ΔE_v (eV)	**0.53**	**0.46**	**0.40**

lated by the second order perturbation theory as reported by Pollak and Cardona.[85] The strain Hamiltonian for this system is given by

$$H = \tfrac{1}{4}\delta E_{001}\left[3\left(\tilde{L}_x\right)^2 - \mathbf{L}^2\right] - \tfrac{3}{4}\delta E_{111}\left[3\left(\tilde{L}_z\right)^2 - \left(\tilde{L}_y\right)^2\right], \tag{4-29}$$

with

$$\delta E_{001} = -4b(S_{11} - S_{12})\left(X_{001} - \tfrac{1}{2}X_{110}\right), \tag{4-30}$$

$$\delta E_{111} = \frac{d}{\sqrt{3}} S_{44} X_{110}. \tag{4-31}$$

Here, $\mathbf{L}$ denotes an angular momentum operator and $\tilde{L}_x$ etc. are components of $\mathbf{L}$ after a rotation transformation. Then, the VBM for *hh* and *lh* bands measured from CVBM are acquired as

$$E^u_{hh} = \tfrac{1}{3}\Delta_{so} - \tfrac{1}{4}\left(\delta E^2_{001} + 3\delta E^2_{111}\right)^{1/2} + \tfrac{3}{32}\left(\delta E_{001} - \delta E_{111}\right)^2 / \Delta_{so} + \ldots, \tag{4-32}$$

$$E^u_{lh} = \tfrac{1}{3}\Delta_{so} + \tfrac{1}{4}\left(\delta E^2_{001} + 3\delta E^2_{111}\right)^{1/2} + \tfrac{1}{4}\left(\delta E_{001} + 3\delta E_{111}\right)^2 / \Delta_{so} + \ldots. \tag{4-33}$$

Obtained values of E^u_{hh} and E^u_{lh}, which are more significant than the hydrostatic strain effect, are also shown in Table IV-V. From $a_{//}$ and $a_{\perp}$ the band gap of strained InAs E^{cs}_{cv} is also calculated as listed in Table IV-V.

XPS measurements of $\Delta E_{\text{In } 4d\text{-Ga } 3d}$ were carried out on GaAs (7 ^{110}ML)/InAs (2 ^{110}ML)/GaAs structures. One ^{110}ML, which indicates a thickness of one monolayer coverage on a (110) plane, is smaller than that on a (100) plane by a factor of $1/\sqrt{2}$. An InAs buffer layer, a GaAs buffer layer, 2 ^{110}ML-thick InAs layer and a capping GaAs layer were successively grown on (110)-oriented *n*-type GaAs substrates at the same growth condition as used for the growth of an AlAs/GaAs (110) structure. $\Delta E_{\text{In } 4d\text{-Ga } 3d}$ is evaluated from two experiments to be 1.59±0.03 eV, which is almost the same as the value measured on the (100) interface. By combining this value with calculated ones, the band offsets are given as listed in Table IV-V. Mostly because of a difference in the non-hydrostatic strain components, the VBO becomes

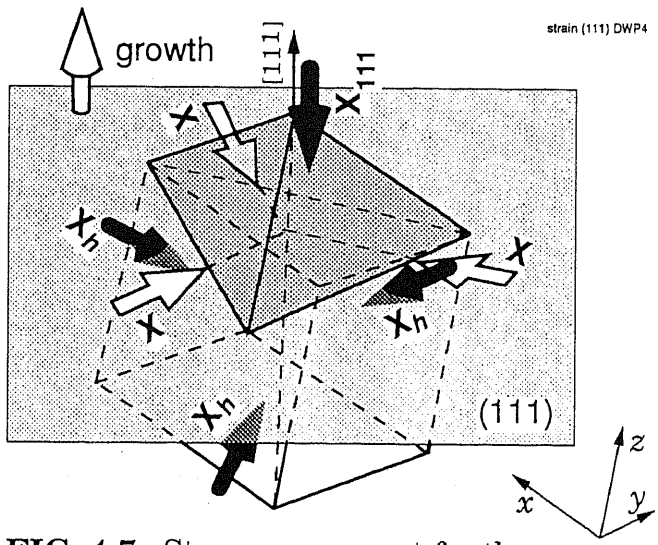

FIG. 4-7. Stress component for the strained InAs layer at a heterostructure grown on (111) surface. Stress can be divided into three **X**'s in the (111) plane or $\mathbf{X}_h$'s (hydrostatic part) + $\mathbf{X}_{111}$ (uniaxial part).

smaller than that for a (100) interface.

4.5.2 A (111) interface

For a (111) heterostructure grown on GaAs substrate, an InAs layer is compressed in the (111) plane. From a symmetry, the stress can be divided into three components parallel to $(\bar{1}01)$, $(01\bar{1})$, and $(1\bar{1}0)$ directions which have the same magnitude X as shown in Fig. 4-7. Then, X is given by

$$X = \left(\frac{a_{//}}{a_0} - 1\right) \Big/ \left(S_{11} + 2S_{12} + \tfrac{1}{4}S_{44}\right). \tag{4-34}$$

A deformation along the [111] growth axis is given by

$$\frac{a_{\perp}}{a_0} - 1 = \left(S_{11} + 2S_{12} - \tfrac{1}{2}S_{44}\right)X. \tag{4-35}$$

Then, a change in volume is obtained by

$$\Delta V/V \sim (2 - D_{111})\left(\frac{a_{//}}{a_0} - 1\right), \tag{4-36}$$

with

$$D_{111} \equiv -\left(\frac{a_{\perp}}{a_0} - 1\right) \Big/ \left(\frac{a_{//}}{a_0} - 1\right) = -\frac{S_{11} + 2S_{12} - \frac{1}{2}S_{44}}{S_{11} + 2S_{12} + \frac{1}{4}S_{44}} = 2\frac{C_{11} + 2C_{12} - 2C_{44}}{C_{11} + 2C_{12} + 4C_{44}}. \tag{4-37}$$

The hydrostatic strain effect is calculated by using Eq. (4-4~6, 28, 36, 37) to be 0.03 eV to raise the VBM in InAs.

In order to calculate effects of uniaxial strain component, rewrite the strain component by using uniaxial and hydrostatic strain components, X_{111} and X_h defined by

$$e_{xx} = e_{yy} = e_{zz} = (S_{11} + 2S_{12})X_h + \tfrac{1}{3}(S_{11} + 2S_{12})X_{111}, \tag{4-38}$$

$$e_{yx} = \tfrac{1}{6}S_{44}X_{111}, \tag{4-39}$$

as

$$X_{111} = -\tfrac{3}{2}X, \tag{4-40}$$

$$X_h = \tfrac{3}{2}X. \tag{4-41}$$

By substituting this X_{111} into a formula for a strain parallel to (111), strain induced shifts in the hh and lh bands are given by[86]

$$E^u_{hh} = \tfrac{1}{3}\Delta_{so} - \tfrac{1}{2}\delta E_{111}, \tag{4-42}$$

$$E^u_{lh} = \tfrac{1}{3}\Delta_{so} + \tfrac{1}{2}\delta E_{111} + \tfrac{1}{2}(\delta E_{111})^2 / \Delta_{so}, \tag{4-43}$$

with

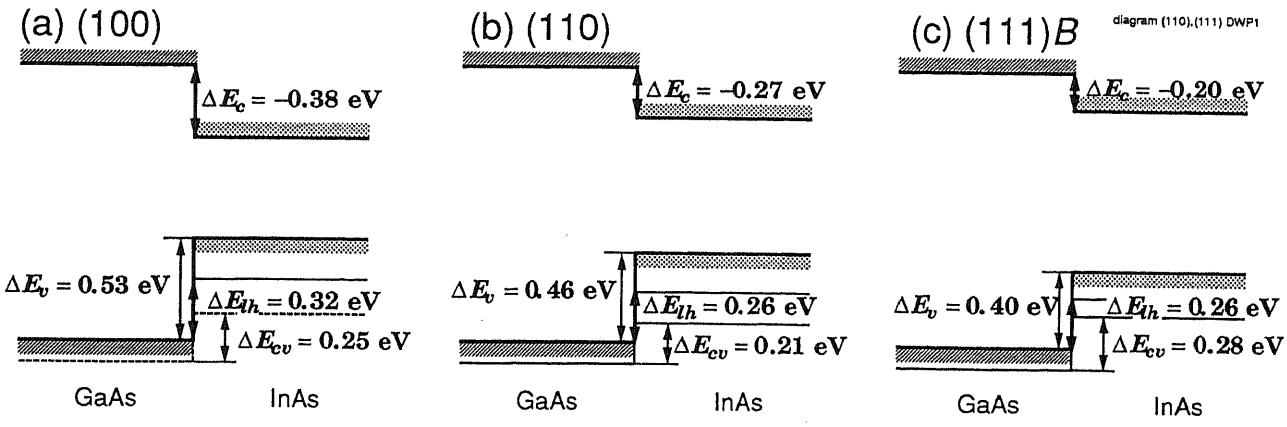

FIG. 4-8. Energy band diagrams for InAs/GaAs heterojunctions grown on (100)-, (110)-, and (111)*B*-oriented GaAs substrates.

$$\delta E_{111} = \frac{d}{\sqrt{3}} S_{44} X_{111}. \tag{4-44}$$

All of the results on the (111) interface are summarized in Fig. 4-8. It is found that the (111) axis is more symmetric than (100) and (110) to make smaller the split of VBMs.

XPS measurements on GaAs/InAs (2 ^{111}ML)/GaAs structures were performed to determine the energy difference $\Delta E_{\text{In } 4d\text{-Ga } 3d}$. Here, one ^{111}ML (=^{100}ML $\times 2/\sqrt{3}$) shows one monolayer thickness on the (111) plane. By two experiments as listed in Table IV-V, it is determined to be 1.66±0.02 eV, which is slightly larger than (100) and (110) interfaces. Then, the VBO is determined as listed in Table IV-V. Figure 4-6 summarizes the determined VBOs for InAs/GaAs structures grown on (100)-, (110)-, and (111)*B*-oriented GaAs substrates. It is found for a (111)*B* interface the VBO is smaller than that on a (100) interface by 0.15 eV.

4.6 Conclusions

$\Delta E_{\text{In } 4d\text{-Ga } 3d}$ in InAs/GaAs heterostructures measured by XPS only slightly depends on the in-plane lattice constant. By taking into account the strain-induced shifts in the core level binding energies relative to VBM, the offset of the centroid of VBM, ΔE_{cv}, is determined to be 0.25 eV for type I (InAs strained case) and 0.30 eV for type II (GaAs strained case).

By adding the effects of the uniaxial part of strain, the valence band offset ΔE_v is determined to be 0.53 eV for type I and −0.16 eV for type II, demonstrating an effect of strain on the band lineups.

Unlike the lattice matched systems, HBOs for a strained InAs/ GaAs system depends

on its orientation; i.e. the VBO is smaller by 0.15 eV for a (111) interface than that for a (100) interface.

Chapter 5 Can We Control Heterojunction Band Offsets?

In order to realize a control of heterojunction band offsets, an energy band diagram at a GaAs/Si/AlAs heterostructure has been studied. A main role of the Si layer is not a control of a valence band offset as proposed by Sorba *et al.* [Phys. Rev. B **43**, 2450 (1991)], but an introduction of band bending in an over-grown layer. To achieve a modification of the true VBO, a precise control of Si occupation site is necessary. Our experiment using a thin *p*-type Si-doped layer and a Si δ-doping of a heterointerface, however, shows a possibility of a true control of a valence band offset at a GaAs/AlAs heterointerface.

5.1 Introduction

A lot of works have been devoted to realize a control of heterojunction band offset because of its technological importance. As described in the previous chapter, the band offset at an isovalent heterostructure such as GaAs/Al(Ga)As is a constant VBO determined by their bulk properties. A VBO can, however, be controlled by using a heterovalency of an interface or by *p*- and *n*-type doped layers which forms an interface dipole as shown in Fig 5-1 (c). Cappasso *et al.* proposed a doping interface dipole, which consists of donor and acceptor layers near a heterointerface.[87] This technique, however, cannot form an abrupt offset at the junction because it needs ~100Å thick *n*- and *p*-type doped layers. Another idea is a usage of a heterovalency of interfaces. At a heterovalent interface such as CdS/Ge[88] and SiO_2/Si,[89] a thin insertion layer may modify a VBO. In these systems, an interface dipole formed by an insertion layer plays a key role. This idea, a manipulation of an interface dipole, can also be applied to more commonly used heterointerfaces such as GaAs/AlAs. Harrison *et al.* showed that a heterovalency of an interface varies an interface dipole at a GaAs/Ge interface to change a valence band offset (VBO).[5] Then, what would happen when an ultrathin

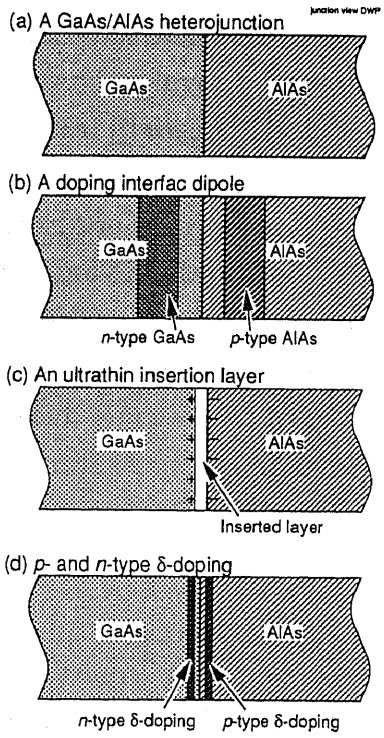

FIG. 5-1. Ideas proposed to control HBO.

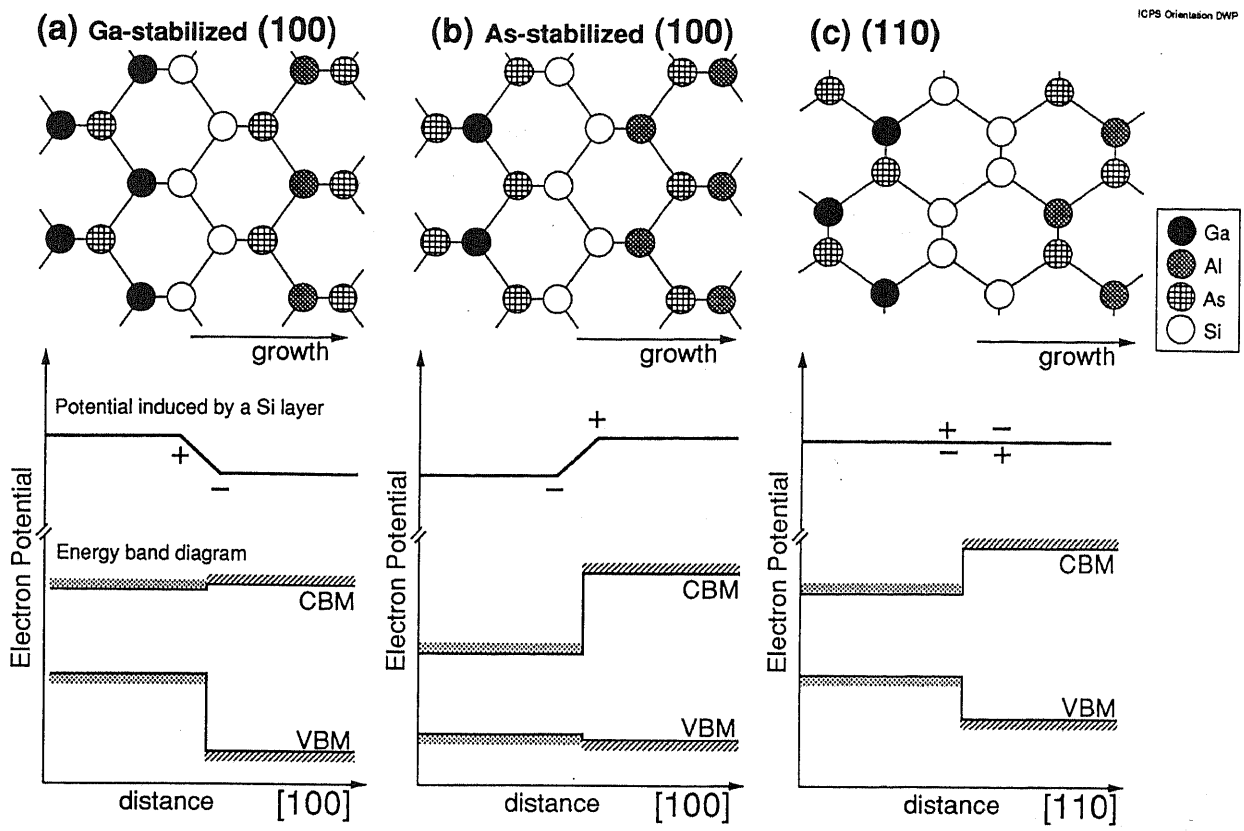

FIG. 5-2. Schematic illustrations of atomic configurations and energy band diagrams at GaAs/Si/AlAs heterointerfaces grown on (a) Ga-stabilized (100), (b) As stabilized (100), and (c) (110) oriented substrates. Potential variations due to the Si layer are also shown.

group IV-element layer is inserted at a III-V semiconductor heterointerface? By a self-consistent calculation, Muños *et al.* showed that a Ge double insertion-layer forms an interface dipole, which can tune the VBO on (100) and (111) crystal planes.[6] That idea is schematically shown in Fig. 5-2. Figure 5-2 displays atomic configurations, dipole potentials induced by Si layers, and expected variations in the energy band diagrams for Si inserted AlAs/GaAs heterointerfaces grown on As- and Ga-stabilized (100) and (110) surfaces. An important point to be noticed is that the interface dipole strongly depends on an interface crystal orientation. Sorba *et al.* reported that the VBO at a GaAs/AlAs (100) heterointerface determined by XPS can be changed from 0.02 to 0.78 eV by inserting a Si layer.[7] When the Si layer is thinner than 0.5 monolayer (ML), their result agrees with a theoretical prediction assuming an interface dipole.[90]

In the following section, however, it will be shown that the main role of the Si layer is not a true control of the VBO but an introduction of a band bending in the XPS probing area. It is mainly because the Si occupation site at the interface is not easily controlled and in most cases Si plays a role of an *n*-type dopant to cause a band bending.

In order to overcome this difficulty, we propose a new structure to realize an effective control of HBO. Figure 5-2(d) shows a GaAs/AlAs heterostructure incorporating two δ-doping layers, which is an intermediate of (b) and (c). By placing highly (~10^{20}cm^{-3}) Si δ-doped layers in a spacing of a few monolayers, one can get a HBO-controlled abrupt heterointerface. In order to realize that idea, an effective *p*-type doping as well as a well-confined δ-doping must be accomplished. An MBE-grown (311)*A* GaAs doped with Si is reported to be *p*-type because of surface bond configurations.[91] We found a Si δ-doped (311)A GaAs is *n*-type and a uniformly Si-doped (311)*A* GaAs grown by MBE shows a *p*-type conductivity (at the maximum p~10^{20}cm^{-3}). Further, by combining a 50Å-thick *p*-type GaAs layer and an interface δ-doping with Si, a preliminary experiment has been made to control a band alignment at GaAs/AlAs heterointerface.

5.2 Roles of Si layer at GaAs/Si/AlAs heterointerfaces

5.2.1 Possible band diagrams

As has been claimed previously, for a correct VBO to be deduced by XPS measurements, an energy band diagram in a sample must be flat in the XPS probing area (≲100 Å). Figure 5-3(a) and (b) show energy band diagrams of an AlAs/GaAs heterostructure on different scales. As a doping density is very low in our sample (n~1×10^{16}cm^{-3}), the surface band bending can be neglected in the XPS probing region as shown in Fig 5-3(b). By rewriting Eq. (2-1) to explicitly show a flat band condition, a VBO is shown by

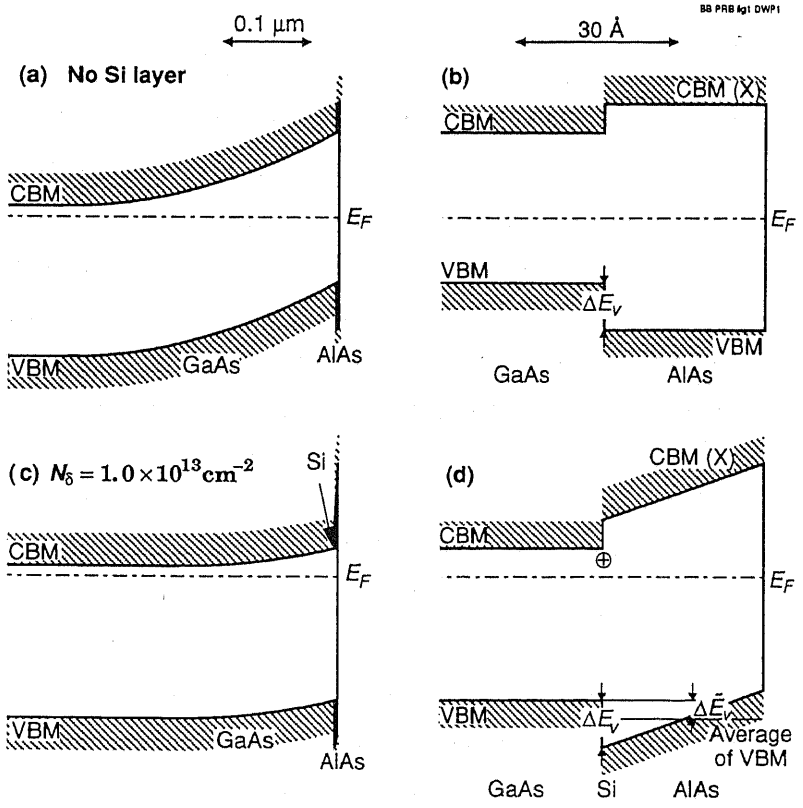

FIG. 5-3. Energy band diagrams in (a, b) AlAs/GaAs and (c, d) AlAs (30Å)/Si/GaAs (the Si donor density at the interface, N_δ, is 1×10^{13} cm^{-2}) structures estimated by the band bending model. (b) and (d) show blowups of (a) and (c), respectively, near the surface, where XPS probes. The GaAs layer is doped with Si (n~1×10^{16} cm^{-3}). Diffusion and/or segregation effects of inserted Si atoms are ignored for simplicity.

$$\Delta E_v = \Delta E_{\text{Ga } 3d\text{-Al } 2p}(\text{flat band}) - 53.97\text{eV}. \quad (5\text{-}1)$$

$\Delta E_{\text{Ga } 3d\text{-Al } 2p}$(flat band) is the energy difference between Ga $3d$ and Al $2p$ core levels measured on an AlAs/GaAs heterostructure. Sorba *et al.* applied this method to the AlAs/Si/GaAs system to derive the VBO.[7] However, this is not generally true, because the flat band condition is not always fulfilled in this system. The following three factors should be taken into account to draw a true band diagram.

(1) Excess charges induced by ionized Si-impurities near the interface due to a "δ-doping" effect. This is likely because Si preferentially occupies a Ga-site to form donors in MBE-grown GaAs.
(2) The surface Fermi level pinning due to surface states.
(3) A possible segregation of Si into an over-grown layer.[92]

The first two factors cause a band bending in the over-grown layer and the third factor induces a non-linear variation of the band bending.

The band bending in the over-grown layer changes the energy separation between Ga $3d$ and Al $2p$ peaks in the XPS spectra and hence it is necessary to separate the true VBO-change from the band bending effect when deriving the VBO from XPS spectra. In order to clarify this situation, let's consider a case where an AlAs thin layer is grown on a Si/GaAs layer (the structure is denoted as AlAs/Si/GaAs) and a band bending due to Si donors is present in the AlAs layer as shown in Fig. 5-3(c) and (d). A band bending in the GaAs layer is negligibly small because the doping density in the GaAs layer is very low and a Si diffusion into the GaAs layer is negligible under the present experimental condition. The measured peak of an Al $2p$ level consists of a superposition of photoelectrons with different energies emitted from different depths from the surface. Therefore, the peak energy shifts and the Al $2p$ line width is broadened by the band bending. On the other hand, when only the VBO changes and no band bending is present, no line-width broadening should be observed. This fact can be used to separate the two effects. Moreover, the interface dipole potential at a heterovalent interface is much dependent on the interface orientation, in contrast to the band bending which is primarily independent since it is determined by the ionized-donor concentration. Furthermore, if the energy shift is due to a band bending, separation of the two peaks should vary with increasing the AlAs over-grown layer thickness, while if it is due to the true VBO-change, it should remain constant. We will use these three factors to test which effect dominantly takes place in the present AlAs/Si/GaAs structures. In the following, we discuss an "average valence band difference," $\Delta\tilde{E}_v$, which is defined as

$$\Delta\tilde{E}_v = \Delta E_{\text{Ga } 3d\text{-Al } 2p}(\text{meas}) - 53.97 \text{ eV}. \quad (5\text{-}2)$$

Here, $\Delta E_{\text{Ga } 3d\text{-Al } 2p}$(meas) is the measured energy separation between Ga 3*d* and Al 2*p* peaks and dependent on both a band-bending and a change of a true VBO as mentioned above. This value is identical to the VBO when the interface dipole is formed and no band bending exists.

5.2.2 Samples and an analysis on peak line-widths

The sample structure used in the experiment is a 1 μm-thick GaAs buffer layer, an ultrathin Si inserted layer and an AlAs over-grown layer, which were successively grown by MBE on *n*-type (100), (110), and (311)*A* GaAs substrates. For (100) substrates, both As-stabilized and Ga-stabilized surfaces were studied. A Ga-stabilized surface was obtained by heating a sample at 550~600°C with a liquid-nitrogen cooled shroud one day after the growth of a GaAs layer to eliminate the residual As_4 flux from the shroud. The RHEED pattern changed from (2×4) to (4×2). The sample on a (110) substrate was grown under a high As_4 flux (an As_4 to Ga ratio was 15~30) at 400~450°C. The GaAs layer was lightly doped with Si (1×10^{16} cm^{-3}), except for the samples grown on (311)*A* substrates, which were undoped. A thickness of a Si layer was measured in a unit of monolayer (ML), where 1 ML = 6.25×10^{14} cm^{-2}; i.e. one ML corresponds to a full coverage of Si on either group-III or -V atom sites on a (100) GaAs surface. The growth temperatures were 600 °C, 400 °C, and 450 °C for a GaAs layer, a Si inserted-layer, and an AlAs over-grown layer, respectively, both on (100) and (311)*A* substrates. The thickness of GaAs and AlAs layers was calibrated by the RHEED intensity oscillations and the Si deposition rate was determined from a sepa-

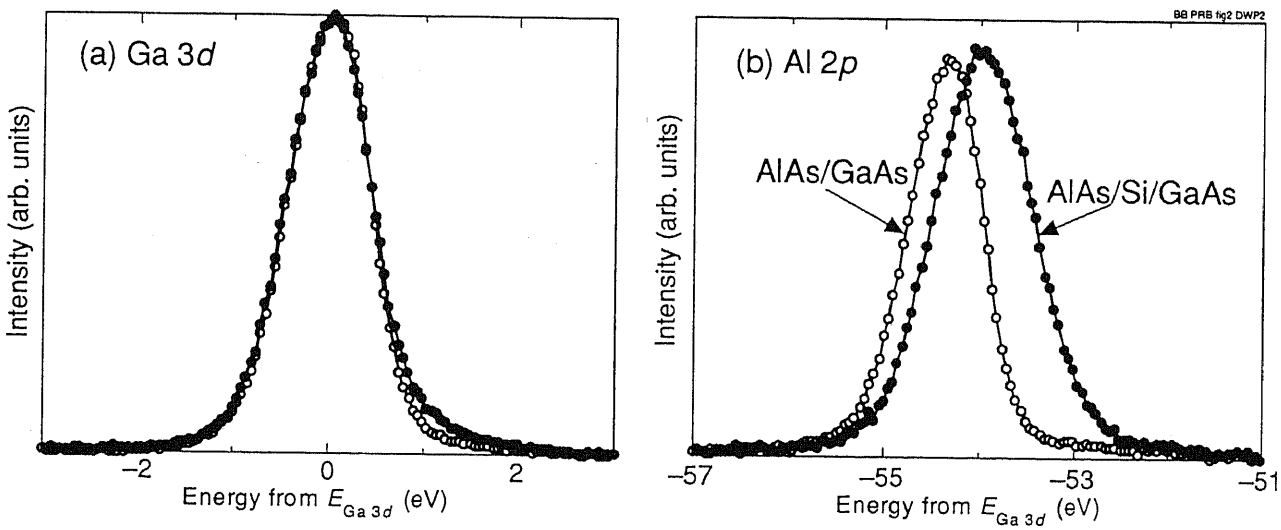

FIG. 5-4. XPS spectra of (a) Ga 3*d* and (b) Al 2*p* core levels taken from AlAs (30 Å)/(311)*A* GaAs (open circles) and AlAs (30 Å)/Si (0.2 ML)/(311)*A* GaAs (dots) heterostructures.

rate measurement of electron concentration in a uniformly Si-doped GaAs sample.[93] A Si deposition was performed by using a conventional effusion cell with a cell temperature of 1100°C. (It takes 26 minutes to complete a Si monolayer growth.) The samples were immediately transferred to the analysis chamber to be analyzed by XPS.

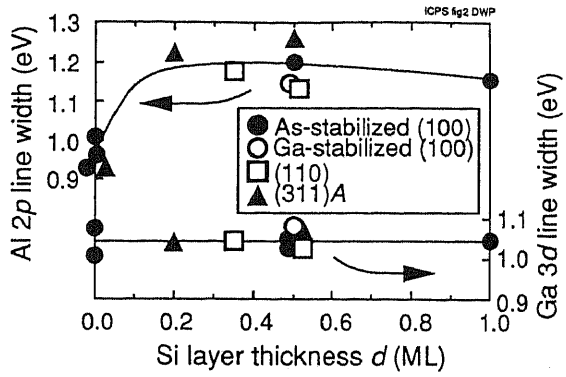

FIG. 5-5. Peak line widths (in the FWHM) of Ga 3*d* and Al 2*p* peaks plotted as functions of the Si layer thickness, *d*.

Figure 5-4 shows typical XPS spectra of (a) Ga 3*d* and (b) Al 2*p* levels taken from AlAs (30Å)/GaAs and AlAs (30 Å)/Si (0.2 ML)/GaAs samples grown on (311)*A* substrates. For each spectrum the origin of energy scale is set at the Ga 3*d* peak energy. As seen from Fig. 5-4(b), the Al 2*p* peak energy shifts by ~ + 0.4 eV, indicating that $\Delta\tilde{E}_v$ is modified by a Si insertion. The Al 2*p* line width is broadened from 0.93 eV to 1.22 eV in the FWHM, while the Ga 3*d* level retains its intrinsic line width. This indicates that a band bending in the AlAs over-grown layer affects the XPS spectra. The unchanged lineshape of the Ga 3*d* peak indicates that the band bending in the GaAs layer is very small. A small shoulder observed at the higher energy side of the Ga 3*d* peak is due to a chemical shift of a Ga atom bonded to Si atoms. (This will be discussed in detail later.) Figure 5-5 shows line widths of the Ga 3*d* and Al 2*p* levels measured on AlAs (30Å)/Si (*d* ML)/GaAs structures grown on Ga- and As-stabilized (100), (110) and (311)*A* surfaces as a function of the Si layer thickness *d*. It is found that in all the samples the Al 2*p* line width is broadened by ~0.3 eV when a Si layer is inserted and the Ga 3*d* level has a constant line width within an experimental uncertainty (± 0.03 eV). This result indicates that there exists a large band bending in the AlAs layer.

5.2.3 Orientation dependence and band bending model

In Fig. 5-6, the average valence band difference, $\Delta\tilde{E}_v$, is plotted as a function of the inserted Si layer thickness *d* for As- and Ga-stabilized (100), (110), and (311)*A* interfaces. For reference, the results by Sorba *et al.* are also included. As easily seen from the figure, $\Delta\tilde{E}_v$ decreases by a Si insertion layer and saturates at *d* ~ 0.5 ML in all the samples and the data points except for (311)*A* fall on a single curve. In Fig 5-6, the theoretical curves of Si-induced shifts in the VBO calculated for Ga- and As-stabilized (100) (shown by (100)Ga and (100)As, respectively) and (110) interfaces are shown by broken lines.[94] In agreement with a simple estimation shown in Fig 5-2, the calculated VBO increases with increasing *d* on (100)Ga and only slightly changes on (110)

interface. This result completely disagrees with the experimental observations clearly indicating that the interface dipole model is not applicable in this system.

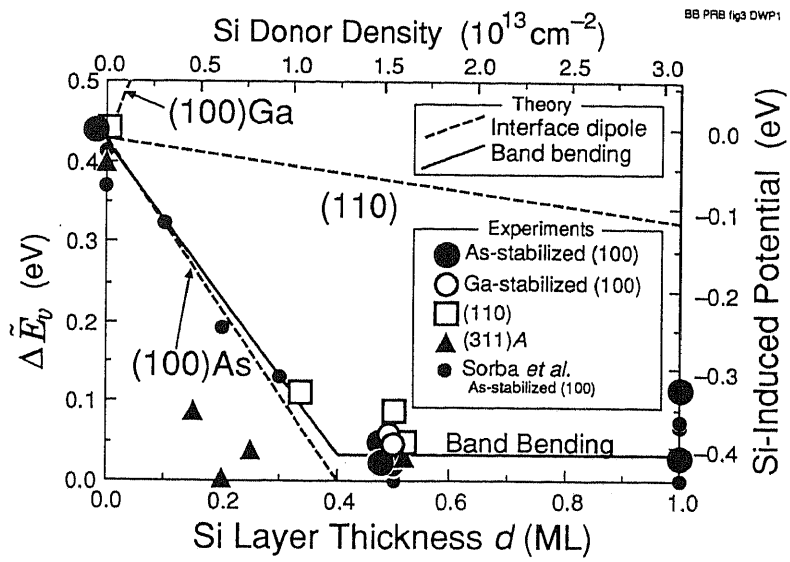

FIG. 5-6. The average valence band difference, $\Delta\tilde{E}_v$, measured on As- and Ga-stabilized (100), (110), and (311)*A* interfaces as a function of inserted Si layer thickness d. The broken lines show theoretical predictions of the interface dipole potential induced by a Si layer calculated for Ga-stabilized (100) (denoted by (100)Ga), As-stabilized (100) ((100)As), and (110) interfaces. The solid line shows a theoretical variation of $\Delta\tilde{E}_v$ as a function of Si donor density, N, which is shown in the top axis, obtained by the "capacitor model."

Alternatively, these results are well explained by a model which assumes a band bending in the AlAs over-grown layer (the band-bending model). Parts of Si atoms deposited at the interface form donors and shift the Fermi level toward the CBM, while the surface Fermi level is pinned. Since the Fermi level should be spatially constant at the thermal equilibrium, the band bends in the AlAs layer. The band bending is expected to saturate at a certain Si donor density, because when the Fermi level reaches the CBM, free electrons are accumulated and hence the CBM no more changes significantly.

By assuming that the band bending is linear in the AlAs layer,[95] we can estimate a variation of $\Delta\tilde{E}_v$, by considering a simple "capacitor" in the AlAs layer. Because of surface states of AlAs, the surface Fermi level is pinned and the excess electrons induced by Si ions are mostly trapped by these states. The potential drop in the AlAs layer, E_{BB}, is, then, given by

$$E_{BB} = \frac{t}{\kappa_0 \varepsilon_0} e^2 N, \qquad (5\text{-}3)$$

where t is a thickness of the AlAs over-grown layer (30 Å in the present case), κ_0 is the low frequency dielectric constant of AlAs, ε_0 is the dielectric permittivity of vacuum, and N is the areal density of ionized Si donors, which is equal to the density of excess

electron at the surface states in the present "capacitor" model. Then, we can estimate the variation of $\Delta\tilde{E}_v$ as

$$\begin{aligned}\Delta\tilde{E}_v &= E_{\mathrm{Ga}\ 3d} - E_{\mathrm{Al}\ 2p}^{average} - 53.97\mathrm{eV} \\ &= E_{\mathrm{Ga}\ 3d} - E_{\mathrm{Al}\ 2p}^{bottom} - 53.97\mathrm{eV} - \left[E_{\mathrm{Al}\ 2p} - E_{\mathrm{Al}\ 2p}^{bottom}\right]^{average} \\ &= \Delta E_v - \int_0^t (1-x/t)E_{BB}\exp(-x/\lambda_e)dx \Big/ \int_0^t \exp(-x/\lambda_e)dx,\end{aligned} \tag{5-4}$$

where $E_{\mathrm{Al}\ 2p}^{average}$ denotes the Al $2p$ peak energy averaged over the XPS probing region, $E_{\mathrm{Al}\ 2p}^{bottom}$ denotes the energy at the bottom of the AlAs layer (= heterointerface), and λ_e is a photoelectron escape depth. For t = 30 Å and λ_e = 25 Å, Eq. (5-4) gives $\Delta\tilde{E}_v - \Delta E_v$ = 0.60 E_{BB}. As seen in Fig. 5-6, the measured shift, ($\Delta\tilde{E}_v - \Delta E_v$), at t = 0.5 ML is ~ 0.40 eV, which leads to E_{BB} = 0.67 eV. From Eq. (3) N is 1.2×10^{13} cm^{-2}. This is a reasonable value because a carrier concentration obtained by a δ-doping with Si up to 2.7×10^{13} cm^{-2} has been reported.[96] By a separate UPS measurement, we have found that the surface Fermi level pinning position for an undoped AlAs is 1.07 ± 0.1 eV-higher than the VBM.[97] Then, E_{BB} is estimated by

$$\begin{aligned}E_{BB} &= 1.43\ \mathrm{eV}(\text{band gap of GaAs}) + 0.44\ \mathrm{eV}(\mathrm{VBO}) - 1.07\ \mathrm{eV} \\ &= 0.80\ \mathrm{eV}\ .\end{aligned} \tag{5-5}$$

This value is slightly larger than the experimental one. The discrepancy may be due to a non-linearity of the band bending. Further, we can calculate $\Delta\tilde{E}_v$ from Eqs. (5-3) and (5-4) as a function of N, which can be converted to the Si-layer thickness by assuming the "activation efficiency" is 0.05 (constant) for $d \le 0.4$ ML. This "activation efficiency" is also reasonable as compared with the reported value[98] which ranges from 0.01 to 0.1. The calculated curve is shown by a solid line in Fig. 5-6. On the top of the figure, ionized Si donor density is also shown. This curve agrees with experimental observation for $d \le 0.4$ ML. For $d > 0.4$ ML, the Fermi level at the interface no more changes (degenerates) and the $\Delta\tilde{E}_v$ saturates.

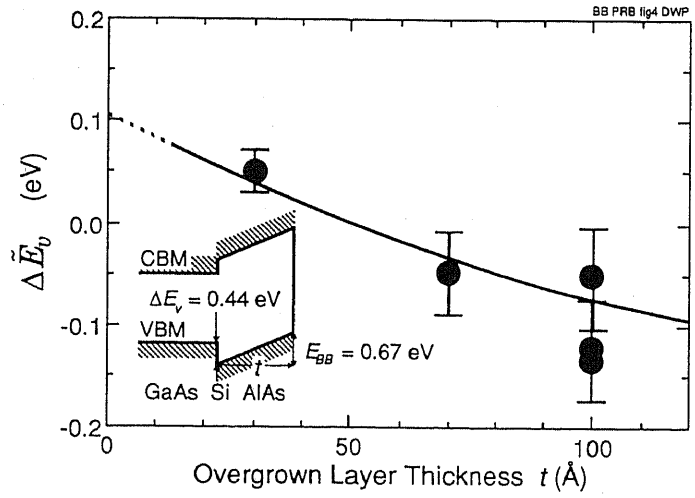

FIG. 5-7. The average valence band difference, $\Delta\tilde{E}_v$, plotted as a function of the AlAs layer thickness t. The solid line shows the theoretical prediction when there is a band bending as shown by the inset.

For the (311)*A* substrates $\Delta\tilde{E}_v$ is smaller than the other cases when $d < 0.5$ ML, suggesting a higher "activation efficiency." Although Si is known to be an acceptor on a (311)*A* substrate under a certain growth condition, it is an efficient donor with δ-doping under a large As_4 to Ga ratio.[99] Bratina *et al.* reported that a change in $\Delta\tilde{E}_v$ at AlAs/Ge/GaAs structures is three times as large as that at AlAs/Si/GaAs when $d \leq 0.15$ ML,[100] which is very similar to our (311)*A* case. All these experimental results can be explained in the band-bending model by assuming different "activation efficiencies" of δ-doped Si.

To further confirm the validity of the band-bending model, we measured a dependence of $\Delta\tilde{E}_v$ on the AlAs layer thickness t in AlAs (t Å)/Si (0.5 ML)/GaAs structures grown on an As-stabilized (100) substrate. Figure 5-7 shows $\Delta\tilde{E}_v$ as a function of t. $\Delta\tilde{E}_v$ does decrease by ~ 0.1 eV with increasing t from 30 Å to 100 Å. The solid line in Fig. 5-7 is the calculated $\Delta\tilde{E}_v$ by using Eq. (5-4) for $E_{BB} = 0.67$ eV, $\Delta E_v = 0.44$ eV, and $\lambda_e = 25$ Å. An excellent agreement between the measurement and the calculation again supports that the main role of a Si insertion layer is not a control of VBO but an introduction of the band bending. The Al 2*p* line width slightly decreases with increasing t, reflecting that a band bending near the surface decreases when t increases.

In addition, we have studied a variation of $\Delta\tilde{E}_v$ in reversed GaAs/Si (0.35~0.5 ML)/AlAs (110) structures as well as AlAs/Si/GaAs (110). Figure 5-8 shows $\Delta\tilde{E}_v$ as a function of Si layer thickness for the both structures. It is found that $\Delta\tilde{E}_v$ increases for the reversed structure indicating that the band bending formed in the

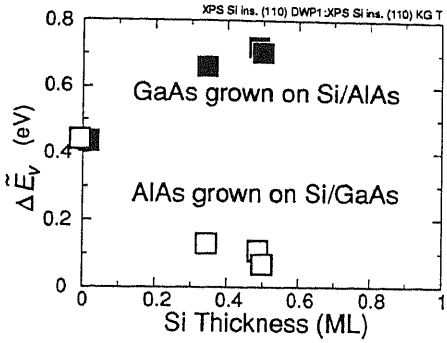

FIG. 5-8. $\Delta\tilde{E}_v$ for AlAs/Si/GaAs (110) and reversed GaAs/Si/AlAs (110) structures.

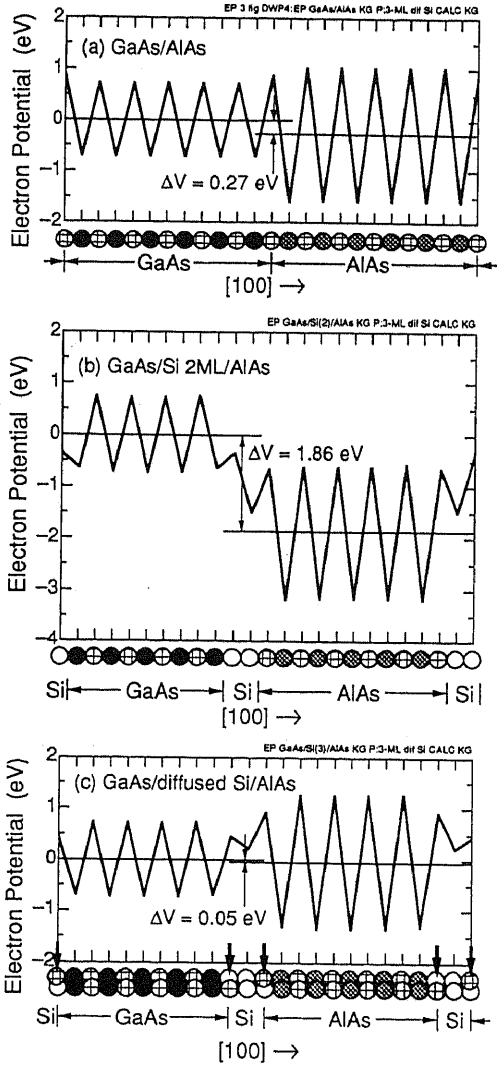

FIG. 5-9. Spatial variations of electron potential for (a) GaAs/AlAs (100) and (b, c) Si inserted GaAs/Si 2 MLs/AlAs. (c) assumes Si atoms occupy a half of As sites beside an interface group-V monolayer.

top GaAs layer raises the average of the VBM in the GaAs layer to raise $\Delta\tilde{E}_v$. Although, Muños and Hernández showed that an interface dipole may decrease ΔE_v when Si occupy only As sites at the interface,[101] this experiment disagrees with their theory and it shows that the main role of Si layer is an introduction of a band bending. It is because if the interface dipole predicted by Muños *et al.* is formed on the (110) surface to change the $\Delta\tilde{E}_v$, the VBO must decrease (or at least remain constant) when the reversed GaAs/Si/AlAs structure is studied.

5.2.4 Why the HBOs are not controlled?

In the above discussion, it is now clear that an interface dipole layer with equal densities of Si_{Ga} and Si_{As}, which is necessary to control the VBO leaving no band bending, was not successfully formed under the present experimental conditions. There considered are a few reasons for it. First, Si preferentially occupies a Ga-site under a normal growth condition. Therefore, even if double Si monolayers are deposited, Si might change its site from As to Ga and only Si_{Ga} is left after the growth is completed. Thus, no dipole is formed. Another possibility is that dipoles with opposite polarities, Si_{Ga}-Si_{As} and Si_{As}-Si_{Ga} may simultaneously be formed and a polarity cancellation, may take place.[102] For example, when Si-atoms spread over 3 atomic layers (i.e., Si occupy a half of As sites, full of interface group-III sites, and a half of As sites at the interface), Si-induced dipole moment is mostly canceled. Figure 5-9 shows a theoretical potential diagram obtained by a self-consistent calculation for an AlAs/GaAs (100) heterointerface and Si inserted AlAs/Si/GaAs (100) structures.[103] It is clearly shown that when Si-atoms occupy three layers a change in the electrostatic potential is very small as compared with a case when Si-atoms completely occupy both Ga and As planes at the interface. This indicates that a precise control of Si sites is required to achieve a control of VBO as predicted by the theory. In addition, the densities of donors and acceptors should be exactly equal. However, it is rather difficult to experimentally achieve such a condition.

5.3 UPS analysis of a Si reaction and GaAs/Si/GaAs structures

A control of the occupation site of inserted atoms is very important to realize a control of the HBOs. The XPS analysis of bonding states of Si atoms by using Si 2*p* spectrum is, however, difficult because of its low photoemission cross section and a small magnitude of chemical shift.[104] In this section Ga 3*d* UPS spectra taken on Si/GaAs and GaAs/Si/GaAs structures are discussed to clarify bonding states of Ga and Si atoms. Even when Si is deposited on an As-stabilized surface, a considerable density of Ga-Si bonds are found. This fact suggests a difficulty of a control of Si sites. Further, a

TABLE V-I. Samples and the growth conditions.

	Structure	Growth procedure
(i)	GaAs	A lightly Si-doped (n ~ 10^{16}cm^{-3}) GaAs (1μm) was grown on an n^+-type GaAs (100) substrate. The growth temperature was T_s~600°C, a V/III flux ratio was 3~5, and a growth rate was ~0.6 μm/h
(ii)	Si/GaAs	2 monolayers (1.3×10^{15}cm^{-2})-thick Si layer was deposited on (i) (after a UPS measurement). The deposition temperature is very low. (The substrate heater has been turned off. Although, a thermocouple located behind the sample holder indicates ~100°C, the sample can be heated by a radiation from the Si cell to be 200~300°C.) Si cell temperature is 1100°C. No As flux was provided during the Si deposition.
(iii)	Si/(Ga) GaAs	After a GaAs buffer layer is grown as identical to the sample (i), a sample was kept in a transfer chamber for 1~2 days. The sample is, then, heated up to ~600°C (It is nearly the oxide desorption temperature of GaAs.) with liquid nitrogen cooled shroud to obtain a Ga-stabilized surface. 2 ML-thick Si layer is deposited on the Ga-stabilized surface as that has been done for the sample (ii).
(iv)	GaAs/Si/GaAs	GaAs layers were grown on samples (ii) and (iii) after a measurement. Ga and As beams were alternatively supplied to enable a very low temperature growth. (The substrate temperature was T_s~300°C with a thermocouple preset is 500°C. An As deposition was made much longer than a time one monolayer of As coverage needs, since a reduction of an As reaction has been reported.[105])

GaAs/Si/GaAs structure is studied and discussed from two viewpoints; a change in VBO and a band bending.

5.3.1 UPS spectrum of Si deposited GaAs samples

First, in order to clarify the bonding states of Ga atoms in a Si-deposited GaAs sample, three samples (reference GaAs, Si-deposited GaAs, and Si-deposited Ga-stabilized GaAs) were grown by MBE. Details of the growth conditions are summarized in TABLE V-I. The sample was transferred to the analysis chamber immediately after its growth and a UPS spectrum was measured. An ultraviolet source is differentially pumped to keep a pressure

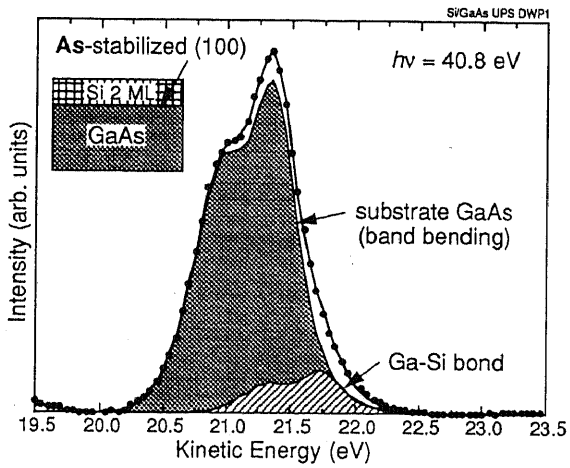

FIG. 5-10. A UPS spectrum taken from a Si-deposited As-stabilized GaAs. Dots show the experiment and a solid line shows a fitting curve obtained by adding two components as described in the text. A hatched region is a signal from Ga atoms bonded to Si atoms.

in the sample chamber ~1.5×10^{-9} Torr during the experiment. By integrating the signal over 5.5 hours, a peak intensity of ~30 Kcounts (~120 Count/s) is obtained with an analyzer energy of 2.5 eV (an instrumental resolution is better than 0.1 eV).

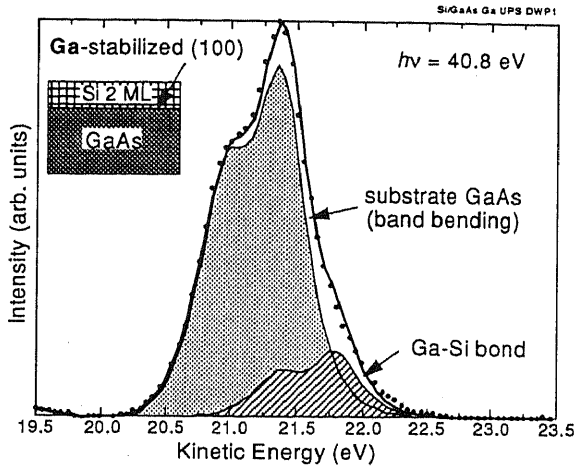

FIG. 5-11. A UPS spectrum taken from a Si-deposited Ga-stabilized GaAs. Definitions of symbols are identical to as in Fig. 5-10.

Figure 5-10 shows a UPS spectrum taken from a Si-deposited GaAs sample (sample (ii)). This spectrum has a small shoulder at the higher energy side of the main peak. This feature has also been found in the XPS spectrum shown in FIG. 5-4(a). It has been reported that a Ga atom bonded to Si shows a chemical shift of +0.4~+0.7 eV from that of GaAs depending on the substrate crystal orientation.[106] The shoulder of the Ga 3*d* spectrum is, thus, considered to be a signal of Ga-Si bonds. In order to evaluate a density of surface Ga-Si bonds, a least squares fit is made by using a substrate GaAs signal. The XPS spectrum (an intensity I is given as a function of an energy, E) for Si deposited GaAs, $I_{\mathrm{Si/GaAs}}(E)$ is shown by

$$I_{\mathrm{Si/GaAs}}(E)=\sum_{i=1}^{\infty}\exp\left(-\frac{i}{\lambda_e}\right)I_{\mathrm{GaAs}}\left[E-(i-1)E_{BB}^{layer}\right]+CI_{\mathrm{GaAs}}(E-E_{\mathrm{Ga\text{-}Si}}), \qquad (5\text{-}6)$$

with $I_{\mathrm{GaAs}}(E)$ the XPS spectrum from reference GaAs, E_{BB}^{layer} the magnitude of a band bending in GaAs (in eV/layer), C the concentration of Ga-Si bonds in the surface Ga atoms, and $E_{\mathrm{Ga\text{-}Si}}$ the chemical shift for the Ga-Si bonds. By substituting an electron escape depth λ_e = 8Å,[107] E_{BB}^{layer}, $E_{\mathrm{Ga\text{-}Si}}$, and C are obtained by a least squares fit as shown by the solid line in Fig. 5-10. Then the surface Ga-Si bonds are estimated to be ~1/3 of Ga atoms at the top layer. Figure 5-11 shows a UPS spectrum from another sample, for which Si (2 ML) was deposited on a Ga-stabilized (100) surface (sample (iii)). As seen from the figure, a signal corresponding to Ga-Si bonds is observed also in this sample. However, its magnitude is yet less than the expected value. Only a half of Ga atoms located at the top Ga layer are considered to be bonded to Si atoms. This indicates that on the Ga-stabilized surface Si atoms are bonded to both Ga and As atoms.

5.3.2 GaAs/Si/GaAs structures

McKinley *et al.* reported that a so called homojunction band offset can be formed in a Ge (thick over-layer) /Ga (1 atomic layer)/As (1 atomic layer)/Ge (substrate) structure.[108] They measured photoemission spectra from samples which consist of Ga, As, and Ge layers evaporated on a Ge substrate and deconvoluted the spectra to obtain the band offset. Although their spectra shift to suggest a formation of a band offset, their spectra become somewhat broader by depositing GaAs and Ge overlayer. It can be considered in the following two ways:

(i) There is a band bending in the overgrown layer. (Then, the band offset is not formed by the Ga and as layer insertion.)
(ii) A spectrum broadening might be due to a crystallinity of a sample. Since they used a simple evaporation to form a junction, the crystallinity of their samples is questionable.

In this work, we perform UPS measurements on GaAs/Si 2 monolayers/GaAs structures to check a possibility to form a VBO in this system. GaAs layers were overgrown on Si/GaAs samples as listed in Table V-I (iv) after UPS measurements. In order to suppress Si diffusion and to maintain a crystallinity of the overgrown GaAs layer, an MBE-growth of a sample has conducted at a very low temperature (~300°C) and the Ga and As fluxes were alternatively supplied.[109] Figure 5-12 displays UPS spectra from GaAs/Si 2 ML/GaAs structures with various overgrown GaAs layer thickness. All of the spectra were taken from one sample by depositing GaAs layers successively. A spectrum from a GaAs and that from a Si deposited GaAs sample are also shown for comparison.
The following features are found from the spectra;

(1) A Ga 3*d* peak energy shifts by increasing a GaAs overgrown layer thickness.
(2) Ga 3*d* peak line width becomes broader than those of a GaAs sample.

Since, even when d=18 ML, which is much thicker than the photoelectron escape depth (8~10 Å for an electron energy of 21 eV) the Ga 3*d* spectrum is broader than that from the

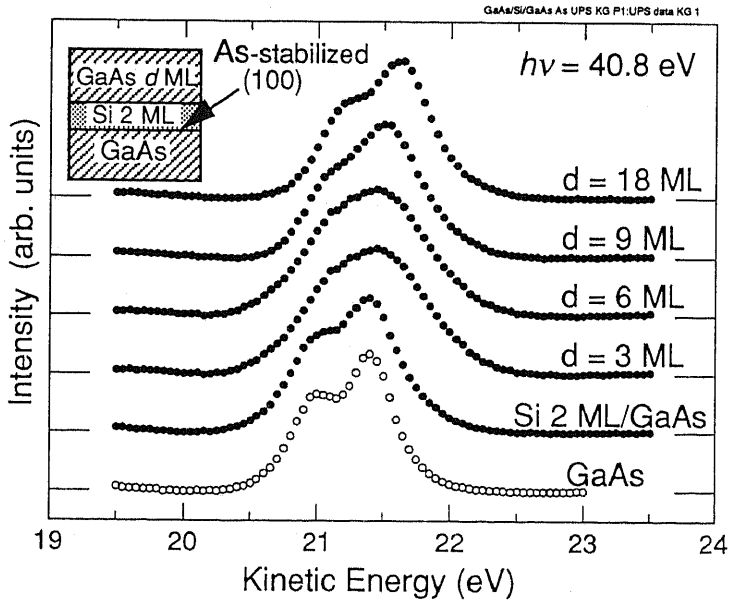

FIG 5-12. UPS spectra taken from GaAs, Si (2 ML) deposited GaAs, and GaAs (*d* ML)/Si (2 ML) /GaAs structures.

reference GaAs sample. This effect indicates that a band bending in the top GaAs layer is significant in this sample.

Figure 5-13 shows UPS spectra from the samples which consist of Si 2 monolayers and GaAs layers overgrown on a Ga-stabilized GaAs substrate as shown by the inset. These spectra show very similar variations as appeared in those from samples grown on an As-stabilized substrate (Fig 5-12). This behavior reflects that a Si occupation site is not controlled by changing a substrate surface.

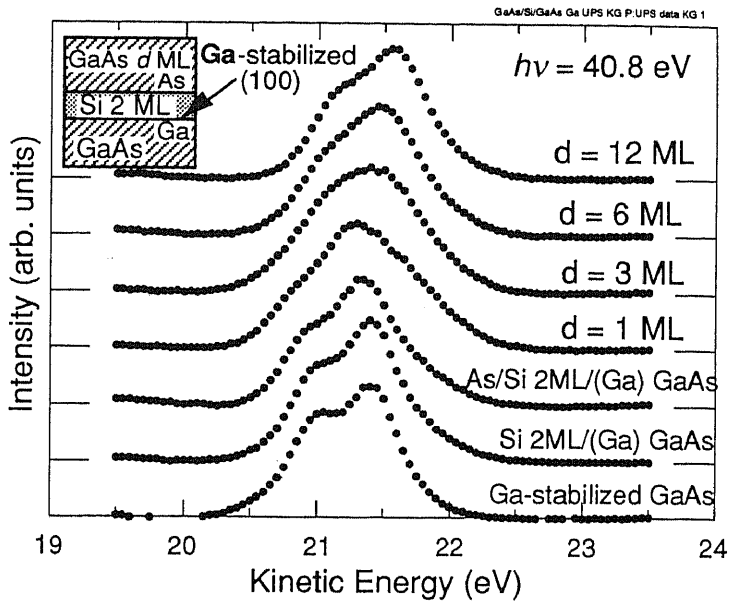

FIG. 5-13. UPS spectra taken from Ga-stabilized GaAs, Si (2 ML) deposited on Ga-stabilized GaAs, Si-deposited Ga-stabilized GaAs exposed to an As flux, and GaAs (*d* ML)/Si (2 ML)/Ga stabilized GaAs structures.

Shifts in a Ga 3*d* peak is considered in the following two ways;

(1) Inserted Si atoms play a role of donor impurities. A line width broadening is well explained by considering a band bending. Then, a shift in energy of the Ga 3*d* peak is explained by considering the following speculation. With a Si layer insertion, the interface Fermi level approaches to the CBM of GaAs, then depending on a surface state density the surface Fermi level shift for lower energy in the band gap from its value for a semi-insulating sample. Although the surface state density is not clear for our sample, the band bending found on the AlAs/GaAs interface is smaller than a value determined by Eq. (5-5) suggesting a possibility of 10^{13} cm^{-2} of interface states slightly (0.1~0.2 eV) lower the pinning position of the surface Fermi level in the particular sample designed for a photoemission measurement.

(2) A slight valence band offset can be formed. As appeared in Fig 5-9, a small change in the VBO might originate due to Si-layer insertion even if its occupation site is not ideally controlled. Moreover, an MBE-growth is not a process of the thermal equilibrium and a cancellation of the interface dipole formed by Si_{As}-Si_{Ga} and Si_{Ga}-Si_{As} may not be always complete, although it seems to be the most stable when the same density of Si_{As}-Si_{Ga} and Si_{Ga}-Si_{As}. Then, the remained interface dipole can form a VBO at the GaAs/Si/GaAs junction. It was also reported

that when one insert thick (several atomic layers) Si layer in a GaAs/AlAs interface, the VBO can be modified by ~0.2 eV due to a difference between the top and bottom interfaces.[110]

These experiments do not deny a possibility of the latter case, although the change in VBO (0.2 eV) is much smaller than can be formed by completely site-controlled Si layers. However, a difficulty in changing a modification direction (It can only raise the VBM in the overgrown layer.) makes this technique much less useful for one to apply this to a device fabrication.

5.4 A Control of HBOs by *p*- and *n*-type δ-doping

When one inserts a Si mono-layer at an interface, it is very difficult to control its occupation site to form an interface dipole. As an alternative idea, an insertion of separate two layers which are *p*-type and *n*-type (monolayer) sheets is considered to control a VBO. As are seen from the XPS spectra of an AlAs/Si/GaAs structure, a Si δ-doping sheet is *n*-type with a doping density of $1\sim3\times10^{13}$ cm^{-2} depending on the interface orientation. Although to our knowledge a *p*-type δ-doping in GaAs with Si is not reported so far, it may be realized by a choosing a growth condition or doping elements other than Si such as Carbon or Zinc.

In this work, we concentrate our attention to a Si doping on (311)*A* GaAs substrate. Because of the surface bond configuration, MBE-grown uniformly Si-doped (311)*A* GaAs shows *p*- and *n*-type conductivity depending on the growth condition. Its conduction type can be easily controlled by changing As_4/Ga ratio.[111] Si is known as a relatively stable material among many possible dopants commonly used for GaAs. When a (311)A GaAs substrate is δ-doped with Si, it seems to be an *n*-type as suggested by the XPS experiments on AlAs/Si/GaAs structures.[112] Instead of a *p*-type δ-doping, a *p*-type very high doping was used in the experiment. We have confirmed a hole concentration up to $\sim1\times10^{20}$ cm^{-3} by uniformly doping GaAs with Si.[113] Briefly described in the following is a trial to effectively control a VBO by combining the two dopings with Si on (311)*A* GaAs substrate; a 50Å-thick *p*-type ($1.5\sim5\times10^{19}$ cm^{-3}) sheet and an interface δ-doping.

After a growth of a 1 μm-thick GaAs buffer (not intentionally doped) and a 50 Å-thick Si doped GaAs on a Si-doped n^+ (311)*A* GaAs substrate, a sample is cooled down to ~450 °C and a Si δ-doping and a growth of a 30 Å-thick AlAs top layer were carried out. The 50 Å-thick GaAs bottom doped layer was grown for 21 seconds with Si-cell temperature 1100 °C and 1150 °C, which correspond to an acceptor concentration of

p~1.5×10^{19} cm^{-3} and p~5×10^{19} cm^{-3}, respectively. A δ-doping with Si was performed at the same Si beam flux as used for the p-type layer and a doping duration was varied so as to match the p- and n-type effective dopant concentrations. An XPS measurement was performed immediately after growth of each sample. After the measurement, we grew an additional 40 Å-thick AlAs layer, to study a band bending in the top AlAs layer.

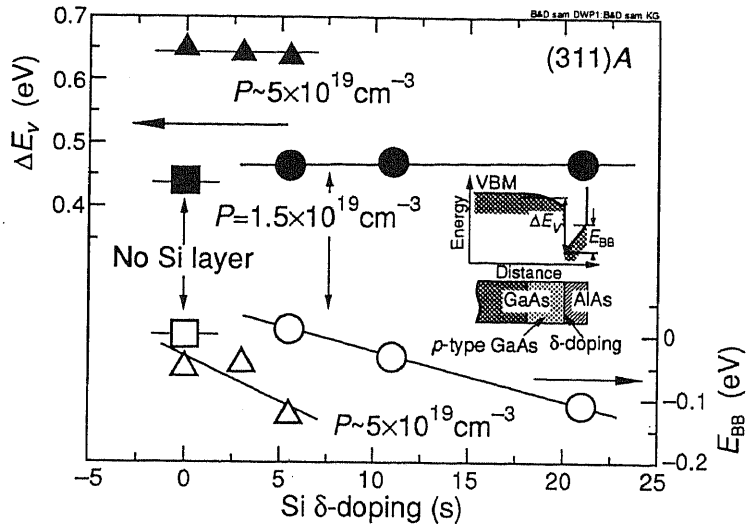

FIG. 5-14. A variation of a VBO and a residual band bending plotted as a function of a Si δ-doping duration. The inset shows the sample structure and a schematic energy diagram of the VBM. p-type (Si-doped) GaAs was grown for 21s with the same Si cell temperature as was used for an interface δ-doping.

A band bending E_{BB} is evaluated by substituting values of VBOs at t=30 Å (after the first growth) and at t=70 Å (with a deposition of an additional AlAs layer) into Eq. (5-4). Figure 5-14 summarizes an effective valence band offset defined by an energy difference between the average of the VBM in GaAs and the VBM at the bottom of AlAs.[114] As shown from the inset, this value is obtained by subtracting a band bending E_{BB} from an apparent valence band difference given by Eq. (5-2). It is found that when p- and n-type layers were formed a valence band offset is raised from 0.44 to ~ 0.65 eV. Although, a band bending in the top AlAs layer is not removed completely, its dependence on the interface Si density shows that the band bending is due to a difference between acceptor and donor concentrations. This result confirms that by controlling a Si occupation site we can modify the VBO, although it remains a technical difficulty to form a thin and precise p-type doping layer.

5.5 Conclusions

A Si insertion layer in an AlAs/Si/GaAs structure does not modify the VBO but introduces a band bending in the layer grown over the Si layer. The band bending model proposed in section 5.3.3 explains the following experimental observations.

(1) A peak line width is broadened in the Al 2p XPS spectrum from AlAs/Si/GaAs samples.

(2) The apparent variations in XPS-deduced VBO do not depend on the crystal orientation (among As- and Ga-stabilized (100), (110), and (311)*A*).
(3) That apparent valence band difference varies when the overgrown layer thickness increases.

In order to realize a true control of a VBO, we have to control a Si occupation site, since a Si atom tends to occupy a Ga site to be a donor.

By forming a *p*-type doping and an interface δ-doping, a modification of the VBO is accomplished to show a possibility of combining *p*- and *n*-type δ-doping sheets to control a VBO.

Chapter 6 Conclusions

To conclude this thesis, main features found on the HBOs are summarized. Displayed are the determined HBOs for GaAs/AlAs and InAs/GaAs systems and a transient of electronic structure which has been found experimentally. Finally, the role of Si layer inserted in GaAs/AlAs and a possibility of controlling HBOs are shown.

6.1 Determination of HBOs and Origin of HBOs

(1) Heterojunction band offsets have been determined by XPS measurements as shown by Fig. 6-1.

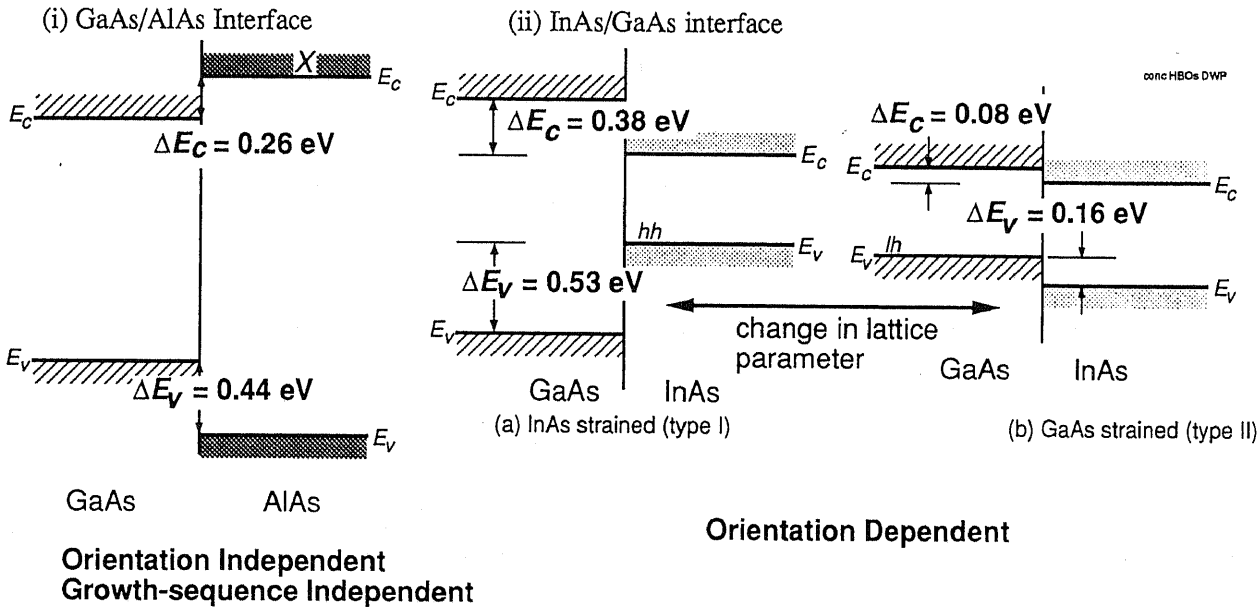

FIG. 6-1. HBOs determined for (i) GaAs/AlAs and (ii) InAs/GaAs systems.

ΔE_v's determined on (100), (110), (111)*B* and (311)*A* interfaces are independent of the crystal orientation for the (lattice matched) GaAs/AlAs system, which suggest the VBO and the interface dipole potential (if it is) are constant determined by choosing materials. This result supports a validity of the theories, which predict HBOs from bulk properties of constituent materials.[15-20]

(2) By measuring, as a function of the distance from the interface, energies of Ga 3*d* and Al 2*p* levels near the GaAs/AlAs heterointerface, we found the followings.

(i) As shown in Fig. 6-2, there are interface chemical shifts of Ga 3*d* and Al 2*p* levels as;

$\delta E_{\mathrm{Ga}\ 3d}(1) = -\delta E_{\mathrm{Al}\ 2p}(1) = -57 \pm 20$ meV ,

$\delta E_{\mathrm{Ga}\ 3d}(2) = -\delta E_{\mathrm{Al}\ 2p}(2) = -25 \pm 20$ meV ,

and

$\delta E_{\mathrm{Ga}\ 3d}(3) = -\delta E_{\mathrm{Al}\ 2p}(3) = -7 \pm 20$ meV .

These values mean that Ga 3*d* (Al 2*p*) level becomes deeper (shallower) in the vicinity of the heterointerface.

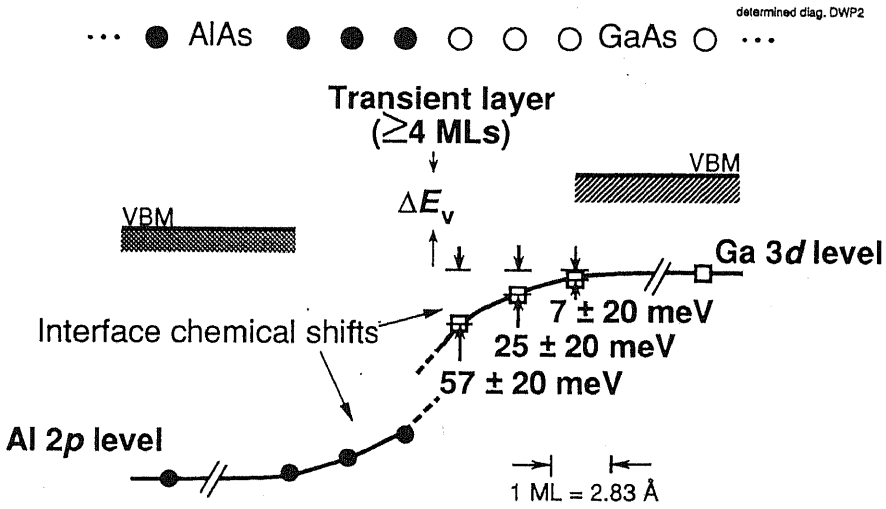

FIG. 6-2. Transient layer and measured chemical shifts.

(ii) There is a transient in the electronic structure at the interface (no thinner than ~11Å). This result presents us a caution that the atomically abrupt HBOs are not a real picture.

(3) $\Delta E_{\mathrm{Ga}\ 3d\text{-}\mathrm{Al}\ 2p}$ is 140 meV-smaller for AlGaAs alloy indicating a 140 meV of chemical shift in the alloy.
This value agrees with our experiments on heterostructures and confirms the validity of the measured interface chemical shifts.

(4) Stained InAs/GaAs heterojunctions were studied. By taking into account the strain-induced shifts in the core level binding energies relative to VBM, and by adding the effects of the uniaxial part of strain, the VBOs are obtained as shown in Fig. 6-1.

(i) VBO depends on the substrate lattice parameter by ~0.7 eV.
(ii) Unlike the lattice matched systems, VBO at InAs/GaAs depends on its orientation; i.e. the VBO is smaller by 0.15 eV for a (111) interface than that for a (100) interface.

6.2 A Control of HBOs

(1) As a candidate to control HBOs, roles of a Si layer inserted at GaAs/AlAs are studied. A Si insertion layer, however, does not modify the VBO but introduces a band bending in the layer grown over the Si layer. This is supported by the following experimental observations.

(1) A peak line width is broadened in the Al 2*p* XPS spectrum from AlAs/Si/GaAs samples. This fact shows that there is a band bending in the AlAs layer.
(2) The apparent variation in XPS-deduced VBO does not depend on the orientation of the substrate (As- and Ga-stabilized (100), (110) and (311)*A* surfaces were studied). This result disagrees with a prediction assuming an interface dipole formation to control HBOs.
(3) That apparent valence band difference varies when the overgrown layer thickness increases. This variation also cannot be explained unless there is a band bending in the top layer.

In order to realize a control of a VBO, we have to control a Si occupation site, since a Si atom tends to occupy a Ga site to be a donor.

By forming a *p*-type doping and an interface δ-doping, a modification of the VBO is accomplished to show a possibility of combining *p*- and *n*-type δ-doping sheets to control a VBO.

Acknowledgments

All the works described in this thesis have been accomplished at the Prof. Ikoma's laboratory, Institute of Industrial Science (IIS), University of Tokyo. The author wants to express his sincere thanks to the following people.

Professor Toshiaki Ikoma (the dissertation supervisor) has given me a good chance to get in touch with fascinating topics and provided an excellent apparatus and advises to accomplish those works.
Professor Kazuhiko Hirakawa (IIS, Univ. Tokyo) has let me know a lot of superb ideas and presented several significant discussions.

The following people of Prof. Ikoma's laboratory have assisted the author.
Dr. Toshio Saito supported the experiments shown in this thesis by his theory and discussed about those works.
Genichi Tanaka and **Kenichi Agawa** have worked with me for the control of HBOs.
Mitsuhiro Noguchi, Hideki Sakakibara, S. N. Wang, Dr. Toshiro Hiramoto, Dr. Takahide Odagiri, and **Dr. Xin Wei Zhao** have given me a lot of discussions and supported on experiments. **Ms. Yukiko Kurihara** has often encouraged me.

Professor Y. Iye (Institute for Solid State Physics (ISSP), Univ. Tokyo) discussions at meetings and an important idea for the experiments.
Professors H. Sakaki, Y. Arakawa, and **Homma** (IIS, Univ. Tokyo) and **Professor Yasuoka** (ISSP, Univ. Tokyo) and lot of people in their laboratories allowed the author to use several apparatuses needed in the experiments and have given some interesting discussions.

Dr. Detlev M. Hoffman, Dr. Kalid Ismail, Dr. Trevor J. Thornton,
have stayed in the laboratory to bring fresh *air*, ideas, and a chance for me to acquire some linguistic knowledges.

They are gratefully acknowledged.

GaAs substrates including (110), (111)*B*, (111)*A*, and (311)*A* orientations were kindly provided by **J. Nakagawa** (Hitachi cable).

References

[1]See for example, *Heterojunction Band Discontinuities: Physics and Device Applications*, edited by F. Capasso and G. Margaritondo (North-Holland, Amsterdam, 1987); *Electronic Structure of Semiconductor Heterojunctions*, edited by G. Margaritondo (Kluwer, Milano, 1988), and references cited and/or included therein.

[2]R. L. Anderson, Solid-State Electron. **5**, 341 (1962).

[3]H. L. Stömer, A. Pinczuk, A. C. Gossard, W. Wiegmann, Appl. Phys. Lett. **38**, 691 (1981).

[4]J. Nishizawa, H. Abe, and T. Kurabayashi, J. Electrochem. Soc. **132**, 1197 (1985); N. Kobayashi, T. Makimoto, Y. Horikoshi, Inst. Phys. Conf. Ser. **79**, 737 (1986).

[5]W. A. Harrison, E. A. Kraut, J. R. Waldrop, and R. W. Grant, Phys. Rev. B **18**, 4402 (1978).

[6]A. Muños, N. Chetty , and R. M. Martin, Phys. Rev. B **41**, 2976 (1990).

[7]L. Sorba, G. Bratina, G. Ceccone, A. Antonini, J. F. Walker, M. Micovic, and A. Franciosi, Phys. Rev. B. **43**, 2450 (1991).

[8]For example various papers included in Applied Surface Science **56-58** (1992).

[9]W. R. Frensley, H. Kroemer, Phys. Rev, B **16**, 2642 (1977).

[10]D. M. Bylander and L. Kleinman, Phys. Rev. B **36**, 3229 (1987); Phys. Rev. B **34**, 5280 (1986); Phys. Rev. B **38**, 7480 (1988).

[11]S. Baroni, R. Resta, A. Baldereschi, and M. Peressi, in *Spectroscopy of Semiconductor Microstructures* edited by G. Fasol (Plenum, 1989) pp 251; A. Baldereschi, S. Baroni, R. Resta, Phys. Rev. Lett. **61**, 734 (1988).

[12]A. Oshiyama and M. Saito, Phys. Rev. B **36**, 6156 (1987).

[13]S. Massidda, B. I. Min, and A. J. Freeman, Phys. Rev. B **35**, 9871 (1987); Phys. Rev. B **38**, 1291 (1988).

[14]W. R. L. Lambrecht, B. Segall, and O. K. Andersen, Phys. Rev. B **41**, 2813 (1990).

[15]J. Tersoff, Phys. Rev. Lett. **52**, 465 (1983).

[16]J. Tersoff, Phys. Rev. **30**, 4874 (1984).

[17]F. Flores and C. Tejedor, J. Phys. C **12** 732 (1979).

[18]M. Cardona, N. E. Christensen, Phys. Rev. B **35**, 6182 (1987).

[19]C. G. Van de Walle and R. M. Martin, Phys. Rev. B **35**, 8154 (1987).

[20]W. A. Harrison and J. Tersoff, J. Vac Sci. Technol. B B, 1068 (1986); W. A. Harrison and J. E. Klepeis, Phys. Rev. B **37**, 864 (1988) W. A. Harrison, *Electronic Structures and Properties of Solids* (Freeman, San Francisco, 1980).

[21]G. B. Bachelet and N. E. Christensen, Phys. Rev. B **31**, 879 (1985).

[22]S.-H. Wei and A. Zunger, Phys. Rev. Lett. **59**, 144 (1987); J. Vac Sci. Technol. B **5**, 1239 (1987).

[23]See for example, *Electron Spectroscopy: Theory, Techniques, and Applications* volume 1-5 edited by C. R. Brundle and A. D. Baker (Academic, London 1977), and various text books published for the electron spectroscopy.

[24]H. Sakakibara, Master thesis, University of Tokyo (to be published 1993).

[25]H. Fellner-Feldegg, U. Gelius, B. Wannberg, A. G. Nilsson, E. Basulier, and K. Siegbahn, J. Electron Spectroscopy and Related Phenomena, 5, 643 (1974)

[26]A sample of a GaAs/AlAs heterostructure has been measured by XPS. When the sample is placed level and raised from the point at which the maximum XPS intensity is obtained, peak energies of Ga 3*d* as well as Al 2*p* levels increases by ~ 0.15 eV.

[27]P. H. Citrin and G. K. Wertheim, Phys. Rev. B **27**, 3160 (1983).

[28]U. Gelius, E. Basilier, S. Svensson, T. Bergmark, and K. Siegbahn, J. Electron Spectroscopy and Related Phenomena, 2, 405 (1974).

[29]A. D. Katnani and G. Margaritondo, Phys. Rev. B 28, 1944 (1983).

[30]E. A. Kraut, R. W. Grant, J. R. Waldrop, and S. P. Kowalczyk, Phys. Rev. Lett. **44**, 1620 (1980); J. R. Waldrop and R. W. Grant, Phys. Rev. Lett. **43**, 1686 (1979); S. P. Kowalczyk, E. A. Kraut, J. R. Waldrop, and R. W. Grant, J. Vac. Sci. Technol. 21, 482 (1982); J. R. Waldrop, S. P. Kowalczyck, R. W. Grant, E. A. Kraut, and D. L. Miller, J. Vac. Sci. Technol. 19, 573 (1981).

[31]We consider our determination of $\Delta E_{v\text{-}CL}$ is more accurate than Kraut *et al.* at least in the accuracy of the theoretical DOS and in the sharpness of the observed spectrum. However, the agreement of theoretical DOS and the spectra is not sufficient for us to give an accuracy of ± 0.03 eV as Kraut *et al.* claimed. A still better value of ± 0.02 eV, which had appeared in their early paper, has been amended later [J. R. Waldrop, R. W. Grant, and E. A. Kraut, J. Vac. Sci. Technol. B **5**, 1209 (1987)].

[32]Although the most important point to be fit is the VBM, the spectrum is too featureless to be fit accurately. We made least squares fit for two energy regions, (i) –2 ~1 eV from

VBM in the theoretical DOS and (ii) –1~1 eV of DOS. After acquiring two values, we averaged those value to determine the VBM energy. Kraut *et al.* seems to have been used –1~2 (or 3) eV of the DOS.

[33]J. Ihm and J. D. Joannopoulos, Phys. Rev. B 24, 4191 (1981).

[34]J. R. Chelicowsky and M. L. Cohen, Phys. Rev. B **14**, 556 (1976).

[35]G. I. Gualtieri, G. P. Schwartz, R. G. Nuzzo, R. J. Malik, and J. F. Walker, J. Appl. Phys. **61**, 5337 (1987).

[36]At a certain growth condition, an inter-diffusion of Ga has been reported. In this section, however, we will discuss an interface effect on electronic structure when an ideal junction is formed.

[37]A. C. Gossard, P M. Petroff, W. Wiegmann, R. Dingle, and A. Savage, Appl. Phys. Lett. **29**, 323 (1976).

[38]H. Sakaki, M. Tanaka, and J. Yoshino, Jpn. J. Appl. Phys. **24**, L417 (1985).

[39]H. Munekata, L. L. Chang, S. C. Woronick, and K. H. Kao, J. Cryst. Growth **81**, 237 (1987).

[40]G. Tanaka, K. Hirakawa, H. Ichinose, and T. Ikoma, in 18th Proc. Int. Symp. GaAs and Related Compounds (1991).

[41]L. Vina and W. I. Wang, Appl. Phys. Lett. **48**, 36 (1986).

[42]As a guideline to preset an experimental duration, each of the peak XPS intensity should be more than ~10 Kcounts (Not a value in counts/s but that in counts are important) to get an accuracy of ~±20 meV and ~30 Kcounts is desirable to give an accuracy of better than ~±10 meV. However, when there is a significant magnitude of foreign background intensity such as a satellite intensity due to As excitation appearing around the Al 2*p* signal, the determination of a peak energy can be less accurate. An As 3*d* line creates plasmon satellites in lower kinetic energy than the intrinsic line. Unfortunately, a broad biplasmon satellite peak of As 3*d* level cover the Al 2*p* peak, reducing an accuracy of GaAs/AlAs structure with low Al 2*p* signal. Although a background subtraction procedure described in chapter 2 enhances the accuracy, it depends also on the quality (a signal to noise ratio) of the subtracting background spectrum.

[43]This uncertainty includes the unstability of the spectrometer, which changed the energy difference from 54.41 eV to 54.38 eV for a single heterojunction. This will be discussed in section 3.3.6. The data point for (311)A sample in Table III-II is measured a few years later then other samples and the same term as we measured the type II structure of section 3.3. The datum 53.36 eV is then considered to be 53.39 eV by substituting the instrumental artifacts.

[44]J. R. Waldrop, R. W. Grant, and E. A. Kraut, J. Vac. Sci. Technol. B **5**, 1209 (1987).

[45]H. Ohno, H. Ishii, K. Matsuzaki, and H. Hasegawa, J. Cryst. Growth **95**, 367 (1989).

[46]Due to a photoemission process, a number of electrons are ejected from the sample surface. Then, if a sample has relatively high resistance, a shortage of a current supplied from the bottom of the sample, which is connected to the earth level of the apparatus, breaks an thermal equilibrium condition and leads a voltage fluctuation in the XPS probing region.

[47]J. R. Waldrop, S. P. Kowalczyk, R. W. Grant, E. A. Kraut, and D. L. Miller, J. Vac. Sci. Technol. **19**, 573 (1981).

[48]Because we consider a spatial variation of potential, energies must be measured from a reference for which the location is identified or spatial constancy is fulfilled. In the experiment Al 2p level are used as a reference for GaAs inserted (type I) and type II samples. For XPS energy scale is often shown by a binding energy, which is measured from a VBM of the Fermi level in a solid sample.

[49]C. S. Fadley, in *Electron Spectroscopy Theory, Techniques, and Applications* Vol. 2, edited by C. R. Brundle and A. D. Baker, p. 80 (Academic Press, London, 1978).

[50]S. Baroni, R. Resta, and A. Baldereschi, in *Band Structure Engineering in Semiconductor Microstructures*, edited by R. Abrams and M. Jaros, NATO ASI series, p. 51 (Plenum, New York, 1988).

[51]By considering one monolayer roughness for type II experiment, the trend found in Fig. 3-7 can be explained by only a1 and a roughness. However, the experiment on type I sample cannot be explained by considering one monolayer roughness only. Further the energy difference found on type II sample which is ~0.5 eV smaller than that from type I reflect that the interface is more flatly formed for those samples.

[52]A shutter for the As beam flux is closed during a growth interruption on an AlAs surface. Then the As beam flux is reduced from ~1×10^{-6} Torr to ~2×10^{-7} Torr.

[53]When the RHEED intensity oscillation does not coincides to the designed one monolayer growth, possibly due to a roughness of the initial AlAs layer and/or the practical problems such as a fluctuation of sample angle, noise etc., we have regrown on it a 1000Å-thick n-type GaAs buffer and the probing layers.

[54]In order to prevent any systematic error cause a trend appear in Fig 3-7, we made three series of experiments. The first and

the second series were performed within one week, on an identical substrate (This minimize an ambiguity arising from a difference in a growth condition and sample position during measurements, because it tend to vary depending on a sample or sample holder.), and successively. Since an order of measurement is d=0 ML (first), $d = \infty$ ML (second), d =1 ML, and d = 2 ML (last), a trend found on Fig. 3-7 is not due to a systematic error which shift the measured difference depending its order of experiment.

[55]When there are several core level peaks which are separated by energy much smaller (≤10%) than the XPS core level line width (~1 eV), the resulting spectrum is a single peak whose apparent position is very well approximated by averaging the energy positions by multiplying the intensity ratio. $\Delta E_{\text{Ga 3}d\text{-Al 2}p}$'s are smaller for type II than for type I. This is mainly because heterointerfaces are more flat in type II samples.

[56]K. Hirakawa, Y. Hashimoto, and T. Ikoma, Surf. Sci. **267**, 166 (1992).

[57]T. M. Duc, H. Hsu, and J. P. Faurie, Phys. Rev. Lett. **58**, 1127 (1987).

[58]R. Ludeke, L. Ley, and K. Ploog, Solid State Commun. **28**, 57 (1978).

[59]P. J. Ireland, L. L. Kazmerski, and R. F. Fisher, J. Vac. Sci. Technol. A **2**, 1129 (1984).

[60]H. Okumura, I. Yoshida, S. Misawa, and S. Yoshida, J. Vac. Sci. Technol. B **5**, 1622 (1987).

[61]C. K. Shih and W. E. Spicer, Phys. Rev. Lett. **58**, 2594 (1987).

[62]Theoretical DOS for $Al_xGa_{1-x}As$ alloy is obtained by the weighted average of the DOS of GaAs and AlAs which were calculated by J. Ihm and J. D. Joannopoulos [Phys. Rev. B **24**, 4191 (1981)]. B. I. Min, S. Massidda, and A. J. Freeman [Phys. Rev. B **38**, 1970 (1988)] calculated the DOS for GaAs, AlAs, and also the $(GaAs)_1(AlAs)_1$ superlattice (SL) and demonstrated that the DOS for the SL is very similar to the rigid sum of the DOS for GaAs and AlAs, suggesting the systematic error caused by the above assumption for the DOS of $Al_xGa_{1-x}As$ is negligible.

[63]The experiments on AlGaAs alloy has been performed in the same term as we measured the samples described in section 3.2 and type I samples of the section 3.3. So the energy difference for the heterojunction used to be compared with that of alloy is not 54.39 eV but 54.41 eV, which is the value before the spectrometer's gain has been changed.

[64]J. Nithianandam and S. E. Schnatterly, Phys. Rev. B **42**, 3038 (1990).

[65]J. Nithianandam and S. E. Schnatterly [Phys. Rev. B **42**, 3038 (1990)] deduced a natural energy lineups by assuming that the Hg 5d and Cd 4d level energy is absolutely constant. However, this assumption does not seem to valid for the AlGaAs system.

[66]K. Akimoto, Y. Mori, and C. Kojima, Phys. Rev. B **35**, 3799 (1987).

[67]G. Osbourn, Phys. Rev. **B27**, 5126 (1983); T. Yao, Jpn. J. Appl. Phys. **23**, L521 (1983).

[68]O. Brandt, L. Tapfer, R. Cingolani, K. Ploog, M. Hohenstein, and F. Phillipp, Phys. Rev. **B41**, 12599 (1990).

[69]H. Nakao and T. Yao, Jpn. J. Appl. Phys. **28**, L352 (1989); G. L. Price, Appl. Phys. Lett. **53**, 1288 (1988).

[70]S. P. Kowalczyk, W. J. Schaffer, E. A. Kraut, and R. W. Grant, J. Vac. Sci. Technol. **20**, 705 (1982).

[71]K. Hirakawa, Y. Hashimoto, and T. Ikoma, Phys. Rev. B **44**, 1734 (1991).

[72]G. P. Schwartz, M. S. Hybertsen, J. Bevk, R. G. Nuzzo, J. P. Mannaerts, and G. J. Gualtieri, Phys. Rev. **B39**, 1235 (1989). In their paper, the authors calculated strain-induced shifts in the core to VBM energies in pseudomorphic Si/Ge heterostructures by self-consistent linear muffin-tin-orbital method. However, their calculation does not take into account the XPS core-hole relaxation effect.

[73]C. G. Van de Walle and R. M. Martin, Phys. Rev. **B34**, 5621 (1986).

[74]R. Enderlein and W. A. Harrison, Phys. Rev. **B30**, 1867 (1984). Since these authors did not take into account the spin-orbit interaction, the energy position of VBM denoted by E_{VBM} in their paper corresponds to E_{cv}.

[75]By using a Born-Haber cycle with the Z+1 approximation, the core level binding energy measured from CVBM is expressed as Eq. (4-10) in the text. Here, the photoemission is treated as a process of exciting one core electron to CVBM (the Fermi level is assumed to be at CVBM position) and incrementing the atomic number from Z to Z+1, which approximately represents the core hole in the final state.
Within the framework of tight binding theory, the bond formation energy of the XAs (X = Ga, In) compound, $E_{bond}(X\text{As})$, is expressed as;

$$E_{prom}(X\text{As}) = \tfrac{1}{8}\left(2e_p^X - e_s^X - e_s^{\text{As}}\right).$$

Here, $E_{prom}(X\text{As})$ denotes the promotion energy, $V_2(X\text{As})$ the covalent energy, and $V_3(X\text{As})$ the polar energy. $E_{prom}(X\text{As})$, $V_2(X\text{As})$, and $V_3(X\text{As})$ are respectively given by;

$$E_{bond}(X\text{As}) = 2E_{prom}(X\text{As}) - 2\left[V_2^2(X\text{As}) + V_3^2(X\text{As})\right]^{\frac{1}{2}},$$

$$V_2(XAs) = -3.22\frac{\hbar}{md^2},$$

$$V_3(XAs) = \tfrac{1}{2}\left(e_h^X - e_h^{As}\right).$$

Here, m denotes the free electron mass, $\hbar$ the reduced Planck constant, and d the bond length. e_s and e_p are the atomic s- and p-orbital energies, respectively, and $e_h^{X,As}$ the hybrid energy which is defined by

$$e_h^{X,As} = \tfrac{1}{4}\left(e_s^{X,As} + 3e_p^{X,As}\right)$$

for X and As atoms. The energy difference in E_{bond} between in the initial and final states, ΔE_{bond}, is obtained by;

$$\Delta E_{bond} = 4\left[E_{bond}({}_{Z+1}XAs) - E_{bond}(XAs)\right].$$

Here, ${}_{Z+1}X$ denotes an atom with an atomic number of $Z+1$.

Under unstrained or hydrostatically strained condition, the energy position of CVBM, E_{cv}, is given by;

$$E_{cv} = \tfrac{1}{2}\left(e_p^X + e_p^{As}\right) + \tfrac{1}{2}\left(\frac{1.28}{3.22}\right)^2 V_0(XAs) - \left[\left(\frac{e_p^X - e_p^{As}}{2}\right)^2 + \left(1.28\frac{\hbar^2}{md^2}\right)^2\right]^{\frac{1}{2}},$$

with

$$V_0(XAs) = \frac{V_2^2(XAs)}{\left[V_2^2(XAs) + V_3^2(XAs)\right]^{\frac{1}{2}}}.$$

Here, $\frac{1}{2}\left(\frac{1.28}{3.22}\right)^2 V_0(XAs)$ is the nonorthogonality shift.

Metallization correction, E_{met}, represents the energy shift originating from the interaction between an X-As bond and the neighboring antibonding orbitals. To calculate the shift ΔE_{met} in the metallization correction, we have to consider the case where the X atom in an X-As bond loses an electron and also the case where the X atom in the neighboring X-As antibonds loses an electron. Then, we have;

$$\Delta E_{met} = -4\left[E_{met}(XAs|O) - E_{met}\left({}_{Z+1}XAs|O\right)\right] - 12\left[E_{met}(XAs|O) - E_{met}\left(XAs|_{Z+1}X\right)\right].$$

Here, $E_{met}(XAs|O)$ and $E_{met}\left({}_{Z+1}XAs|O\right)$ represent the metallization energies for X-As and ${}_{Z+1}X$-As bonds, respectively, and $E_{met}\left(XAs|_{Z+1}X\right)$ the metallization energy for the X-As bond next to the ${}_{Z+1}X$-As antibond. I_{core} denotes the atomic ionization energy, which is specific to the atom species. The d-dependence of ΔE_{bond}, E_{cv}, and ΔE_{met} give the energy shift in E_{CL}^{cv}. The obtained energy shift, $[E_{CL}^{cvs}(theor) - E_{CL}^{cvo}(theor)]$, is – 0.11 eV for InAs strained case (type I) and 0.02 eV for GaAs strained case (type II).

[76] *Landolt-Börnstein: Numerical Data and Functional Relationships in Science and Technology*, edited by O. Madelung (Springer-Verlag, Berlin, 1982).

[77] F. H. Pollak and M. Cardona, Phys. Rev. **172**, 816 (1968).

[78] J. R. Chelicowsky and M. L. Cohen, Phys. Rev. **B14**, 556 (1976).

[79] XPS spectra used to fit the spectrum from the heterostructure are Ga 3*d* and In 4*d* spectra, which were taken from bulk GaAs and InAs samples, respectively, and backgrounds due to inelastic photoelectrons were subtracted. The peak intensities and peak kinetic energies were least squares fit to determine $\Delta E_{\text{In 4d-Ga 3d}}$. Although the bulk XPS spectra seem to be slightly broader than the signal from inserted layer possibly due to a surface chemical shift, the accuracy of the determination is ~0.02 eV for the energy difference.

[80] Yu *et al.* [E. T. Yu, E. T. Croke, T. C. McGill, and R. H. Miles, Appl. Phys. Lett. **56**, 569 (1990)] measured the core level binding energies from VBM on strained Si/Ge heterostructures.

[81] J. Menéndez, A. Pinczuk, D. J. Werder, S. K. Sputz, R. C. Miller, D. L. Sivco, and A. Y. Cho, Phys. Rev. **B36**, 8165 (1987).

[82] M. Cardona and N. E. Christensen, Phys. Rev. **B35**, 6182 (1987).

[83] C. Priester, F. Allan, and M. Lannoo, Phys. Rev. **B38**, 9870 (1988).

[84] A. Taguchi and T. Ohno, Phys. Rev. **B39**, 7803 (1989).

[85] By replacing factors for δE_{001} and δE_{111} in the equation (11) of F. H. Pollak and M. Cardona [Phys. Rev. **172**, 816 (1968)], uniaxial strain effect are deduced for (110) interfaces by second order perturbation theory.

[86] *ibid*, equation (9).

[87] F. Cappasso, K. Mohammed, and A. Y. Cho, J. Vac. Sci. Technol. B **3**, 1245 (1985).

[88] D. W. Niles, G. Margaritondo, P. Perfetti, C. Quaresima, and M. Capozi, Appl. Phys. Lett. **47**, 1092 (1985).

[89] P. Perfetti, C. Quaresima, C. Coluzza, C. Fortunato, and G. Margaritondo, Phys. Rev. Lett. **57**, 325 (1986).

[90] M. Peressi, S. Baroni, and R. Resta, Phys. Rev. B **43**, 7347 (1991).

[91] W. I, Wang, E. E. Mendez, T. S. Kuan, and L. Esaki, Appl. Phys. Lett. **47**, 826 (1095).

[92] O. Brandt, G. E. Crook, K. Ploog, J. Wagner, and M. Maier, Appl. Phys. Lett. **59**, 2730 (1991).

[93] Si deposition rate is calibrated by a van del Pau electron concentration measurement on

an uniformly Si doped GaAs sample. The sample consisted of 1μm-thick Si doped layer embedded by barrier AlGaAs layers and capped with thin GaAs layer grown at 600 °C on a semi-insulating (100) GaAs substrate. The Si cell is heated to 1100°C. And Si cell shutter is opened discontinuously so as to reduce a Si concentration down to ~1×10^{18}cm^{-3}.

[94]Y. Hashimoto, T. Saito, K. Hirakawa, and T. Ikoma, 19th Proc of Int. Symp. GaAs and Related Compounds, (Sept. 1992) to be published: T. Saito and T. Ikoma, unpublished.

[95]A non-linear band bending is expected in the AlAs layer. By taking into account the Si segregation effect as well as a band bending due to the interface Si donor and the surface states a band diagram shown by the next figure is expected. However, the exact profile of Si donor concentration is needed to draw the band bending completely. By neglecting the Si segregation/diffusion effect, which is reduced by 450 °C-growth, a simple linear band-bending is used to estimate the average valence band difference in the text.

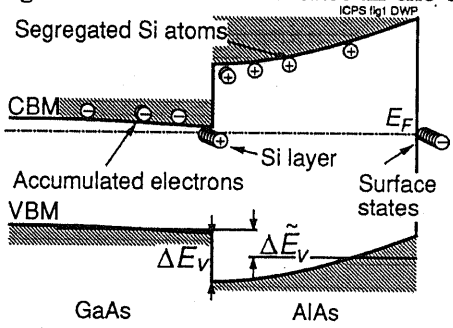

A sketch of a band diagram at AlAs/Si/GaAs structure. Here, Si segregation and electron accumulation effects are taken into account.

[96]G. Gillman, B. Vinter, E. Bardier, and A. Tardella, Appl. Phys. Lett. **52**, 972 (1988).

[97]UPS measurements were performed on a sample consisting of a 1 μm-thick Si-doped (1×10^{16} cm^{-3}) GaAs buffer layer and a 100 Å-thick undoped AlAs layer successively grown on an *n*-type (100) GaAs substrate as well as a reference gold sample. A He I radiation of a UV lamp ($h\nu$=21.2 eV) was used to excite a sample. Because from an AlAs sample any of He II related A kinetic energy for the AlAs VBM is determined by linearly extrapolating a valence spectrum. The Fermi level is also determined by the UPS spectrum from a gold sample. Since an instrumental resolution of UPS is ~0.1 eV. The ambiguity of the determined energy from a VBM of AlAs to the Fermi level is ~0.1 eV.

[98]K. Ploog, A. Fischer, and E. F. Schubert, Surf. Sci. **174**, 120 (1986).

[99]P. N. Uppal, J. S. Ahearn, and D. P. Musser, J. Appl. Phys. **62**, 3766 (1987).

[100]G. Bratina, L. Sorba, A. Antonini, G. Biasiol, and A. Franciosi, Phys. Rev. B **45**, 4528 (1992).

[101]A. Muños, P. Rodríguez-Hernández, Phys. Rev. B **45**, 4502 (1992).

[102]M. E. Greiner and J. F. Gibbons [Appl. Phys. Lett. **44**, 750 (1984)] have reported a polarity change (Si_{Ga}-Si_{As} $\rightleftarrows$ Si_{As}-Si_{Ga}) during a Si diffusion into GaAs by a thermal process.

[103]T. Saito, Y. Hashimoto, and T. Ikoma, unpublished.

[104]G. Tanaka, Master Thesis University of Tokyo 1992.

[105]Y. Horikoshi, M. Kawashima, and N. Kobayashi, J. Cryst. Growth, **111**, 200 (1991).

[106]R. D. Bringans, M. A. Olmstead, R. I. G. Uhrberg, and R. Z. Bachrach, Phys. Rev. B **36**, 9569 (1987).

[107]Photoelectron escape depth λ_e is estimated by measuring AlAs/GaAs structures. We compared an intensity ratio of a Ga 3*d* peak and a valence DOS (dominated by the signal from AlAs when AlAs is thick) among AlAs *d* ML/GaAs structures (d=0, 5, and 10). A decrease in an intensity of a Ga 3*d* signal with increasing *d* is fit by λ_e=8Å.

[108]J. T. McKinley *et al.* J. Vac. Sci. Technol. A **9**, 917 (1991).

[109]Y. Horikoshi, M. Kawashima, and H. Yamaguchi, Jpn. J. Appl. Phys. **25**, L868 (1986); F. Brionez, D. Golmayo, L. Gonzales, and A. Ruiz, J. Cryst. Growth, **81**, 19 (1987).

[110]L. Sorba, *et al.* Phys. Rev. B **46**, 6834 (1992).

[111]W. Q. Li, P. K. Bhattacharya, S. H. Kwok, and R. Merlin, J. Appl. Phys. **72**, 3129 (1992).

[112]A decrease in the apparent ΔE_V is due to an *n*-type doping sheet at the interface. We also tried to evaluate a carrier concentration by a Hall electron or hole concentration measurement. However, the conduction type of Si δ-doped (311)*A* GaAs varies with samples. It might be due to a part of Si atoms segregated or diffused from the doped sheet are different type of dopants: i.e. a doping sheet is *n*-type and the neighbor of the sheet is slightly *p*-type.

[113]K. Agawa, Y. Hashimoto, and T. Ikoma, unpublished.

[114]Because the *p*-type GaAs layer is relatively thick, a band bending in the *p*-type GaAs layer affects the XPS spectra. If an acceptor concentration is constant in the Si-doped GaAs layer, a quadratic curve in VBM is estimated. Then, the offset between the VBM at the bottom of *p*-type layer and the AlAs layer changes twice as much as the XPS determined effective VBO changes.

Related publications

[1] K. Hirakawa, Y. Hashimoto, and T. Ikoma, "Orientation independence of heterojunction-band offsets at GaAs-AlAs heterointerfaces characterized by x-ray photoemission spectroscopy", Appl. Phys. Lett. **57**, 2555 (1990).

[2] K. Hirakawa, Y. Hashimoto, and T. Ikoma, "Strain effect on band offsets at pseudomorphic InAs/GaAs heterointerfaces characterized by x-ray photoemission spectroscopy," Phys. Rev. B **44**, 1734 (1991).

[3] Y. Hashimoto, G. Tanaka, K, Hirakawa, and T. Ikoma, "Role of Si insertion layer at GaAs/AlAs heterointerface determined by x-ray photoemission spectroscopy," submitted to J. Vac. Sci. Technol. B.

[4] Y. Hashimoto, K. Hirakawa, T. Ikoma, and Y. Iye, "Local electronic structure in the extreme vicinity of GaAs/AlAs heterointerfaces," submitted to Phys. Rev. Lett.

[5] Y. Hashimoto, G. Tanaka, K. Hirakawa, and T. Ikoma, " Role of ultrathin Si layer in GaAs/Si/AlAs heterostructure," to be published in Proc. 21st Int. Conf. Physics of Semiconductors, Beijing, CHINA, 1992.

[6] Y. Hashimoto, T. Saito, K. Hirakawa, and T. Ikoma, "Roles of ultrathin Si layer inserted at GaAs/AlAs heterointerface," to be published in Proc. 19th Int. Symp. GaAs and Related Compounds, Karuizawa, JAPAN, 1992.

[7] Y. Hashimoto, K. Hirakawa, K. Harada, and T. Ikoma, "Strain induced change in heterojunction band offsets at pseudomorphically grown InAs/GaAs heterointerfaces characterized by X-ray photoelectron spectroscopy", J. Cryst. Growth **111**, 393 (1991) (6th Int. Conf. Molecular Beam Epitaxy, San Diego, USA, Aug, 1990).

[8] K. Hirakawa, Y. Hashimoto, and T. Ikoma, "Transient of microscopic valence-charge distribution and electrostatic potential at GaAs/AlAs heterointerfaces", Surf. Sci. **267** (Proc. 5th Int. Conf. Modulated Semiconductor Structures, Nara, July 1991), 166 (1992).

[9] Y. Hashimoto, K. Hirakawa, and T. Ikoma, "Microscopic charge distributions at GaAs/AlAs heterointerfaces characterized by X-ray photoelectron spectroscopy", 17th Int. Symp. GaAs and Related Compounds, Jersey, UK, Sep. 1990 (Inst. Phys. Conf. Ser. No 112) pp 225-230.

[10] K. Hirakawa, Y. Hashimoto, and T. Ikoma, "Transient of electrostatic potential at GaAs/AlAs heterointerfaces characterized by x-ray photoemission spectroscopy", SPIE vol. 1361 Physical Concept of Material for Novel Optoelectronic Device Applications pp 255-261 (1990).

[11] K. Hirakawa, Y. Hashimoto, T. Saito, and T. Ikoma, "Direct experimental estimation of interface dipole effect of GaAs/AlAs heterojunction band offset by x-ray photoelectron spectroscopy", Proc. 16th Int. Symp. GaAs and Related Compounds, Karuizawa, Japan, 1989, (Inst. Phys. Conf Ser. No 106) pp 345-350.

[12] Y. Hashimoto, K. Hirakawa, K. Harada, and T. Ikoma, "Strain induced change in band offsets at pseudomorphic InAs/GaAs heterointerfaces characterized by X-ray photoelectron spectroscopy", 9th Symp. on Alloy Semiconductor Physics and Electronics, Izunagaoka, July, 1990 pp 341.

[13] Y. Hashimoto, K. Hirakawa, and T. Ikoma, "Natural band lineups of valence band maximum and core levels in AlGaAs", 10th Symp. on Alloy Semiconductor Physics and Electronics (Nagoya, July, 1991) pp 277.

Presentations have been made on papers 5,6,8,9,12, and 13.